



Universidade do Minho
Escola de Engenharia

Maria João Correia Varela de Almeida

**Biomechanical Analysis
of the Human Gait Cycle
for Different Scenarios**

Dissertação de Mestrado
Ciclo de Estudos Integrados Conducentes ao
Grau de Mestre em Engenharia Biomédica

Trabalho realizado sob a orientação de
Professor Doutor João Paulo Flores Fernandes
Universidade do Minho

Professor Doutor José Mendes Machado
Universidade do Minho

*To my grandparents, my parents and my brother,
for their love.*

*Special thanks to my supervisors Professor João Paulo Flores
Fernandes and Professor José Mendes Machado from
University of Minho as well as Professor Marco Ceccarelli
from University of Cassino and South Latium, for their
brilliant guidance.*

RESUMO

O objectivo geral do presente trabalho é a caracterização experimental da biomecânica da marcha humana através do *Cassino Tracking System (CaTraSys)*. O *CaTraSys*, concebido no *Laboratory of Robotics and Mechatronics, University of Cassino and South Latium*, é um sistema que avalia a posição/orientação e força exercida por sistemas multicorpo ao longo de grandes trajectórias usando um conjunto de cabos em arquitectura paralela. É um sistema económico e de fácil operação. O sistema proposto poderia ter aplicação clínica como dispositivo de avaliação, por exemplo no campo das terapias de reabilitação.

No presente trabalho é usada uma configuração de três cabos ligados ao joelho e outros três ligados ao tornozelo (configuração 3-3). O *set-up* experimental consiste em um tapete rolante não motorizado e a população testada encontra-se entre os 20 e os 28 anos de idade. Diferentes condições experimentais são avaliadas: um teste de referência, em que o sujeito anda a uma velocidade seleccionada pelo próprio (estimado para 5 km/h); um teste de carga, em que a marcha é efectuada com um peso extra de 6 kg; um teste de calçado, onde é pedido ao sujeito que realize o teste com um calçado diferente; e por fim um teste de velocidade rápida, em que a velocidade de marcha é aumentada, sem que ocorra corrida (estimado para 8 km/h).

O princípio de funcionamento do *CaTraSys* é baseado nos cálculos de trilateração, que resumidamente determinam a posição do *end-effector* a partir de três comprimentos de cabos. No campo da aquisição de dados, o procedimento de calibração e cálculo de forças são também abordados. O *software* usado para o processamento de dados é o *LabVIEW* e o *MATLAB*.

Para a análise de dados, diferentes técnicas são usadas. Primeiramente é necessário proceder ao pré-tratamento do sinal, pelo que é usado o filtro *Butterworth*. Para a obtenção da trajectória média, um tratamento estatístico é elaborado. O ângulo da perna apresentado durante o teste é calculado. O método das diferenças finitas é usado para o cálculo da velocidade e aceleração a partir dos dados de trajectória.

Características básicas dos padrões de marcha 2D e 3D são discutidas, para os resultados experimentais de trajectória, ângulo da perna, velocidade, aceleração e forças do *end-effector*. Diferentes condições de teste e características antropométricas são avaliadas a fim de estudar a sua influência sobre a marcha da população. Para que uma análise objectiva seja possível, são determinados parâmetros espaciotemporais.

ABSTRACT

The general purpose of the present work is the experimental characterization of the biomechanics of human walking using Cassino Tracking System (CaTraSys). CaTraSys, conceived at Laboratory of Robotics and Mechatronics, University of Cassino and South Latium, is a system for the estimation of pose and force exerted by multibody systems along large trajectories using a set of wires in parallel architecture. It is a low cost and easy operable system. The proposed system could have clinical application as an assessing device, for example in the field of the rehabilitation therapies.

In the present work a configuration of three cables attached to the knee and other three attached to the ankle point is used (3-3 configuration). The experimental set-up uses a non-motorized treadmill and the population understudy is between the 20 and 28 years old. Different experimental modes are evaluated: a reference test, where the subject walks on a self-selected velocity (estimated for 5 km/h); a loading test, where the walking is performed with an extra weight of 6 kg; a footwear test, where the subject is asked to perform the test with different shoes and at last a fast test, where the walking velocity is increased, with no running (estimated for 8 km/h).

The operating principle is based on the trilateration computations, which basically determine the position of the end-effector from three cables length. In the field of the data acquisition, the calibration procedure and the forces computation are also covered. The software used for the data processing is the LabVIEW and MATLAB.

For the data analysis, different techniques are required. Firstly, it is necessary to do the signal pre-processing, in which it is used the Butterworth filter. In order to obtain an average trajectory curve, a statistical treatment method is devised. Shank angles are calculated. The finite-difference method is used for the computation of the velocity and acceleration from the trajectory data.

Basic characteristics of the 2D and 3D gait patterns are discussed, for CaTraSys results of trajectory, shank angle, velocity, acceleration and forces of the end-effector. Different test conditions and anthropometric characteristics are evaluated in order to study their influence on the gait of the tested population. In order to accomplish an objective analysis, gait spatio-temporal parameters are determined.

KEYWORDS

HUMAN GAIT

CATRASYS

TREADMILL

3D TRAJECTORY

MEAN TRAJECTORY

GAIT PARAMETERS

PALAVRAS-CHAVE

MARCHA HUMANA

CATRASYS

PASSADEIRA ROLANTE

TRAJETÓRIA 3D

TRAJETÓRIA MÉDIA

PARÂMETROS DE MARCHA

TABLE OF CONTENTS

RESUMO	i
ABSTRACT	iii
KEYWORDS	v
PALAVRAS-CHAVE	v
TABLE OF CONTENTS	vii
CHAPTER 1 - INTRODUCTION.....	1
1.1 - Motivation.....	1
1.2 - Scope and Objectives.....	2
1.3 - Contributions of the Work.....	3
CHAPTER 2 - HUMAN GAIT.....	5
2.1 - Lower Limb Anatomy and Physiology	5
2.1.1 - Bones and Joints.....	5
2.1.2 - Muscles	7
2.2 - Gait Analysis.....	9
2.3 - Pathological Mechanisms.....	12
CHAPTER 3 - CATRASYS.....	15
3.1 - System Description	15
3.2 - Components.....	18
3.3 - Data Acquisition.....	23
3.3.1 - Calibration	24
3.3.2 - Trilateration	27
3.3.3 - Forces Computation	30
3.4 - Clinical Significance	32
CHAPTER 4 - METHODOLOGY	35
4.1 - Experimental Setup.....	35
4.2 - Experimental Modes	35
4.3 - Subjects	38
4.4 - Data Collection Protocol.....	38
CHAPTER 5 - DATA ANALYSIS.....	41
5.1 - Signal Pre-Processing	41

5.2 - Statistical Treatment	46
5.3 - Shank Angle	48
5.4 - Velocity and Acceleration	48
CHAPTER 6 - RESULTS AND DISCUSSION	51
6.1 - Curve Analysis	51
6.1.1 - Linear Kinematics	51
6.1.2 - Kinetics.....	57
6.2 - Comparative Gait Analysis.....	58
6.2.1 - Spatio-Temporal Parameters	58
6.2.2 - Influence of the Test Conditions.....	61
6.2.3 - Influence of the Anthropometric Factors.....	64
CHAPTER 7 - CONCLUDING REMARKS	67
7.1 - Conclusions.....	67
7.2 - Future Work.....	68
REFERENCES	69
LIST OF FIGURES	73
LIST OF TABLES.....	77
APPENDIX A – TECHNICAL SPECIFICATIONS OF CATRASYS COMPONENTS.....	79
A.1 - DAQ Board	80
A.2 - Cable-Extension Position Transducer	83
A.3 - Tension (Compression) Load Cell.....	85
A.4 - Analog Weight Transmitter	86
APPENDIX B – LABVIEW VI.....	87
B.1 - Front Panel	88
B.2 - Block Diagram.....	90
APPENDIX C – FORM FOR CATRASYS EXPERIMENTAL TEST ON HUMAN WALKING CHARACTERIZATION	93
APPENDIX D – INDIVIDUAL TESTS INFORMATION	95
D.1 - Subject 1	96
D.2 - Subject 2	97
D.3 - Subject 3	98
D.4 - Subject 4	99

D.5 - Subject 5	100
D.6 - Subject 6	101
D.7 - Subject 7	102
D.8 - Subject 8	103

CHAPTER 1 - INTRODUCTION

In the present chapter an overview of the thesis is provided. The motivation for the development of the proposed work is presented as well as a description of the objectives and structure of the developed work.

1.1 - Motivation

The problems presented by the use of industrial robots as well as their high cost and difficult implementation demand for alternative measuring systems or proper revision of the existing ones. Cable based parallel manipulators are presented as an alternative. They are robotic cable actuated systems. The cables are connected to the end-effector and to a fixed frame.

This type of manipulators has many advantages. Cable based manipulators ensure very good kinematic and dynamic characteristics. They are characterized by an easy set-up and transportability and good inertial behavior due to the small moving masses consisting of the cables and end-effector. The end-effector can be moved and changed. The calibration procedure does not need to be repeated at each use. The main drawback is the requirement of operating in a reduced workspace, so that cables interference is avoided. The main characteristics are the low cost and easy operation, which are very important for a possible commercial system (Ottaviano *et al.*, 2010; Nunes *et al.*, 2011).

All these features are suitable for clinical applications (Homma *et al.*, 2002). Also, cable based systems can be reconfigured for different therapies, the cables in opposition to the rigid links make the patient adaptation easier and also reduce the constraints. Robotic systems for rehabilitation are commonly used to record information or to guide the movement of a patient limb attached to the device (Ottaviano *et al.*, 2010; Nunes *et al.*, 2011).

In this work, a passive cable based parallel manipulator is proposed, Cassino Tracking System (CaTraSys), with possible application in the clinical field as an assessing device.

1.2 - Scope and Objectives

The general purpose of the present work is the characterization of the biomechanics of human walking using CaTraSys.

The specific goals are listed below:

- To study the fundamentals of human gait;
- To understand CaTraSys and the experimental data acquisition;
- To perform experimental work for characterization of the human gait, taking into account different scenarios;
- To analyze and interpret the experimental data results.

A summary of each chapter will be done hereafter. In chapter one an overview of the thesis is provided, along with a characterization of the state of the art of the human walking CaTraSys investigations.

Chapter two provides a description of the lower limb anatomy and physiology as well as an analysis of the human gait and its pathological mechanisms.

In chapter three an overview of CaTraSys operation and its components is done. The clinical application of the present system is reviewed.

Chapter four presents all the methodology of the experimental tests, including the experimental setup, the modes and the data collection protocol. The subject pool under study is presented in detail.

In chapter five the basis of the digital filters used in biomechanics, mainly the Butterworth filter, is discussed. The smoothing technique is applied to the experimental data. The formulation to access to the average trajectory is fairly covered. Finally, equations used for the estimations of the shank angles are provided, as well as for the velocity and acceleration, where the finite difference technique is used.

In chapter six the linear and angular gait kinematics as well as kinetics of the normal human walking are studied. A quantitative analysis of the effect on human gait of different treadmill walking modes and subjects is conducted.

At last, chapter seven comprises the conclusions of the present work in addition to some suggestions for further improvement of the human walking characterization with CaTraSys.

1.3 - Contributions of the Work

The present work allowed firstly the clear definition of a methodology to the CaTraSys gait tests. An enhancement of the virtual instrument (VI) and its formulation, used to acquire the gait data, was achieved. A data analysis procedure was devised. Particularly, a formulation was conceived for CaTraSys gait tests to obtain a medium trajectory. The formulation also allows the determination of gait spatio-temporal parameters from the average curve, enabling so an objective measure and analysis of it.

Basic characteristics of the 2D and 3D gait patterns were discussed, for CaTraSys results of trajectory, shank angle, velocity, acceleration and forces of the end-effector. Different test conditions and anthropometric characteristics were evaluated in order to study their influence on the gait of the tested population.

CHAPTER 2 - HUMAN GAIT

The present chapter begins by providing an explanation of the lower limb anatomy and physiology. It points out the bones, joints and muscles of the lower limb towards a better understanding of the complex chain that is the human lower body. Then, an analysis of the gait phases and technical terms is given. At last, the pathological conditions responsible for causing the abnormalities on the mechanism of walking are also reviewed. It should be noted this chapter does not pretend to do an exhaustive analysis of these subjects, but instead to provide a general idea of these same subjects.

2.1 - Lower Limb Anatomy and Physiology

The main functions of the lower limb are to support body weight and enable locomotion. Lower limbs are linked to the trunk through the pelvis. They are constituted by the gluteal region, thigh, leg and foot and composed by:

- Bones and Joints;
- Muscles.

2.1.1 - Bones and Joints

The pelvis is constituted by the sacrum, the coccyx and the pelvic girdle (see Fig. 2.1). The sacrum consists of five fused sacral vertebrae. The coccyx is the vestigial tail, made of three to five rudimentary vertebrae. The pelvic girdle consists of two coxal bones, each created through the fibrous union of the ilium, ischium and pubic bones. The right and left coxal bones are joined anteriorly at the pubic symphysis, and connect posteriorly via the sacrum and the two sacroiliac joints that articulate with the fifth lumbar vertebra of the spine. On each side of the lower part of

the pelvis is the hip joint, a spherical big joint located between the pelvic acetabulum and the femoral head (Whittle, 2007). The pelvic girdle and hip joints support a sequence of movements and forces. This complex association of forces and movements in equilibrium allow the maintenance of balance and an upright posture (Hamill and Knutzen, 2009).

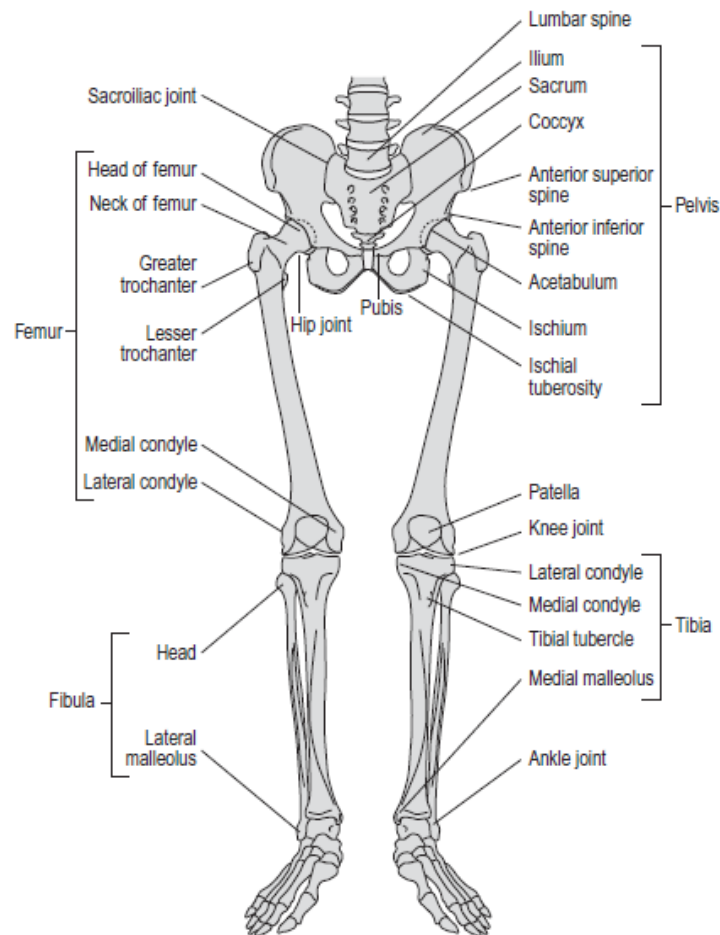


Figure 2.1 - Bones and joints of the lower limbs (Whittle, 2007).

The femur is the bone of the thigh. In its distal extremity, it contacts with the tibia and also articulates with the patella. The patella is the largest sesamoid bone and is surrounded by the tendon of the quadriceps muscle of femur.

The main joint of the knee is the joint between femur and tibia, the tibiofemoral joint. It shares the joint cavity with the patellofemoral joint, the joint between patella and femur. Although the main movements of the knee are flexion and extension, knee joint also allows femur to rotate above tibia. This rotation contributes to the stabilization of the knee when it is totally extended, particularly when the individual is in the stand position (Whittle, 2007).

The leg is constituted by two bones:

- Tibia - it is located in the medial position, it is bigger than fibula and it is the bone that supports the weight;
- Fibula-it is located in the lateral position. Proximally, it forms a small synovial joint (proximal tibiofibular joint) with the inferolateral surface of the lateral condyle of tibia.

Tibia and fibula are connected through its length by an interosseous membrane and in their distal extremities by a fibrous tibiofibular joint, occurring few movements between them (Whittle, 2007). The proximal joint of the foot is the talocrural joint, or ankle joint. It is designed for stability rather than mobility (Hamill and Knutzen, 2009).

The bones of the foot are constituted by the tarsals, metatarsals and phalanges. There are seven tarsal bones organized with the Talus. The tarsal bones articulate with the metatarsal bones (I–IV) forming the tarsometatarsal joints, which allow limited movement of sliding. The independent metatarsals movements are restricted by the metatarsals transverse ligaments, which link the distal heads of the bones in the metatarsophalangeal joints. There is one metatarsal for each one of the five fingers of the foot. Each finger has three phalanges except the first one (Hallux), which only has two. The metatarsophalangeal joints allow flexion, extension, abduction and adduction of the fingers, but the range of movements is more restricted than those found in the hand. The interphalangeal joints are hinge articulations and allow flexion and extension.

The organization of the foot bones is not arranged in a single plane. Instead, the metatarsals and tarsals bones form the longitudinal arches of the foot. The medial arch consists of the calcaneus, talus, navicular, cuneiforms and medial three metatarsals. The lateral arch consists of the calcaneus, cuboid and lateral two metatarsals. The arches are flexible by nature and supported by muscles and ligaments. They absorb and transmit forces when walking and maintaining upright posture (Whittle, 2007).

2.1.2 - Muscles

The muscles of the gluteal region consist predominantly of extensors, abductors and rotators of the hip joint (see Fig. 2.2). The main hip flexors muscles (iliopsoas – psoas major and iliacus) do not originate in the gluteal region or thigh. Instead, they originate in the posterior abdominal

wall and descend through the space between the inguinal ligament and the pelvis bone to be inserted in the proximal end of the femur (Whittle, 2007).

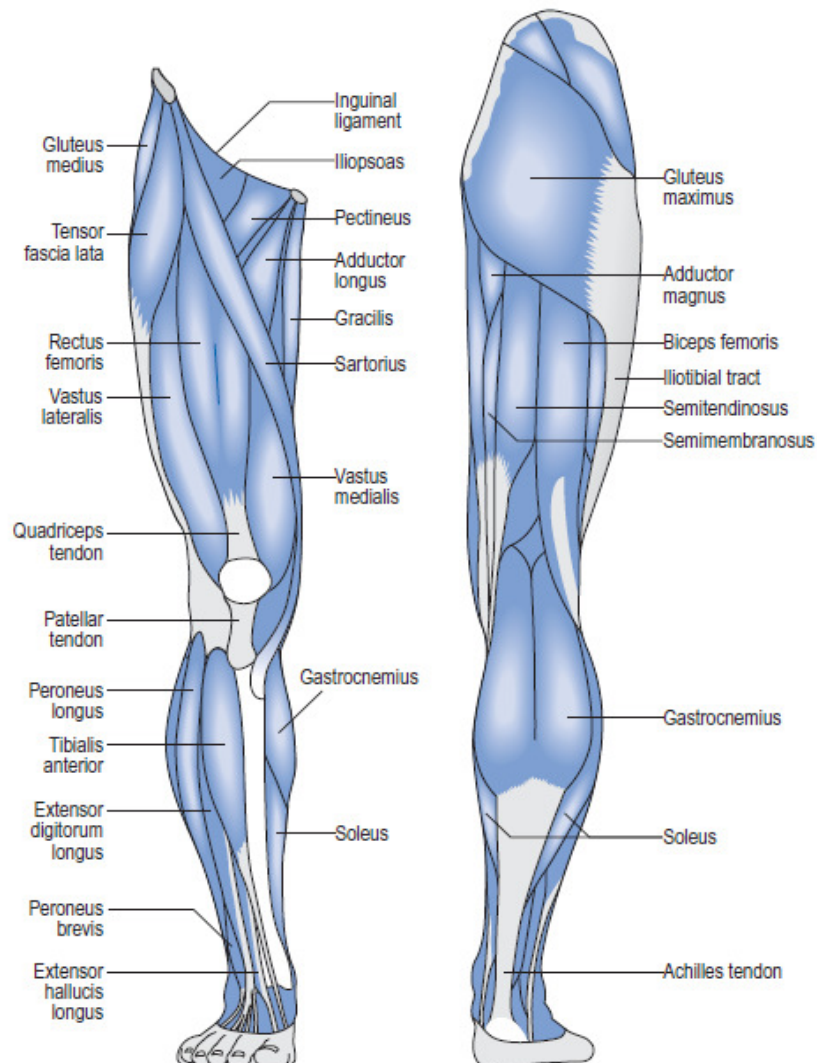


Figure 2.2 - Superficial muscles of the right leg (Whittle, 2007).

The muscles in the thigh and leg are separated into three compartments by layers of fascia, ligaments and bones. In the thigh there are medial (adductor), anterior (extensor) and posterior (flexor) compartments:

- The majority of the muscles in the medial compartment act mainly in the hip joint;
- The muscles (quadriceps femoral) of the anterior compartment mostly extend the knee;
- The large muscles in the posterior compartment act on the hip (extension) and knee (flexion) because they originate in the pelvis and they insert into the bones of the leg.

Leg muscles are divided into lateral, anterior and posterior compartments:

- The muscles of the lateral compartment mostly contribute for the eversion of the foot;

- The muscles of the anterior compartment are responsible for dorsiflexion of the foot and extension of the toes;
- The muscles of the posterior compartment are responsible for the plantar flexion of the foot and the flexion of the toes.

Specific muscles in each one of the three compartments of the leg also enable a dynamic support of the arches of the foot (Hamill and Knutzen, 2009).

2.2 - Gait Analysis

Gait analysis is a branch of biomechanics that studies the locomotion from mechanical point of view. The study includes systematic measurement, description and assessment of quantities representative of the human movement (Racic *et al.*, 2009).

It is important to denote some important definitions of the human motion in the three dimensional (3D) space (see Fig. 2.3). In the anatomical position, the human body can be divided by three reference planes. A sagittal plane is a vertical plane and corresponds to a side view. It divides a body into right and left halves. A coronal plane, also named as frontal plane, is a vertical plane and divides a body into front and back parts. The transverse or axial plane is a horizontal plane cutting through the body at right angles to the sagittal and frontal planes. It divides a body into upper and lower portions.

The six directions of movement relatively to the body centre are described by anterior, posterior, superior, inferior, right and left. Four terms denote the relations within a single part of the body. Medial defines positions towards, whereas lateral defines positions away from the midsagittal plane. Proximal defines closer to torso and distal denotes further away from the torso (Racic *et al.*, 2009).

Generally, the terms walk and gait are used interchangeably. However, *gait* normally refers to the manner or style of walking and *walk* to the process of locomotion (Whittle, 2007). Clarifying, it makes more sense to discuss about differences in gait of two individuals rather than differences in their walking (Racic *et al.*, 2009).

The gait cycle is the period of time between any two identical events in the walking motion. The moment at which one foot hits the ground corresponds to the starting (and completing) event. A gait stride is the distance from initial contact of one foot to the following initial contact of

the same foot. In normal walking, cycles are performed in a continuously and smoothly manner. Also, ground reaction forces (GRFs) are generated against the ground (Moreira, 2009; Racic *et al.*, 2009).

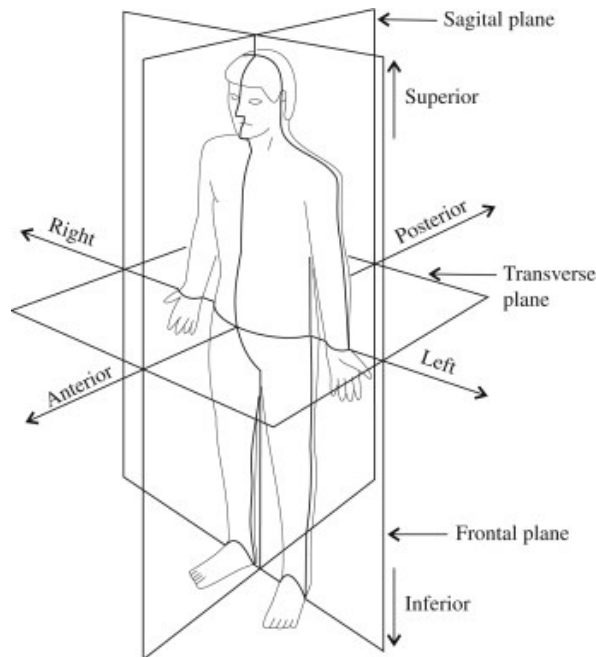


Figure 2.3 - Standardized anatomical position with three reference planes and six fundamental directions (Racic *et al.*, 2009).

The duration of a gait cycle is divided into two periods: stance and swing phase (see Fig. 2.4). The stance phase, also named as support or contact phase, is the time when the foot is on the ground. The swing phase corresponds to the time when the foot is in the air (Racic *et al.*, 2009).

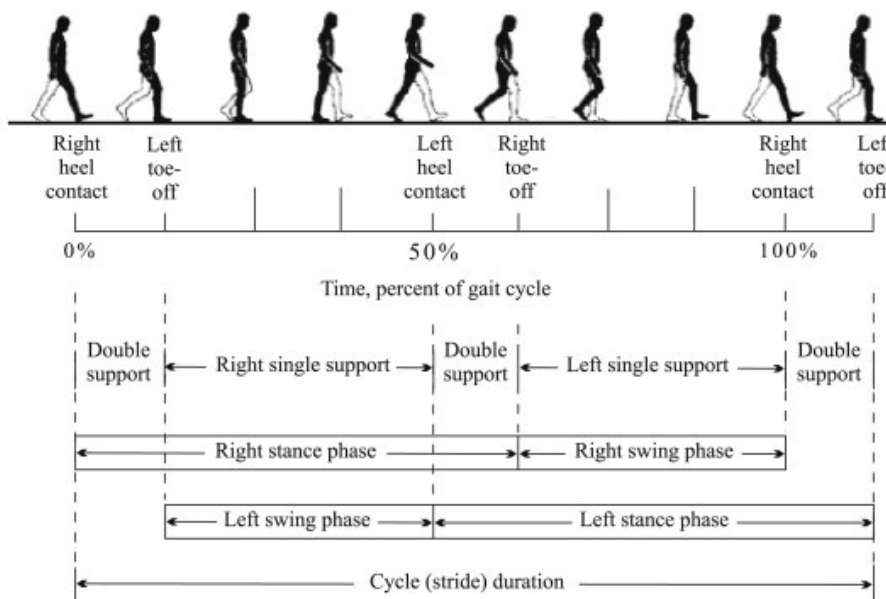


Figure 2.4 - The gait cycle (Racic *et al.*, 2009).

Stance phase is initiated with heel strike (or heel contact) and ends with toe off of the same foot. Swing phase starts at toe off and ends at the next initial contact. The mentioned phases constitute approximately 58 to 61% and 39 to 42% percent of the gait cycle, respectively. Double support is the time in which both feet are in contact with the ground. It occurs at the beginning and the end of stance phase and it represents 16 to 22 % of gait cycle. As velocity increases, double-limb support time decreases. Running is a movement without double-limb support (Winter, 1991).

The stance phase can be further divided into five sub-phases: initial contact, loading response, midstance, terminal stance and preswing:

- 1. Initial Contact** – in this instant the foot of the leading lower limb touches the ground. Normally the initial contact is made by the heel (heel contact);
- 2. Loading Response** – during this phase, the foot contacts totally the floor (foot flat), and body weight is fully transferred to the stance limb. It corresponds to the first 10% of the gait cycle;
- 3. Midstance** – it represents the beginning of the single support. Beginning when the contralateral foot leaves the ground, it continues till the swing-period foot passes the stance-period foot. This phase occurs from the 10 to 30% of gait cycle;
- 4. Terminal Stance** – beginning when the heel lifts the ground (heel off), ends when the contralateral foot contacts the ground, supporting the body weight. This period corresponds to 30 to 50% of the gait cycle;
- 5. Preswing**– it begins when the contralateral foot contacts the ground and ends when the terminal contact is made by the stance limb (toe off).

Likewise, the swing period can be divided into three sub-phases: initial swing, mid-swing and terminal swing:

- 1. Initial Swing** – it initiates with toe off and continues till maximum knee flexion. Corresponds to 60 to 75% of the gait cycle;
- 2. Midswing** – it begins following maximum knee flexion and ends when the tibia is in the vertical position. It corresponds to midstance of the contralateral foot, being the time at which the two feet are side by side. This period corresponds to 75 to 85% of the gait cycle;
- 3. Terminal Swing** – it is the final and deceleration phase, where the tibia passes beyond perpendicular, and the knee fully extends in preparation for heel contact (Perry, 1992; Moreira, 2009).

As shown in Fig. 2.5, three main basic tasks of gait can be distinguished: weight acceptance, single-limb support and limb advancement. Although the preswing is the final stage of the stance phase, it can be also regarded as the preparatory phase for the swing period. Therefore, it is usually considered as an intermediate phase between the stance and swing (Racic *et al.*, 2009).

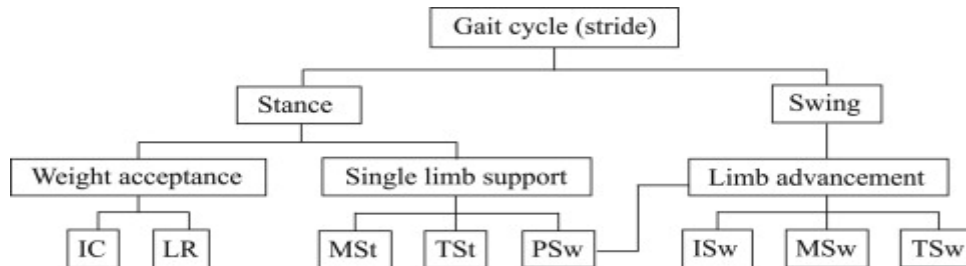


Figure 2.5 - Gait phases and functional tasks: Initial Contact (IC); Loading Response (LR); Midstance (Mst); Terminal Stance (Tst); Preswing (Psw); Initial Swing (Isw), Mid-Swing (Msw); Terminal Swing (Tsw) (Racic *et al.*, 2009).

2.3 - Pathological Mechanisms

In normal walking there is an identifiable normal pattern of walking and a normal range for the measured variables. Those are achieved with no effort, with regular energy consumption and with a complex interaction between the neuromuscular and structural elements of the locomotor system. Abnormal gait may result of an instability of any one of those points (Whittle, 2007).

The pathological conditions cause abnormalities on the mechanism of walking. They can be classified as (Perry, 1992):

- Deformity - When the tissues do not allow enough passive mobility to attain the normal postures and ranges of motion during walking operation. Contracture, abnormal joint contours and ankylosis (bone rigidity) are the most common causes;
- Muscle Weakness—When the patient muscle strength is not enough to walk. Each major muscle group has a postural substitution. Consequently patients with just muscle weakness, reducing the speed, have excellent capacity to substitute and meet the demands of walking, with normal sensation. Causes can be disuse muscular atrophy or neurological impairment;
- Sensory Loss - The subject does not know the position of the body parts and the type of control with the floor. When in greater deficit, the individual cannot use his motor control because he cannot command the motions that occur;
- Pain - The physiological reactions to pain are deformity and muscular weakness. If the abnormal gait results only from the pain, the individual is physically capable of walking normally

but feels comfortable in walking differently (Whittle, 2007). The main causes are the excessive tissue tension, joint distension related to trauma or arthritis;

- Impaired Motor Control (Spasticity) - Muscle selective control and the capacity to substitute are diminished, and consequently timing, muscle intensity and gate phasing are decontrolled. Spastic paralysis results from a central neurological lesion, located in the brain or in the spinal cord. Cerebral palsy, stroke, brain injury, incomplete spinal cord injury and multiple sclerosis are the most common causes of spastic gait.

CHAPTER 3 - CATRASYS

An overview of CaTraSys operation and its components will be presented. The calibration procedure as well as the trilateration and forces computations are extensively explained towards a better understanding of the data acquisition process. The clinical significance of CaTraSys is also reviewed.

3.1 - System Description

CaTraSys, shown in Fig. 3.1a, was conceived at Laboratory of Robotics and Mechatronics (LARM), University of Cassino and South Latium in 1993. Since then it has been continuously evolving in operation and design and it has been used in different applications (Ceccarelli, 2012).

As shown in Fig. 3.1b, CaTraSys is composed of a mechanical part, an electronics/informatics interface unit and a software package. The mechanical part consists of a fixed base and it is named as Trilateral Sensing Platform (TSP). It is basically composed of 6 position sensors T_i ($i=1\dots6$) and 6 force sensors C_i ($i=1\dots6$). The moving platform is the end-effector for CaTraSys and allows the tracking of the movement while it moves. The two platforms are connected by the cables, which in the case of the present work are 6 cables. The electronics/informatics unit is constituted by the 6 amplifiers A_i ($i=1\dots6$), the data acquisition (DAQ) board and the power supply. The software package is the Laboratory Virtual Instrument Engineering Workbench (LabVIEW, 2010). The personal computer (PC) allows the monitoring of the system performance (Ottaviano, 2007).

CaTraSys is classified as a parallel manipulator for the kinematic point of view and as for the operation, it is based on the trilateration technique. It can be modeled as 6 degrees of freedom (DOF) parallel manipulator because cables can be considered as extensible legs connecting the platform and base by means of spherical and universal joints, respectively (Ottaviano et al., 2010). It is a passive cable system and measures large displacements. The system identifies the

6 DOF of a body in the space (Tavolieri et al., 2006), being capable to give 3D pose (position and orientation) and force information (Ceccarelli et al., 1999).

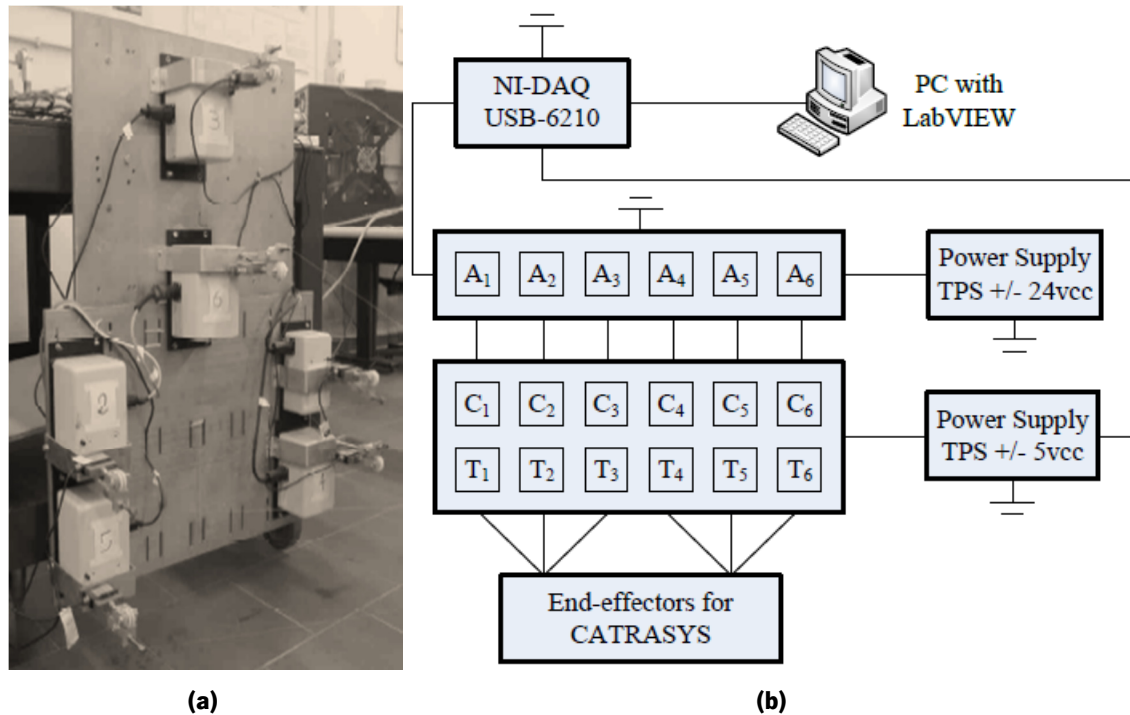


Figure 3.1 - CaTraSys: (a) prototype; (b) scheme (Li and Ceccarelli, 2011).

The present system has been successfully used for the determination of robot workspace and kinematic parameters and more recently performs experimental human tests, determining pose and forces exerted by the tested limb, arm or leg (Ceccarelli *et al.*, 1999; Ottaviano *et al.*, 2001; Ceccarelli, 2010; Ottaviano *et al.*, 2010).

The main objective of CaTraSys is to combine the low-cost, the easy-operability and the mechanical robustness features. It is considered a low-cost system with respect to other available commercial measuring systems such as, for example, video cameras. This is possible because CaTraSys only uses Commercial Off-The-Shelf (COTS) mechanical components, which makes it a low cost system (Ceccarelli *et al.*, 1999). The easy (and fast) operation of CaTraSys is due to the simple method of trilateration, explained below, responsible of determining pose of the moving platform.

Besides the above features, other ones can be pointed out. It is a system of simple calibration. It works in real-time which, for gait monitoring tests is of major importance, since it allows the supervisor (and subject, if desired) to evaluate the test results in real-time (Ceccarelli *et al.*, 2000; Ottaviano and Grande, 2012).

CaTraSys is also very adaptable to different working schemes. The parallel architecture of

the CaTraSys moving platform can be used in diverse configurations, i.e., different number of end-effectors and different number of wires at each attachment. The term 3-2-1, a technical term from Robotics, indicates 3 end-effector points with 3, 2 and 1 cables attached (Ceccarelli, 2011). As for the human tests, 3-2-1 configurations are not possible since the arm or leg are not rigid links, but instead composed of two bodies. Some of the possible configurations are the 3-3 scheme, the one used in the present study (see Fig. 3.1b), or only 1 module of 3 cables attached to a determined point. The last was used by Ottaviano *et al.* (2010). Moreover, the position of the position sensors in the fixed platform can be changed, it can be used along with other measurement instruments and different rigid multibody systems (MBS) can be easily attached to CaTraSys. As an example, CaTraSys attached to PUMA robot is shown in Fig. 3.2 (Tavolieri *et al.*, 2006). Also, movements can be performed in different planes (Ottaviano *et al.*, 2010).



Figure 3.2 - Lay-out of PUMA robot applied to CaTraSys (Ceccarelli *et al.*, 2007).

CaTraSys measurement errors, noise and accuracy have been investigated by Ottaviano *et al.* (2002). Conclusions indicated an average value of accuracy of 1mm for point displacements in a range between 1 and 2m (Ottaviano *et al.*, 2010). The uncertainty band for an acquired measure can be due to calibration errors, devices measuring errors, stiffness of the mechanical components and the robot attached (if it is the case), wire interferences and singular configurations (Ceccarelli *et al.*, 2000; Tavolieri *et al.*, 2006). CaTraSys trilateration technique does not take into account the uncertainties in the measurements. Nevertheless, there are techniques and strategies that can improve the data results (Grandón *et al.*, 2007), such as the hybrid system proposed by Tavolieri *et al.* (2006).

Ottaviano and Grande (2012) compared the results of the motion captured system VICON

(*Motion Capture Systems*) with CaTraSys results for the same subject (see Fig. 3.3). Approximate results were found, which confirms the feasibility of the proposed system. Different self-selected speeds of the two tests can be one of the causes of some of the encountered differences.

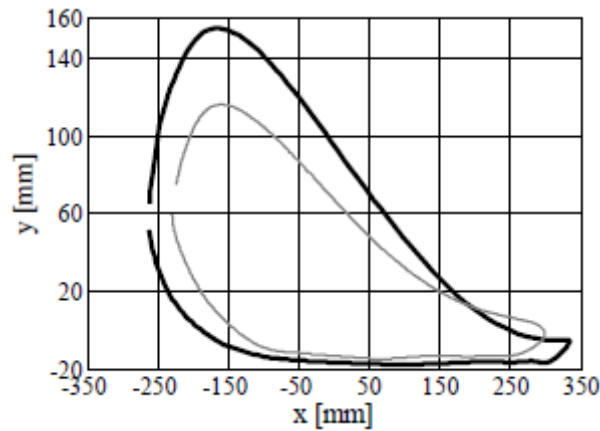


Figure 3.3 - VICON (black line) and CaTraSys (grey line) results for the ankle trajectory (Ottaviano and Grande, 2012).

The application of CaTraSys for human walking characterization began very recently, precisely in 2008. Palmucci et al. (2008) presented the first work. The trajectory and the force exerted by the human limb extremity on the human walking operation were presented. Kinematic parameters for femur and tibia were also determined. Ottaviano et al. (2009) studied the human walking taking into account different trial conditions. It was concluded the human gait is highly influenced by different anthropometric factors. Li and Ceccarelli (2011) presented an overview of the CaTraSys outputs, including trajectory, velocity, acceleration, forces, and shank orientation.

3.2 - Components

A brief appointment will be done for each one of the main components of CaTraSys.

▪ Fixed Platform

The metal large support on which it is directly fixed the position sensors. It has 68 x 91.5cm of size, in order to obtain a compact system (see Fig. 3.1a).

▪ Digital Generator of VDC

The position and force sensors are connected to the power supply ± 5 volts of direct current (VDC). The power supply ± 24 VDC is connected to the amplifiers and to the DAQ board.

▪ DAQ Board

National Instruments (NI) Universal Serial Bus (USB)-6210 DAQ board (NI, 1994) (see Appendix A.1 (National Instruments Corporation, 2009))

A NI multifunction DAQ board (also called device or card) is used (see Fig. 3.4). Considering the work case of analog input, the main characteristics to be considered are:

- 8 differential or 16 single ended channels, with 16 bits of resolution and a maximum sample rate of 250 kS/s;
- 4 digital inputs and 4 digital outputs; two 32-bit counters;
- maximum input voltage of ± 10.4 V.



Figure 3.4 - NI USB-6210 DAQ board used in CaTraSys (National Instruments Corporation, 2009).

▪ Cable-Extension Position Transducers

6 PT-101 position sensors (Celesco Transducer Products Inc., 1994) (see Appendix A.2 (Celesco Transducer Products Inc., 2012))

The position sensors used are of potentiometric type (Ceccarelli *et al.*, 2000). The range covered by the sensor is 2540 mm. Also called string pots, they are rigidly fixed on the fixed base with such an arrangement designed to achieve a small size and also to allow a correct placement of the wires without folding, wrapping or damaging (Ceccarelli *et al.*, 2000).

The hardware inside the plastic corresponding box (see Fig. 3.5a), which is fixed to the metal support, is basically the potentiometer and the spiral spring (see Fig. 3.5b) aligned on the same axis. The cable is attached to the spiral spring in order to maintain its tension, and is conducted, from the pulley housing, to the outside of the plastic box. From here (see Fig. 3.6), it goes first to the lowest positioned pulley, then to the next highest positioned pulley. The final part of the cable is composed by the end-effector structure.

▪ Tension (Compression) Load Cells

6 SA 15 kg load cells (LAUMAS Elettronica S.r.l., 2008) (see Appendix A.3 (S.r.l., 2010))

The selected force cells can bear a maximum weight of 15 kg. COTS force sensors (see Fig. 3.7) are used since their small geometrical dimensions do not justify the need of miniaturized ones. They are used in order to monitor the tension applied to pull the cable and, along with the position sensors, allow CaTraSys to obtain both pose and force information (Ottaviano *et al.*, 2010; Ceccarelli, 2012).



Figure 3.5 - Position transducer: (a) inside view of the plastic protective box; (b) spiral spring.

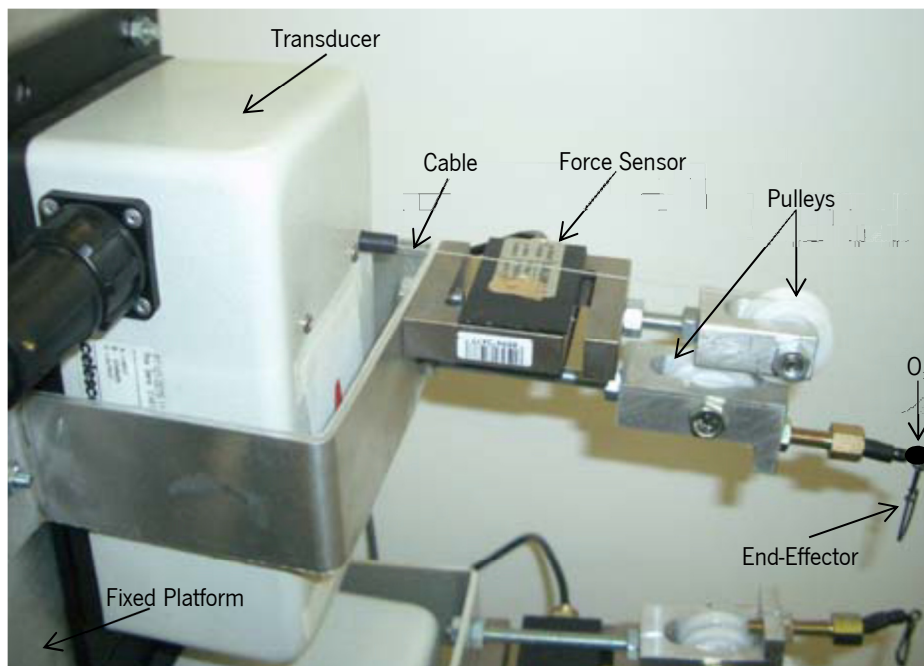


Figure 3.6 - Setup of the transducer, along with the two pulleys and the force sensor.

▪ Analog Weight Transmitters

6 JOLLYTPS ± 5 VDC amplifiers (LAUMAS Elettronica S.r.l., 1994) (see Appendix A.4 (LAUMAS Elettronica S.r.l., 2011))

The signal from the position and force sensors is connected to the amplifiers. 6 amplifiers are used to provide signal amplification (see Fig. 3.8). The amplifiers are connected to the DAQ board (see Fig. 3.1b) (Ceccarelli, 2012).

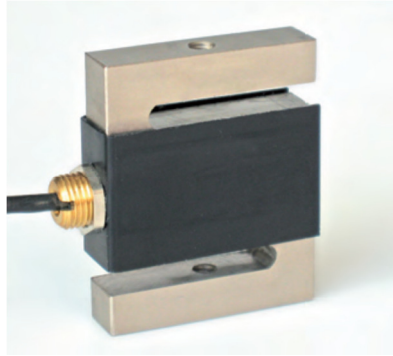


Figure 3.7 - CaTraSys load cell (S.r.l., 2010).



Figure 3.8 - The 6 amplifiers together with the DAQ board.

- Pulleys

- 12 pulleys

The installation in Fig. 3.6, two pulleys attached to each one of the force sensors, maintains the tension of the cables (along with the spiral springs). This is the adopted strategy to reduce the inertial effects, which are due to the cables only. The pulleys have been placed in order to obtain a compact system where the cables can move in a fairly large scope. The adopted scheme avoids the risk of cable folding, wrapping or damaging (Ottaviano *et al.*, 2010).

- Cables

- 6 cables

For the present experimental study, 6 steel wire cables are used in a 3-3 configuration (see Fig. 3.9a). They connect the fixed platform to the end-effectors, allowing so the system to track the movement.

In CaTraSys, the tension of the cables is required to keep them in tension. This tension has a range limit since the cables need a minimum value to avoid cables to become slack, and a maximum value to minimize elastic and inelastic effects (Ottaviano *et al.*, 2010).

▪ End-effectors

2 Velcro® custom straps

For the present experimental study, the end-effectors were tightly strapped to the legs around the two measurement points: medium line of the knee and ankle (as close as possible). The proper positioning at the location of interest is ensured through Velcro straps, which are soft, flexible and adaptable to any subject (see Fig. 3.9b). On the other hand, they can lead to some inaccuracy in the measurements, since the location of the point of attachment is difficult to duplicate from test to test. Also in the same test, some movement of the straps can occur, although the straps are tightly attached. The movement is more likely to occur in the ankle, once the strap in this point is not so easy to fix as in the knee. Ceccarelli and Romdhane (2009) and Ceccarelli and Romdhane (2010) outlined some potential solutions to the end-effector. For example, Ceccarelli and Romdhane (2010) proposed a specific application for the human leg.

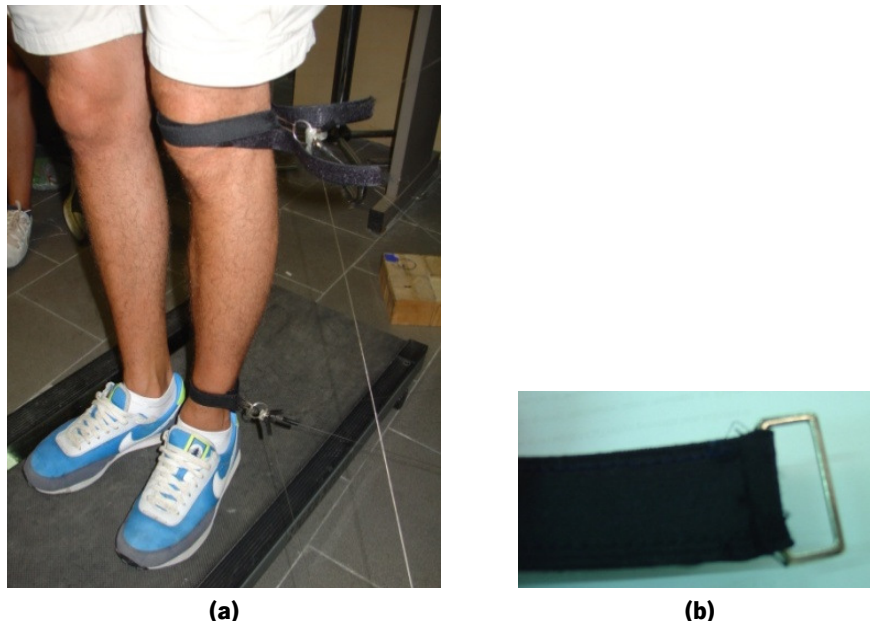


Figure 3.9 - CaTraSys end-effector: (a) attached to the knee and ankle in 3-3 configuration; (b) zoomed view.

The previous presentation of the system components allows the understanding of CaTraSys as a low-cost system, since it is totally composed of COTS components.

3.3 - Data Acquisition

The software package used to do the data acquisition and analysis is the LabVIEW. It allows real-time data acquisition, processing, visualization and recording. The real-time visualization is very important for a gait tracking system since the supervisor (and the tested person, if it is wanted) can monitor in real-time the test progression.

The DAQ device is plugged to the PC through the communication ports. Very briefly, in LabVIEW the block diagram comprises the graphical code. The front panel is the user interface. The CaTraSys block diagram (see Appendix B.1) uses the DAQ assistant to collect and calibrate the input data. Using wires, 12 icons collect the length and force data (correspondent to the 6 position sensors and 6 force sensors). The formula node does the trilateration math and forces computation, of which results the knee and ankle point trajectory (6 positions) as well as its force (6 forces) components that are plotted through express VI. The corresponding front panel (see Appendix B.2) displays the 6 length and 6 force plots, as well as the knee and ankle point trajectory components, and knee and ankle forces, all against time. The last set of plots shows force components against each other.

When the test is started, the VI calls the DAQ assistant. The DAQ assistant passes the settings to the DAQ board and receives the data. The analog to digital converter (A/D) in the DAQ device converts its input voltage to a digital number, an integer of 16 bits (sample). The DAQ assistant can convert that integer to mm or N, through the calibration settings previously introduced.

Figure 3.10 shows the settings of the DAQ assistant:

- Sample Rate - 2 kHz;
- Samples to Read- 50;
- Sampling Rate - 40 Hz (2000/50).

Each time the DAQ assistant is called, it samples at 2000 samples per second (1 sample is acquired each 0.5ms). So, for the DAQ assistant to carry out one read, i.e., to *take* 50 samples, 25ms (50 x 0.5) are waited. In 1s, 40 readings are done.

Each reading is a Dynamic Data Type (DDT) which has a waveform with 50 data points. The dynamic data is converted to a single scalar value. It means that only one data point per channel (or per waveform) is recorded, in each reading. So in 1s, 40 readings of 1 point are done, i.e., 40 points are taken.

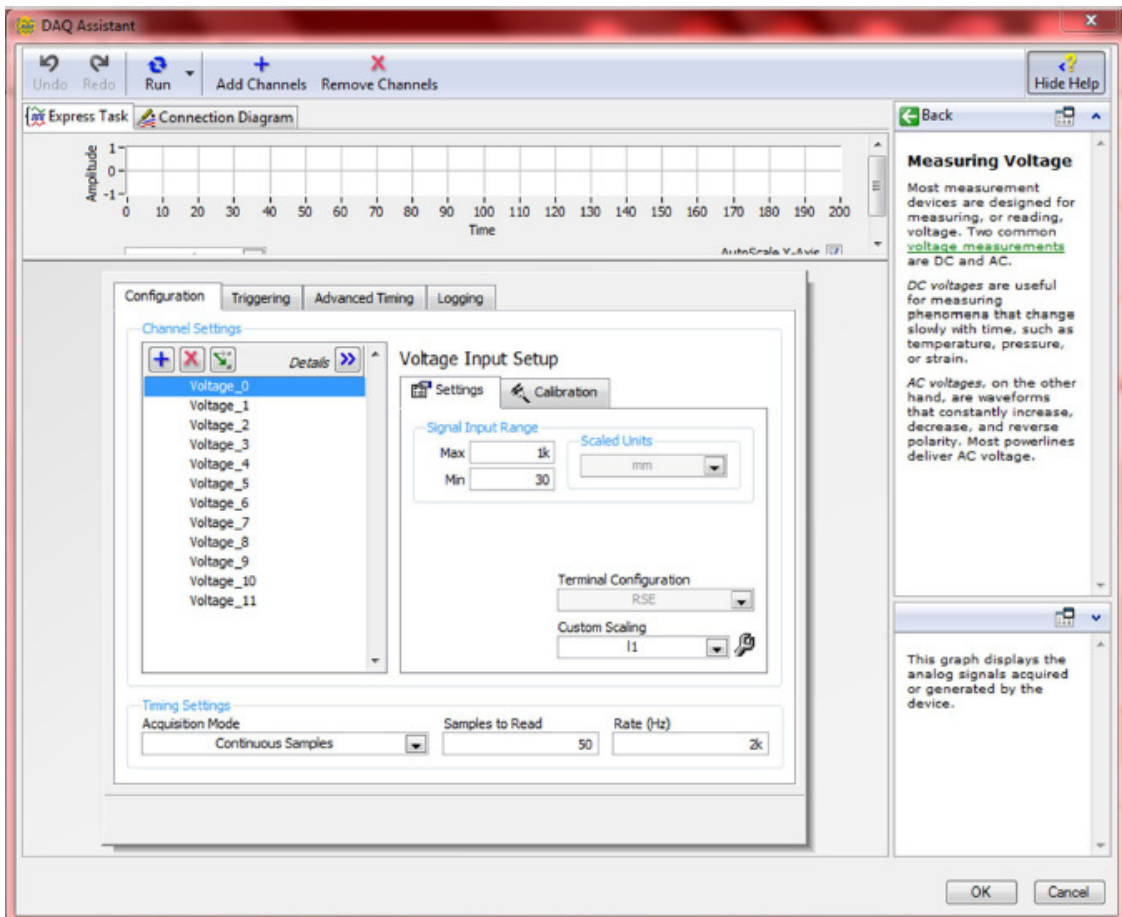


Figure 3.10 - DAQ assistant configuration panel for transducer 1.

3.3.1 - Calibration

In one reading, 50 samples are sent to each channel. In 1s, 40 points are taken to each channel. Besides sampling, the DAQ assistant is responsible for the calibration of the input voltage, i.e., it is responsible to convert the V to the desired units. As the VI has 12 channels, the DAQ assistant converts 12 types of values from V to mm and N. Respectively, they are the 6 lengths from the 6 position sensors and the 6 forces from the 6 force sensors

It will be presented the calibration protocol of the cable 1 length. Opened the NI Measurement & Automation Explorer (MAX) (see Fig. 3.11), it is selected CaTraSys NI board (NI USB-6210 "Dev1") and then the Test Panels setting (in order to see the voltage plot). Here, the channel is chosen (Dev1/a1 to Dev1/a6 for the position sensor 1 to 6), on continuous mode and for Reference Single Ended (RSE) input configuration. The next step is to pull the cable to the desired length (see Fig. 3.12) and take the corresponding voltage in the MAX. With a tape measure, the lengths tested goes from the 30 mm, the initial position when the wire is not

pulled, i.e., when it is totally wrapped, to the 1000 mm, the (almost) maximum length of the wire. Four points are taken for each wire.

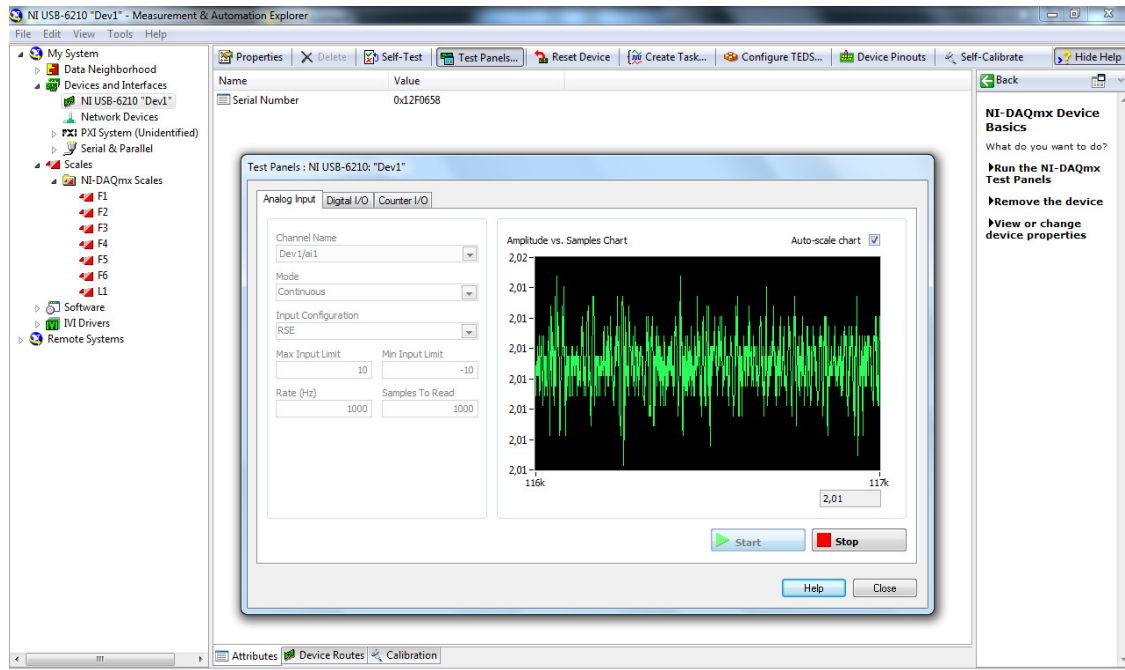


Figure 3.11 - NI MAX settings for position sensor 1.

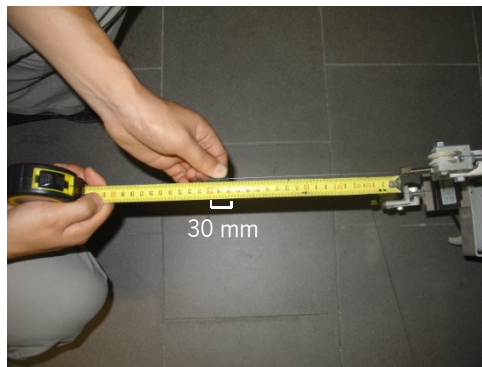


Figure 3.12 - Tape measurement procedure for cable 1.

From the LabVIEW block diagram, it is possible to be directed to the DAQ assistant, where the configuration of the sensors voltage is done (see Fig. 3.10). For the present case, Voltage_0 is selected (Voltage_0 to Voltage_5 refers to the length data). In the custom scaling, if <No Scale> was selected, the output position values in the datasheet would be in voltage. Created the custom scaling L1 (L1 to L6 are the length data custom scales created previously), it is necessary to choose the type of scale to use in the measurement. It was used the table scale type since the length behavior is almost linear, but not completely. The measured points are inserted. The minimum and maximum lengths are also inserted in the signal input range setting.

In what refers to the calibrations of the force results, the procedure is similar, but with some other peculiarities. In the NI MAX, Dev1/a7 to Dev1/a12, corresponding to the load cells 7 to 12, shall be chosen. The force exerted in the pulled cable is measured by an electronic scale device, and it is correspondent to 0.14 kgf in the case of Fig. 3.13. Two points are measured. In the DAQ assistant, custom scaling from F1 to F6 are used. The linear scale type is selected due to the linear relation between the length of the cable and the voltage. The scaling parameters, slope and intercept are then introduced and result from the two previously measured points for each cable. The force corresponding to the initial position, where the wire is not pulled, was not considered as a point since it was consider critical to measure the force at this point.



Figure 3.13 - Electronic scale device measuring the force exerted on the cable.

Summarizing, with DAQ assistant properly calibrated, LabVIEW is capable of acquire the data from the NI-DAQ board in V and convert it to mm and N (length and force, respectively).

Calibration of the system does not need to be repeated each time the system is used. It must be performed when some component of the system is changed and periodically (Ottaviano and Grande, 2012). In the first case scenario and exemplifying, if the cause is only the breaking of one cable, only the position and force sensors correspondent to that cable need to be calibrated. The low sensitivity to the external parameters (e.g.: humidity) may be due to the robustness of CaTraSys. During the procedure, nothing apart from the system length and force should be changed. The desired environmental conditions of the device are specified by the product supplier information.

The 6 cables length and 6 force data is connected to a formula node, in which the trilateration math is computed. So the input of the formula node is the length and force of the 6 cables. The output of the formula node is the three components of the ankle and knee position, and the three components of the ankle and knee force. This totalizes 12 parameters of input and 12 parameters of output, stored in a file (DATA.xls) (see Annex B.2).

3.3.2 - Trilateration

In the VI formula node, the trilateration technique is used to compute knee and ankle positions from the 6 calibrated lengths.

Several systems for position measurement, such as cameras, theodolites, laser tracking systems and wire systems use triangulation or trilateration techniques. These techniques use the geometry of triangles to determine the relative position between points. Whereas triangulation uses measurements of both length and angles, trilateration uses only distances measurements (Ceccarelli *et al.*, 2000). Moreover, these methods of obtaining pose by means of geometric and measured information are also called of computation of direct kinematics. The geometric information is obtained through the design of the robot and the measured information by built-in sensors (Grandón *et al.*, 2007). CaTraSys determines the pose of the end-effector by using the second mentioned technique, trilateration.

Fig. 3.14a and 3.14b represent the 3-3 configuration and trilateration scheme for CaTraSys. H and F stands for the knee and ankle points. Cables 1, 2 and 3 are attached to the knee (H) and cables 4, 5 and 6 are attached to the ankle (F). O_1, O_2 and O_3 are the coordinates of the base points of H cables and d_1, d_2 and d_3 represent the distance between H and O_1, O_2 and O_3 . The distances d_1, d_2 and d_3 can be seen as radii of spheres, whose intersection constitute point H and whose center points is the known O_1, O_2 and O_3 , respectively. This is the basis of the 3D trilateration (Ceccarelli *et al.*, 2000). To determine the relative position of one point (one end-effector) it is necessary at least 3 cables connected to the point at the same time. Using the known locations of three points, together with the distances measured by the position sensors, it is possible to access to the coordinates of the end-effector.

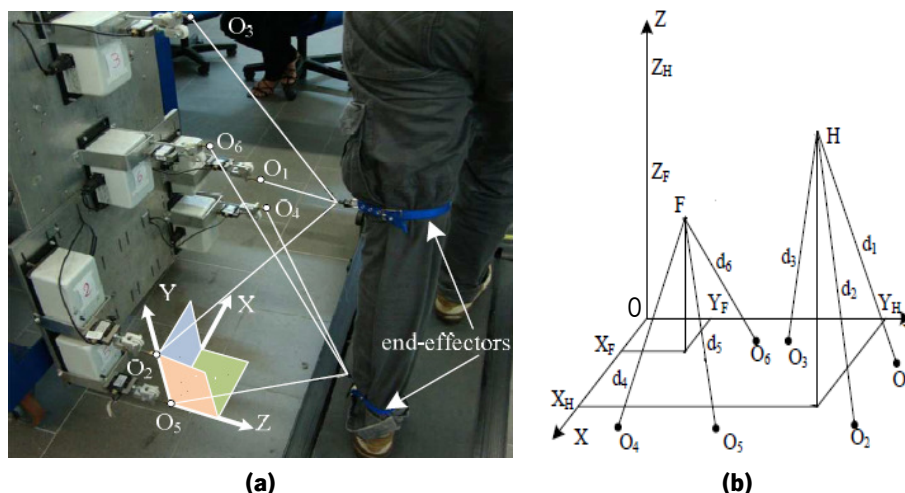


Figure 3.14 - CaTraSys 3-3 configuration: (a) treadmill walking test; (b) trilateration scheme (adapted from (Li and Ceccarelli, 2011)).

The algebraic manipulation involved in the trilateration computations will be referred for point H and follow the notation of Fig. 3.14a. H coordinates are given in Equation (3.1),

$$H = (x, y, z) \quad (3.1)$$

O_1, O_2 and O_3 are stated in Equations (3.2), (3.3) and (3.4) respectively,

$$O_1 = (x_1, y_1, z_1) \quad (3.2)$$

$$O_2 = (x_2, y_2, z_2) \quad (3.3)$$

$$O_3 = (x_3, y_3, z_3) \quad (3.4)$$

Then, trilateration equations are formulated like in Equations (3.5), (3.6) and (3.7)

$$d_1^2 = (x - x_1)^2 + (y - y_1)^2 + (z - z_1)^2 \quad (3.5)$$

$$d_2^2 = (x - x_2)^2 + (y - y_2)^2 + (z - z_2)^2 \quad (3.6)$$

$$d_3^2 = (x - x_3)^2 + (y - y_3)^2 + (z - z_3)^2 \quad (3.7)$$

The development of Equations (3.5), (3.6) and (3.7) leads to Equations (3.8) and (3.9),

$$d_1^2 - d_2^2 = (x - x_1)^2 - (x - x_2)^2 + (y - y_1)^2 - (y - y_2)^2 + (z - z_1)^2 - (z - z_2)^2 \quad (3.8)$$

$$d_2^2 - d_3^2 = (x - x_2)^2 - (x - x_3)^2 + (y - y_2)^2 - (y - y_3)^2 + (z - z_2)^2 - (z - z_3)^2 \quad (3.9)$$

Continuing to develop Equation (3.8), Equation (3.10) is found,

$$x = \frac{d_1^2 - d_2^2 + x_2^2 - x_1^2 + y_2^2 - y_1^2 + z_2^2 - z_1^2 - 2y(y_2 - y_1) - 2z(z_2 - z_1)}{2(x_2 - x_1)} \quad (3.10)$$

Inserting Equations (3.11), (3.12), (3.13) and (3.14),

$$A_i = d_i^2 - x_i^2 - y_i^2 - z_i^2 \quad (3.11)$$

$$X_{ij} = 2(x_i - x_j) \quad (3.12)$$

$$Y_{ij} = 2(y_i - y_j) \quad (3.13)$$

$$Z_{ij} = 2(z_i - z_j) \quad (3.14)$$

in Equation (3.10), it is obtained Equation (3.15),

$$x = \frac{A_1 - A_2 - Y_{21}y - Z_{21}z}{X_{21}} \quad (3.15)$$

Developing Equation (3.9), the expression in Equation (3.16) is obtained,

$$A_3 - A_2 + X_{32}x + Y_{32}y - Z_{32}z = 0 \quad (3.16)$$

Placing Equations (3.10) and (3.16) in the same expression, it is found the y coordinate of H point by Equation (3.17),

$$y = H_y z + E_y \quad (3.17)$$

where H_y and E_y are defined in Equations (3.18) and (3.19),

$$H_y = \frac{X_{32}Z_{21} - X_{21}Z_{32}}{X_{21}Y_{32} - X_{32}Y_{21}} \quad (3.18)$$

$$E_y = \frac{-A_1X_{32} + A_2(X_{21} + X_{32}) - A_3X_{21}}{X_{21}Y_{32} - X_{32}Y_{21}} \quad (3.19)$$

In Equation (3.15), by replacing y by Equation (3.17), the expression which states the x coordinate of H point is found by Equation (3.20),

$$x = H_x z + E_x \quad (3.20)$$

where H_x and E_x are formulated in Equations (3.21) and (3.22),

$$H_x = \frac{-Y_{21}H_y - Z_{21}}{X_{21}} \quad (3.21)$$

$$E_x = \frac{A_1 - A_2 - Y_{21}E_y}{X_{21}} \quad (3.22)$$

Developing Equation (3.9), it can be obtained Equation (3.23) (*quadratic equation*),

$$[H_x^2 + H_y^2 + 1]z^2 + [2H_x(E_x - x_3) + 2H_y(E_y - y_3) - 2z_3]z + [E_x^2 + E_y^2 - A_3 - 2E_x x_3 - 2E_y y_3] = 0 \quad (3.23)$$

Replacing Equations (3.24), (3.25) and (3.26),

$$B_1 = H_x^2 + H_y^2 + 1 \quad (3.24)$$

$$B_2 = 2H_x(E_x - x_3) + 2H_y(E_y - y_3) - 2z_3 \quad (3.25)$$

$$B_3 = E_x^2 + E_y^2 - A_3 - 2E_x x_3 - 2E_y y_3 \quad (3.26)$$

in Equation (3.23), the z coordinate of H point is found by Equation (3.27),

$$z = \frac{-B_2 - \sqrt{B_2^2 - 4B_1B_3}}{2B_1} \quad (3.27)$$

The sign ambiguity in Equation (3.27) was experimentally studied and it was confirmed the use of the minus sign.

Summarizing, if at a determined time, the distances d_1, d_2 and d_3 are known and having the coordinates of O_1, O_2 and O_3 (correspondent to the base points of H wires) defined, it is possible to solve the system of equations composed by Equations (3.8) and (3.9), which mainly represent the trilateration technique. The previously approach can be applied to the ankle end-effector module (F), using the distances d_4, d_5 and d_6 and the coordinates of O_4, O_5 and O_6 . And so, at the end, it is determined the trajectory of the desired point. Trilateration technique

allows so CaTraSys to track the knee and ankle point, while the end-effectors move during the experimental test.

Many configurations of the end-effector can be used. In the case of the 3-2-1 configuration, 3 cables connected to the point at the same time would determine the first point. For the second point, it is just needed 2 cables to be connected to the second since the third cable can be considered the distance between the second point and the first point already known (Ceccarelli, 2012). Once the coordinates of both the first and the second points are known, for computing the coordinates of the third point, it is only necessary one cable. As previously explained, this trilateration scheme cannot be used for human experimental tests.

An alternative to the trilateration technique is the use of the Cayley-Menger determinants (Tavolieri *et al.*, 2006). This method will not be explored in the present study.

3.3.3 - Forces Computation

The formula node of the VI, besides the trilateration math, includes the formulation to find the force exerted by the knee and ankle point, from the initial 6 forces of the cables.

Ottaviano *et al.* (2010) stated that in passive cable-based manipulators, the force of the end-effector is a consequence of the cables tensions, which can be determined as stated in Equation (3.28),

$$F_i(i) = s_0(i) + s(i)l(i) \quad (3.28)$$

where $s(i)$ (for base point $i=1, \dots, \theta$) is the relationship between the i th cable tension and the cable length $l(i)$; and $s_0(i)$ depends on the spring preloading.

Results of experimental studies verified that $F_i(i)$ is not a constant value but it depends on the length of the cables $l(i)$. They also showed the best model is a linear relationship with $s_0(i)$ and $s(i)$ kept as constant values (Ottaviano *et al.*, 2010).

Figure 3.15 pretends to better explain the algorithm used in the present work to determine the force exerted by the end-effector and its components. For the example case, F_4 represents the force applied by the ankle point (F) from the base point O_4 and it is the force measured by the force sensors. Its components are F_{4x} , F_{4y} and F_{4z} . x_F , y_F and z_F are the length components of point F . F_{4r} is the projection of F_4 in the horizontal plane and h is the corresponding length. The first angle to be identified is β , formulated in Equation (3.29),

$$\beta = \tan^{-1} \frac{x_F}{z_F} \quad (3.29)$$

h is determined in Equation (3.30),

$$h = \frac{x_F}{\sin \beta} \quad (3.30)$$

α is expressed in Equation (3.31),

$$\alpha = \tan^{-1} \frac{y_F}{h} \quad (3.31)$$

$F_{F'}$ is expressed in Equation (3.32),

$$F_{4'} = F_4 \cos \alpha \quad (3.32)$$

F_{4x} , the horizontal component of F_4 , is expressed in Equation (3.33),

$$F_{4x} = F_{4'} \sin \beta \quad (3.33)$$

F_{4y} , the vertical component of F_4 , is determined in Equation (3.34),

$$F_{4y} = F_4 \sin \alpha \quad (3.34)$$

F_{4z} , the medio-lateral component of F_4 , can be computed in Equation (3.35),

$$F_{4z} = F_{4'} \cos \beta \quad (3.35)$$

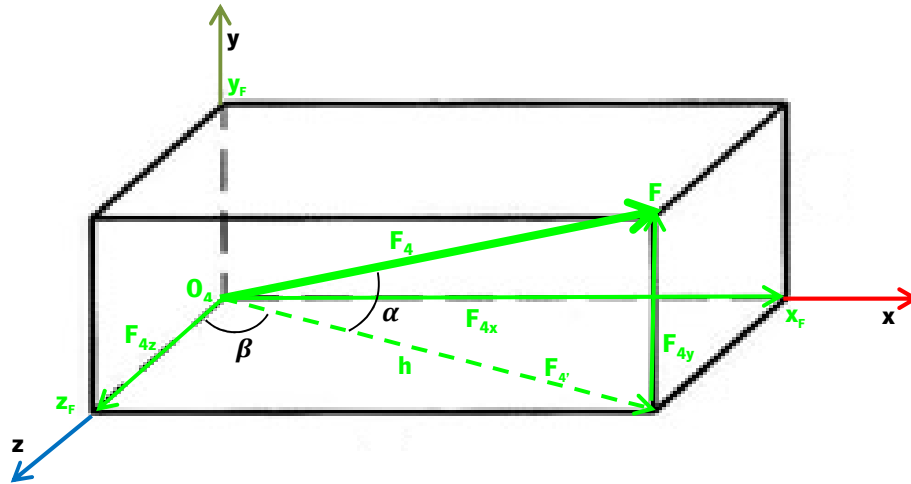


Figure 3.15 - Scheme for the forces computation.

It is of major importance to get the components of F_4 . With those components and the remaining it is possible to find F_H and F_F , force exerted in the knee and ankle point, respectively. Continuing with the example of the ankle end-effector, F_F components are given in Equation (3.36), (3.37) and (3.38),

$$F_{Fx} = F_{4x} + F_{5x} + F_{6x} \quad (3.36)$$

$$F_{Fy} = F_{4y} + F_{5y} + F_{6y} \quad (3.37)$$

$$F_{Fz} = F_{4z} + F_{5z} + F_{6z} \quad (3.38)$$

F_F is found through the vector module, using the Pythagorean theorem, and it is represented in Equation (3.39),

$$F_F = \sqrt{F_{F_x}^2 + F_{F_y}^2 + F_{F_z}^2} \quad (3.39)$$

Adapting this formulation to the knee point F_H , it is possible to obtain the force exerted by the two end-effectors, during the experimental test.

3.4 - Clinical Significance

CaTraSys allows continuous motion capture and various analysis results to be displayed in real-time: trajectory and force exerted by the monitored point. It is a passive device and different robotic schemes can be applied. The system is easy to work with, due to the simple hardware architecture and to the very intuitive interface. After suitable data processing, other type of motion pattern results can be obtained and objective gait spatio-temporal parameters can be found.

Having been proved the essential equivalence of treadmill and overground gait, clinicians are allowed to fairly use treadmill-based protocols (Riley *et al.*, 2007). Besides other applications like evaluating robot characteristics (Ceccarelli *et al.*, 1999), CaTraSys is suitable for medical applications as an assessing device, to record information (Ottaviano *et al.*, 2010). The existence of reference data would make CaTraSys results easy to be analyzed by not specialized entities.

CaTraSys output can give useful information to the clinicians about the individual limb performance. The motion measurements can be archived and then compared in order to assess quantitatively the level of motor recovery or could be compared with suitable reference values of healthy gait patterns (Ottaviano *et al.*, 2010; Nunes *et al.*, 2011). This can be helpful in cases of diagnosis procedures, to evaluate the extent of which the gait pattern has been affected, to plan treatment protocol or surgical prescription and intervention for the disorder.

The system can also constitute an advantage in the field of rehabilitation therapy. In rehabilitation of human limbs, the benefit of repeated movements had already been proved (Nunes *et al.*, 2011). In cases of treadmill walking therapies (eventually along with other devices), CaTraSys would allow the recording of the patient limb performance. Over the last decade,

robotic systems for rehabilitation of lower limb have been developed. However, CaTraSys as a passive device cannot be classified as a treadmill gait trainer (Díaz *et al.*, 2011).

Iida and Yamamuro (1987) studied patients before and after joint replacement and verified the 3D curves of body centre of mass were distorted before the clinical procedure, but tended to normalize after it. This example can be taken as a proof of the clinical capability of CaTraSys.

CHAPTER 4 - METHODOLOGY

In order to run the experimental study a protocol, approved by the University of Cassino and South Latium, was followed. All the trial variables were defined with the aim of being the most suitable for a gait experimental investigation.

4.1 - Experimental Setup

The measurement scenario of the experimental study (see Fig. 4.1) may be described for:

- The Environment - All experiments were conducted at the LARM, located at the University of Cassino and South Latium. Good control of light, noise, temperature and humidity was provided.
- The Walkway - The use of a treadmill as the walkway in an experimental gait study allows the assessment of a large number of consecutive walking cycles, easily and quickly for both the supervisor and the subject. A non-motorized treadmill (*Ercolano*, Italy) with a 1500mm long × 500mm wide conveyor belt, 190kg of mass and an angle of inclination of 7.3° was used. The treadmill was positioned parallel to CaTraSys, in a precise position verified and corrected at each trial. It was activated by the subject himself and so the velocity was not enforced, which encourage active involvement of the individual and allow him to control their stepping performance. As the treadmill belt provides little resistance to motion, subjects needed to hold onto the handlebars located on both sides of the treadmill during the test.

4.2 - Experimental Modes

One of the objectives of the present work was the study of the human gait under several testing conditions. To this purpose, the subject anthropometric features gender, age, weight, and height were evaluated along with four diverse test settings. The first gait assessment task was recorded with the subject walking at a self-selected velocity (estimated for 5 km/h), the *reference test* (see Fig. 4.1a). In the *loading test*, a backpack weighing 6 kg was used. The subject was

tested carrying the backpack on his shoulders, well centered on the back (see Fig. 4.1b). In the next trial condition, volunteer stepped out of the treadmill, changed his shoes and performed the *footwear test* (see Fig. 4.1c). The last two tests were also performed at the self-selected velocity. At last, the participant was asked to increase its step velocity without running, the *fast test* (estimated for 8 km/h) (see Fig. 4.1d). It was defined the fast test to be the last, so that the self-selected velocity was not perturbed. A sequence of a loading test on a male subject is shown in Fig. 4.2.

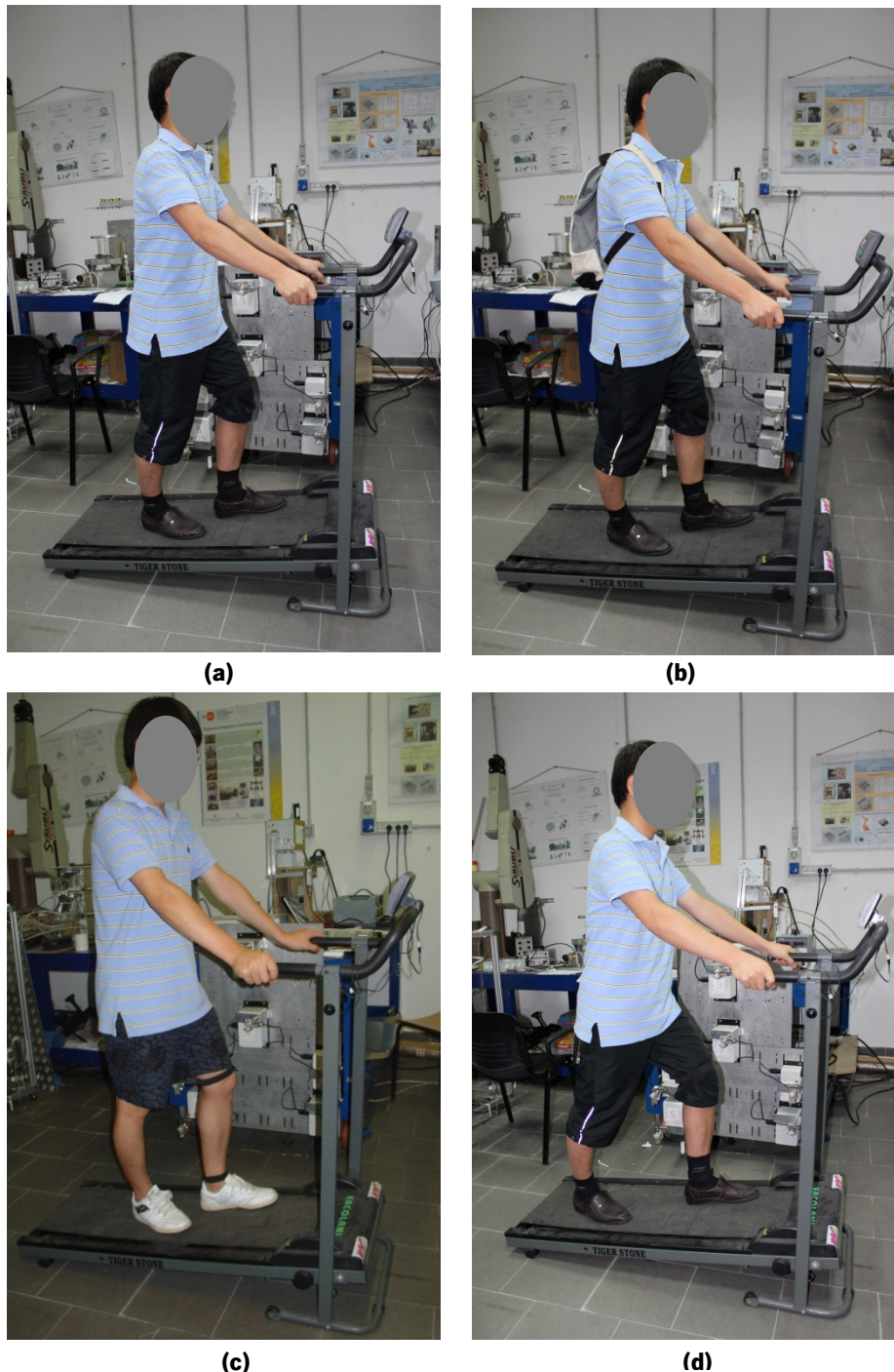


Figure 4.1 - Experimental tests conditions: (a) reference test; (b) loading test; (c) footwear test; (d) fast test.

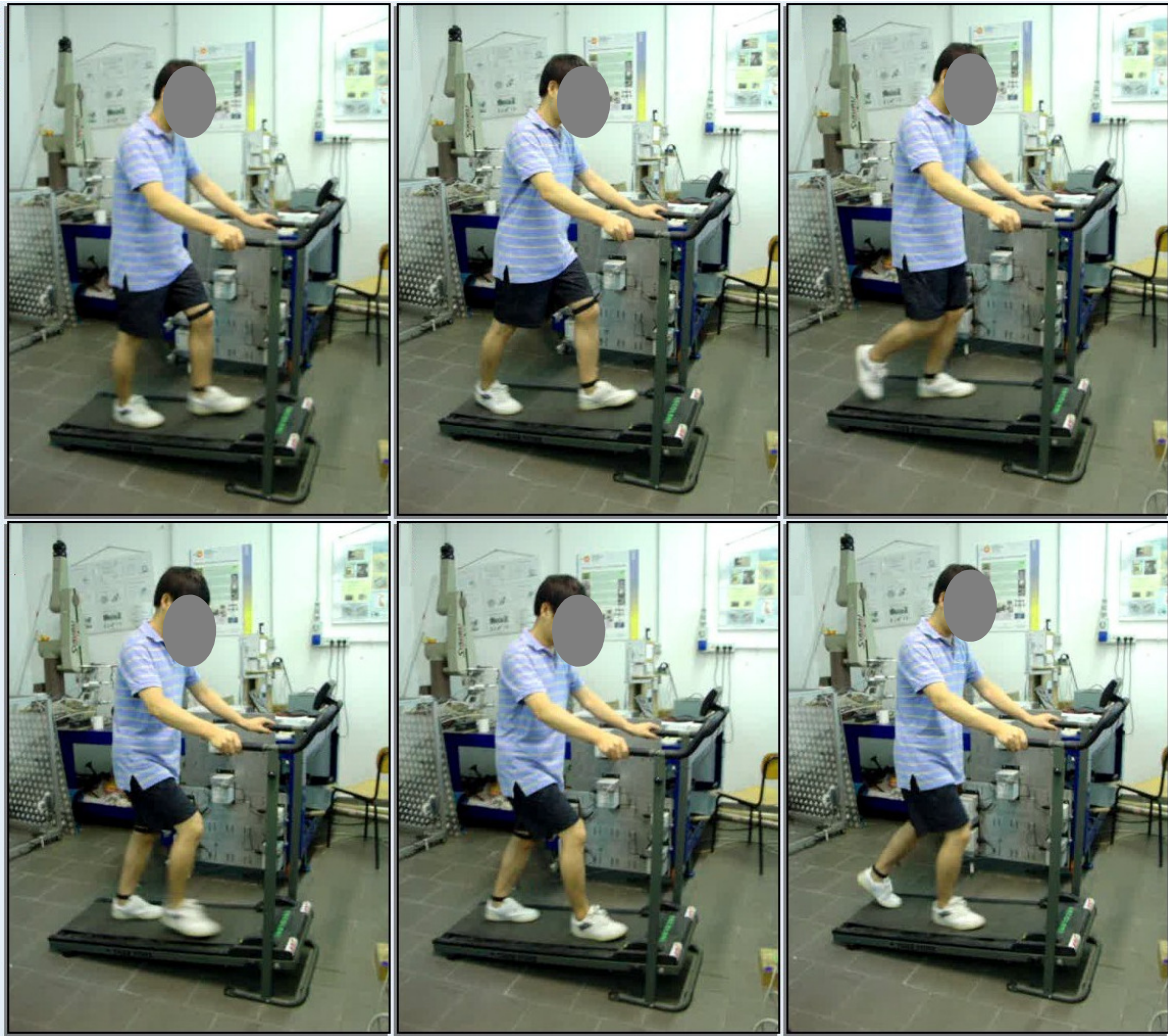


Figure 4.2 - Experimental footwear test for a male subject.

To standardize the dressing protocol, it was defined participants to wear shorts and, as an in-shoe assessment, light casual shoes, i.e., not sportive, high heel, or open toes shoes (see Fig. 4.3a). In the footwear test a particular type of shoes was required. Men were required to wear sport shoes type (see Fig. 4.3b) and women used a specific high heel shoes with 74 cm of heel (see Fig. 4.3c).



(a)



(b)



(c)

Figure 4.3- The different footwear types used in the experimental tests: (a) casual shoes; (b) sport shoes; (c) high heel shoes.

4.3 - Subjects

Prior to the testing, the studied population was asked to fill in a *Form for CaTraSys Experimental Test on Human Walking Characterization* (see Appendix C).

The questionnaire was composed of a first part to the supervisor and a second one to the participant responsibility. The first one, the *Operator Section*, was destined to the supervisor notes: identification of the test, number of validates tests and duration of the validated test. A pre- and after-comment was also required. As for the *Subject Section*, nationality identification and anthropometrical information, including gender, age, height and weight, was asked. The target range of age pretended was between the 20 and 30 years old. Health conditions needed also to be pointed out. It is not objective of the work to study the pathological gait. Hence, subjects were not included if they reported any health disorder. Information about the personal sport activity was also asked. An after-comment to the experimental test was required at the final of the accomplished session. The form was also composed of a private subdivision where namely subject provided his name, contact information, signature and test session date, as a representation of the provided written informed consent (to be filled in prior to the session).

Information of the subjects is provided in Table 4.1. Eight subjects (5 male and 3 female) from the University community volunteered to enroll in the study. The participants age ranged between 20 and 28 years (mean= 24.8 ± 3.6 years); height between 1.55 and 1.80 m (mean= $1,683\pm 0.077$ m); weight between 56 and 82 kg (mean= 62.3 ± 9.6 kg) and shoe size between 36 and 43 (mean= 39.6 ± 2.5).

4.4 - Data Collection Protocol

For all test conditions, forward walking motion was performed in the sagittal plane. Data of the left hand side of the subject was recorded. To this end, the subject was properly equipped with two straps, the CaTraSys end-effectors, banded to the knee and ankle in a 3-3 configuration (see Fig. 3.14).

Considering the intra- and inter-variability of the gait, i.e., the trajectory does not remain constant but varies at each stride in the same individual and between individuals, averaged

curves were defined as a good reflect of the individual ones. To get reproducible averages, i.e., stable and reliable averages, it was determined to acquire 10 cycles per each test (DeVita and Bates, 1988). Considering the methodological problem, Macellari and Giacomozzi (1996) indicated data averaged over 12 steps have an adequate standard deviation (SD) and the increasing of this number improves only slightly the SD. Besides this definition, the number of cycles (and so, the amount of data) acquired per test can always be different since it is impossible to completely control the parameter in a CaTraSys walking test.

Table 4.1 - Subjects anthropometric characteristics, sport activity frequencies and respective comments.

Subject	Nationality	Gender (M/F)	Age (Years)	Weight (kg)	Height (m)	Shoe Size	Sport Activity (Times/Week)	Comments
1	Chinese	M	28	61	1.68	41	No	No
2	Chinese	M	28	65	1.68	39	No	No
3	Romanian	M	28	58	1.75	41	No	Discomfort caused by the ankle end-effector
4	Greek	M	21	82	1.80	43	No	No
5	Italian	M	20	65	1.72	42	Basketball (3)	No
6	Chinese	F	28	49	1.55	36	No	No
7	Portuguese	F	23	56	1.63	37	Swimming (2)	No
8	Spanish	F	22	62	1.65	38	No	Difficult on treadmill walk
Mean	-	-	24.8	62.3	1.683	39.6	-	No
(SD)			(3.6)	(9.6)	(0.077)	(2.5)		

Male (M); Female (F)

In order to assess the repeatability of measure, the same test (subject and type) was performed on two separate occasions, mandatorily different days. The strategy was adopted to avoid occasional factors intrinsic to the subject or not, as the case of wrong software definitions.

Before effective evaluation and in order to control the stepping performance, a 5 minutes familiarization period to treadmill locomotion was provided to the participants. The instructions were to walk so that the subject felt comfortable and used to (*“to walk in a consistent manner as possible”*), achieving so a steady state gait in a self-selected speed (exception for the fast test). Besides holding onto the handlebars as mentioned previously, subjects were asked to look straight ahead and avoid looking at their feet. Simultaneously, they were given verbal cues about

the periodicity of their gait and if they were drifting too far forward or back on the treadmill surface.

After this first adaptation period, each test was always preceded by a 3 min rest period (baseline) with the volunteer standing on the treadmill and becoming acquainted with the next locomotor task. After this moment, subjects were requested to start the treadmill walking in a self-selected speed. Simultaneously, the operator was receiving real-time visual feedback of each cable length and force plotted against time, by the LabVIEW output on the PC monitor. By the time five subsequent curves with periodic feature were visible, i.e., once subjects gait were in steady state, the test was started without subject knowledge. From this moment on, 10 consecutive gait cycles data (at least) were acquired and a 20 s trial (average) was captured. The participant was only informed of the stop walking moment after the record was already shot down in LabVIEW. If the initial steady state was not achieved, the test was stopped and started again.

After each test, supervisor needed to check again the viability of the test by confirming the periodicity of the cables length and force against time plots as well as the low dispersion of the knee and ankle trajectory plots (topic explained afterwards). To conclude the test session, subject and operator complete the initial form, namely the after-comment section.

Table 4.2 presents a sum up of the CaTraSys experimental procedure, with corresponding estimation of the time expended with each test. Four different treadmill test settings were performed in a 55 min session (estimation). Each subject participated in 2 sessions of data collection, resulting in a total of 8 tests per subject.

Table 4.2 - Summary of the CaTraSys experimental protocol and estimative of the time spent with the respective task.

Task	Time (min)
1. Fill in of the form by the operator and subject	10
2. Operator indications	5
3. Set-up arrangement	5
4. Subject adaptation period to the treadmill walking	5
5. Subject experimental tests	20
6. Operator verifications of the test results	5
7. Completion of the form after-comments by the operator and subject	5
	Σ 55

CHAPTER 5 - DATA ANALYSIS

During the present chapter, the proposed CaTraSys formulation will be depicted, including the data pre-processing and statistical treatment, the computation of the shank angle, the velocity and acceleration. The software used for the data processing was LabVIEW and MATrix LABoratory® (MATLAB, 2010).

The reference system adopted for CaTraSys is represented in Fig. 3.14a. The planes directions adopted for CaTraSys are the positive X for the posterior-anterior direction, the positive Y for the inferior-superior direction and the positive Z for the medio-lateral direction. In order to do a clear exposition along the text, it was selected a test result to be used as a reference. The test was selected to be the reference type of test performed by the subject most used to CaTraSys experimental tests. Therefore, when along the text, the term *representative test* is pointed out, it is referred to the reference test of subject 1. The Cartesian coordinates are the type of coordinates used for the analysis of CaTraSys results. It must also be referred that all the averages calculations of the formulation constitute arithmetic means.

5.1 - Signal Pre-Processing

The two smoothing techniques most commonly used in biomechanics are curve fitting and digital filtering. They are also used in many commercial quantitative analysis packages (e.g.: the GCVSPL package determines the ideal smoothing parameter for the spline) (Bartlett, 2007; Kutz, 2009).

Curve fitting is generally based on a least squares difference. Piecewise approximation methods are widely used in human gait studies, being cubic and quintic splines the more common used types. Digital filtering was the method used in the present study. It creates a smoother signal, if sampled at an adequate rate. The concept is based on the fact that any

signal, if sampled at an adequate rate can be recreated from a series of sine and cosine waveforms of varying frequency (Kutz, 2009).

Between the different types of digital filters, Butterworth filter was the selected one since it is very probably the most used one in the biomechanics field (periodic data). A low-pass Butterworth filter strongly attenuates frequencies above the cutoff frequency (high-frequency noise), allowing frequencies below the cutoff to pass through the filter unattenuated (the response at lower frequencies is 1) (Winter, 2005; Bartlett, 2007; Kutz, 2009).

Butterworth filters depend on the type and order of the filter, the sampling frequency, the cutoff frequency and, as a recursive filter, they also depend on the past raw and filtered data. The higher the order of the filter, the sharper the filter response, i.e., the more severely the signals above the cutoff frequency are attenuated (Winter, 2005).

A slightly distortion in the output signal is introduced by the filter. It results from a not complete rejection of the frequency noise and a slight attenuation of the signal around the cutoff frequency. The compromise is always between the signal distortion and the unattenuated noise. Therefore, a choice of a too high cutoff frequency may not filter enough noisy data (less distortion). If a very low cutoff frequency is used, too much filtering may occur, and a signal with high distortion and highly smoothed is obtained. In this last case, and in opposition to the first, rapid changes in activity will not be detected (Winter, 2005; Bartlett, 2007; Payton *et al.*, 2008).

Besides this amplitude distortion in a transition region where the frequencies of signal and noise overlap, Butterworth filters introduce a phase distortion (i.e., events will occur at different moments) in the new signal, which can be removed by a second filtering in the reverse direction. The procedure increases the filter order and reduces the cutoff frequency, bringing the filtered signal back in phase with the unfiltered one (Winter, 2005)

From slower to faster events, those with rapid energy transfers (e.g.: impacts), higher cutoff frequencies are required. As human gait movement is at a low frequency, a cutoff frequency of between 4 and 8 Hz is often used. Besides, it must be considered that, in the same test, different components of the data (X , Y and Z) or different tracked points (e.g.: ankle and knee) can require or not the same cutoff frequencies. In fact, no fixed values can be used in the smoothness process in order to get an effective noise removal (Winter, 2005; Bartlett, 2007)

To implement a Butterworth filter, the main decision is the cutoff frequency value. There is a number of methods that can be used to select an appropriate cutoff frequency, removing some

subjectivity in assessing the ideal cutoff frequency. The approach used in the present work was the residual analysis by Winter (2005).

For a signal of N sample points in time, residuals between the raw (X_i) and filtered data (\hat{X}_i) (of a specific cutoff frequency (f_c)) are calculated by Equation (5.1). This residual amplitude corresponds mathematically to the root mean square (rms) error of the difference between raw and filtered data. In the graphic, the residuals calculated for each cutoff frequency are plotted against the corresponding range of cutoff frequencies. The ideal cutoff frequency is reached when the residuals begin to approach an asymptotic value, as detailed explained in the example given hereafter (Winter, 2005; Bartlett, 2007).

$$R(f_c) = \sqrt{\frac{1}{N} \sum_{i=1}^N (X_i - \hat{X}_i)^2} \quad (5.1)$$

For a better understanding of the residuals method, it will be used the sample signal of the ankle vertical trajectory of the representative test (Fig. 5.1a). It was recorded at a frequency of 40 Hz (sampling frequency) and filtered by a Butterworth low-pass filter second-order, used in two rounds of filtering, forward and reverse, yielding so a fourth order filter.

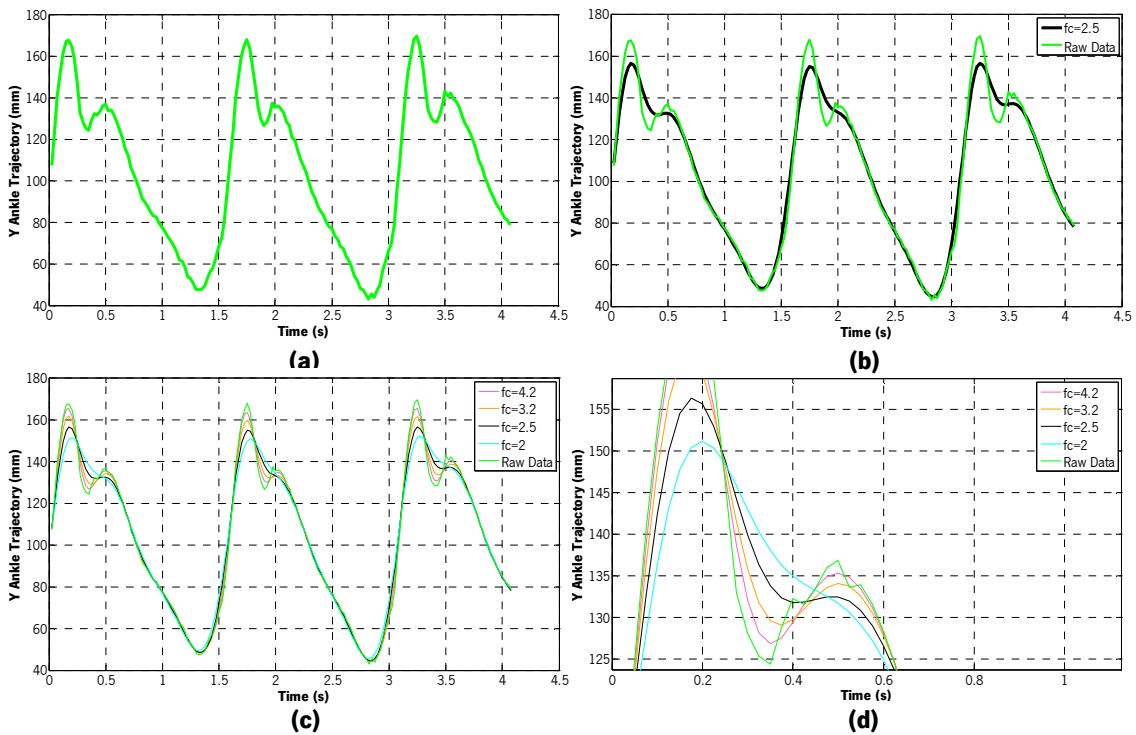


Figure 5.1 - Filtering: (a) raw signal; (b) final signal; (c) application of four cutoff frequencies; (d) zoomed view of (c).

In Fig. 5.2 the residuals are plotted against the corresponding range of cutoff frequencies. The tested frequencies comprehend values between 0 and the Nyquist frequency, i.e., from 0 to $0.5 f_c$ that is 20. In the plot f is the amount of signal distortion and g the noise passed through the filter. Observing the plot, it is also visible the high residual amplitude at lower cutoff frequencies, since at these frequencies the filtered signal would be much more altered than at high frequencies (Winter, 2005).

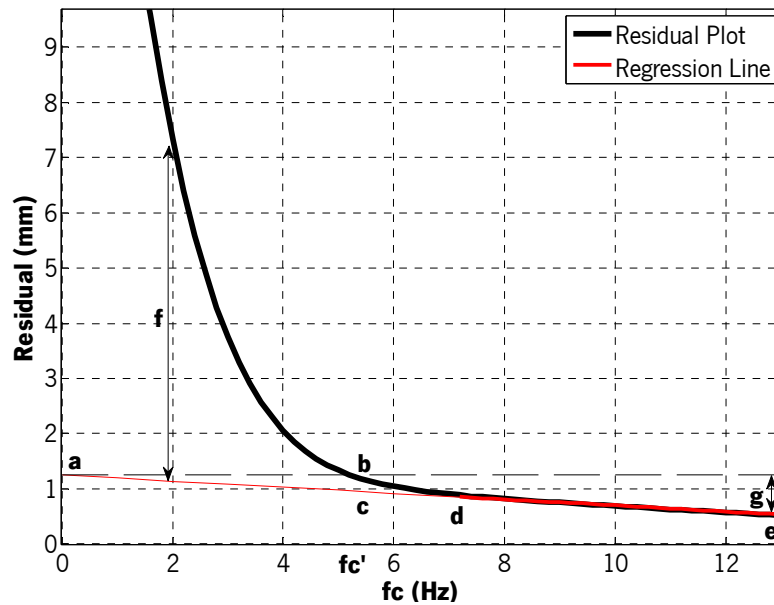


Figure 5.2 - Residual plot for the selection of an optimal cutoff frequency using residual analysis.

The straight regression line $d-e$ represents the noise and was extended to a . If it is decided the amount of signal distortion and noise allowed through are equal it is considered firstly the point a , the y-intercept of the regression line. From this point a horizontal extension is created. Point b is the intersection of this line with the residuals. The vertical line from b finds f_c' , the recommended cutoff frequency (Winter, 2005).

In the present study, in order to find a more accurate way to determine the previous values, the equation of the regression line was determined (see Equation (5.2) and red bold line $d-e$ in Fig. 5.2) taking in account the coefficient of determination R^2 . From it, the value a is found to be 0.8654 (see Equation (5.3)). The next step was to search for the most approximate value of 0.8654 between the residual data. Its corresponding f_c is the desired cutoff frequency (a more accurate method to the approximate value would be an interpolation). For the residual 0.8630 an ideal cutoff frequency of 4.2 was found.

$$y = -0.0406x + 0.8654 \quad (5.2)$$

$$R^2 = 0.9719 \quad (5.3)$$

The attempt to choose the cutoff frequency by the residuals analysis criterion was not completely successful. Instead of a value of 4.2 Hz it was chosen 2.5 Hz, and so a different but yet proximate value of cutoff frequency was used. Observing Fig. 5.1c, and into more detail Fig. 5.1d, the result of the filtering can be seen with four different cutoff frequencies, equal and smaller to the 4.2 Hz. For this raw data, it was verified that from the cutoff 2.5 Hz on, the change in the curve was not significant and so this was the final value adopted for the case study. In Figs. 5.1a and 5.1b it is possible to see the raw data and the smoothed final curve. It can be verified the black line passing through the raw data is a smoothed form of the original signal. No phase lag is observed.

Important considerations will be briefly done about the MATLAB algorithm to obtain the Butterworth filter and residuals. It was used two MATLAB built-in functions. *butter()* designs a Butterworth filter and has as input values the order of the filter and the value of the normalized cutoff frequency. The last is obtained dividing the desired cutoff frequency in Hz by 1/2 of the sampling rate. The other command to be referred is *filtfilt()*. It is used to filter the signal twice (once forwards and once reversed). So, using this command in a Butterworth filter second-order implements a fourth-order filter with zero-phase delay.

The mathematical differentiations when calculating velocity and acceleration magnifies any noise in the original data. The usual way of avoiding this problem is to do the noise removal before calculating other data (e.g. using a low-pass filter on the position data, before differentiation). This procedure is not always satisfactory, especially in gait analysis where transient signals, impacts such as the foot strike, are present (e.g. the high accelerations at the heel strike can be lost). This error is caused by the highly non-linear calculations of the filtering. They can lead to non-linear combinations of random noise, which can affect the split-up of signal and noise by the filter. Bad filtering procedures can lead to wildly erratic or even unusable results. As an example of the first case, it can cause a variation of the distance knee-ankle (Bartlett, 2007).

Bearing in mind these facts, CaTraSys signals were studied and it was verified the pre-treatment need of the positions signal. Besides, velocity and acceleration signals were also filtered after computation, as expected. The causes of the noise in the original signal (raw trajectory signal) could result from the noise of the power supply, the sensibility of the force

sensors, the presence of other electronic devices in the laboratory or even small vibrations of the system.

Different cutoff frequencies were used for different tracked points and component directions. Globally, a range between 2 and 4 was used. The horizontal trajectory was only filtered in two test results. Vertical and medio-lateral trajectory needed filtering, no exceptions were encountered. In what refers to the velocity and acceleration signal, in almost all cases smoothing of the x component was applied.

5.2 - Statistical Treatment

In the most cases, no major differences were found across the results of the two experimental sessions. Since it was used the medium curve for interpretation of the results, to select between the two records, the criterion was to choose the one in which the plot visually showed less dispersion (see Fig. 5.3).

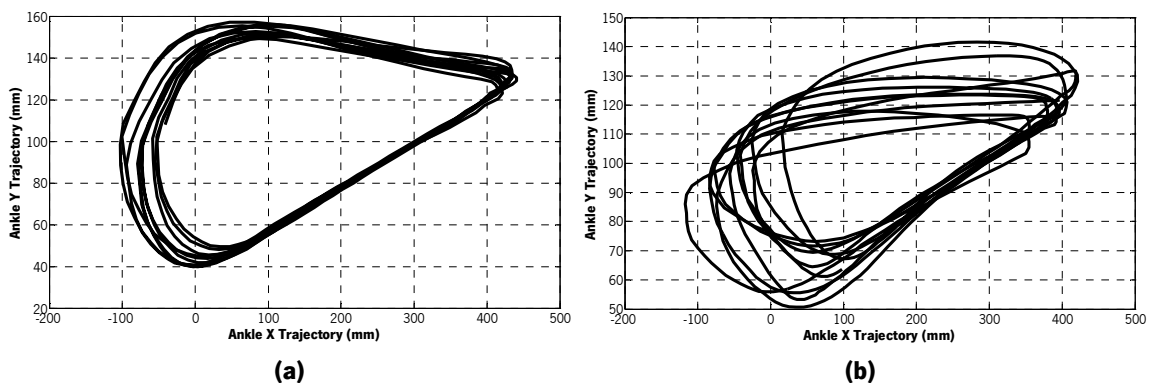


Figure 5.3 - Results of two different sessions (sagittal trajectories): (a) data with less dispersion; (b) rejected data.

With the *best* record, the next step was to find its mean pattern (as justified in chapter 4.4), which means to take the X , Y and Z trajectory of knee and ankle and calculate the corresponding two mean trajectories. The explanation of the formulation will be given for the ankle point.

Figure 5.4a shows the ankle horizontal trajectory of the representative test. Peaks are marked with a black circle and define the beginning of a gait cycle, corresponding so to the heel contact moment.

The algorithm starts so by detecting the peaks on the continuous data sequence. It was verified, even after the pre-treatment of the trajectory signal with the Butterworth filter, the existence of very little glitches at the spikes (see Fig. 5.4b). These local maximums are initially detected by

the algorithm (peak is any highest point between *valleys*, i.e., lower points), and could lead to a mistaken localization of the global maximums, i.e., the beginning of the new gait cycle. The strategy adopted was not to fix the glitches (since they are so small) but instead to skip those by not initiating a new cycle (instead, to continue running) when a peak close to the previous one was found. The first and last peaks were excluded as with in-shoe systems it is common to reject the initial and last cycles (Klika, 2009) (see Fig. 5.4c). The knowledge of the index of these peaks allowed the detection of those indexes in the other directions data. From this step forward, the formulation was run for the three directions at the same time.

After finding the *good* peaks, the algorithm finds the data between each pair of peaks (i.e., cycle by cycle). For averaging purposes, each cycle is normalized to 100 points through spline interpolation. As the cycles have different duration and so different amount of data it is necessary to interpolate before we can average it across the number of cycles (number of peaks minus one). Having 100 points in each cycle, the mean cycle data is calculated (see Fig. 5.4d).

The average cycle data was also time normalized, in order to express it as a percentage of the total gait cycle. 0% corresponds to the left foot initial contact until subsequent foot contact (100%).

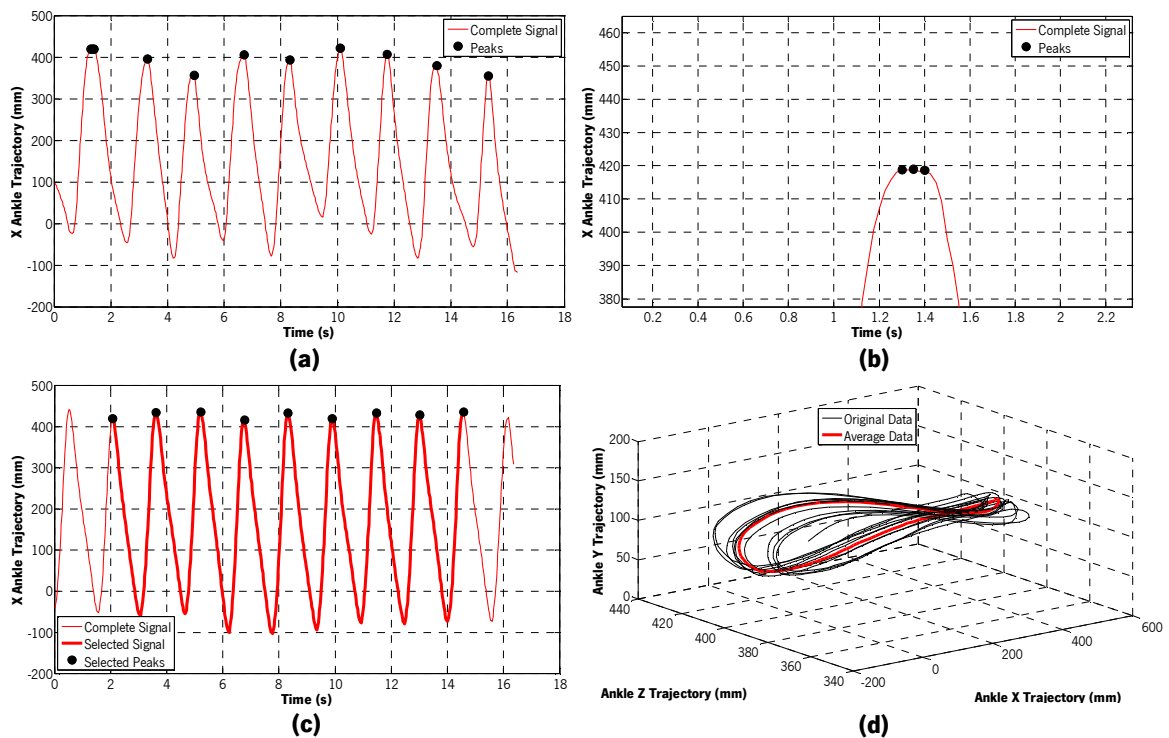


Figure 5.4 - Detection of the heel strike moment in the horizontal trajectory: (a) local and global maximums; (b) zoomed view of (a); (c) global maximums uniquely; (d) original and medium curves.

5.3 - Shank Angle

Taking the coordinates of two points that are in line with the long-bone axis allows calculating the absolute angle of the limb segment in space. For the calculation of the shank angle θ_s (see Fig. 5.5), it was used the position data of knee and ankle (x and y), as showed in Equation (5.4). The angles are positive in a counterclockwise direction in the plane of movement, corresponding the horizontal to 0° (Winter, 2005).

$$\theta_s = \text{tg}^{-1} \frac{y_{knee} - y_{ankle}}{x_{knee} - x_{ankle}} \quad (5.4)$$

As in the experimental tests it was only acquired knee and ankle data, shank angle was the only angle possible to be computed.

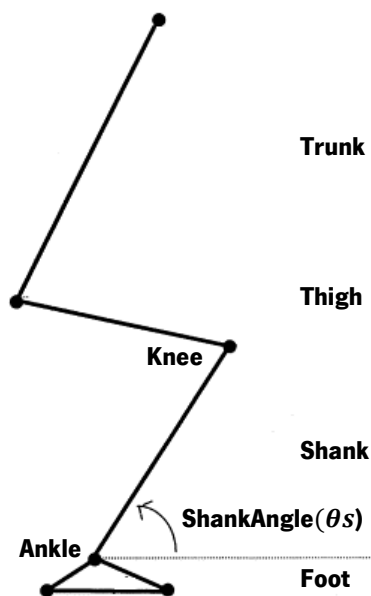


Figure 5.5 - Representation of the shank angle θ_s (adapted from (Winter, 2005))

5.4 - Velocity and Acceleration

To find the velocity and acceleration curve from position data, the finite-difference method was used. As an example, the velocity in the X direction is calculated from $\frac{\Delta x}{2\Delta t}$, where Δx is the difference between x_{i+1} and x_{i-1} and $2\Delta t$ is the time between the samples x_{i+1} and x_{i-1} multiplied per two (Equation 5.5) (Winter, 2005).

$$Vx_i = \frac{x_{i+1} - x_{i-1}}{2\Delta t} \quad (5.5)$$

This velocity is in fact the velocity of a point halfway between the two samples. It is presumed the line joining x_{i-1} to x_{i+1} has the same slope as the tangent to the curve at x_i (see Fig. 5.6) (Winter, 2005).

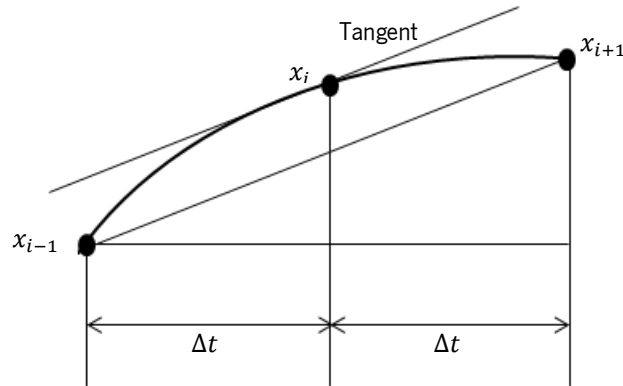


Figure 5.6 - Finite-difference technique (adapted from (Winter, 2005)).

The acceleration calculation is reached likewise, as expressed in Equation (5.6) (Winter, 2005).

$$Ax_i = \frac{Vx_{i+1} - Vx_{i-1}}{2\Delta t} \quad (5.6)$$

As pointed out in chapter 5.1, using the differentiation method to obtain velocity and acceleration from trajectory coordinates results in noisy data. To avoid this problem, accelerometers can be used for the data acquisition (Fig. 5.7). From acceleration data, it is possible likewise to access to spatio-temporal information. For example, the heel contact moment can be detected with the ground reaction force method, the zero-crossing method or the peak detection method (Zijlstra and Hof, 2003).

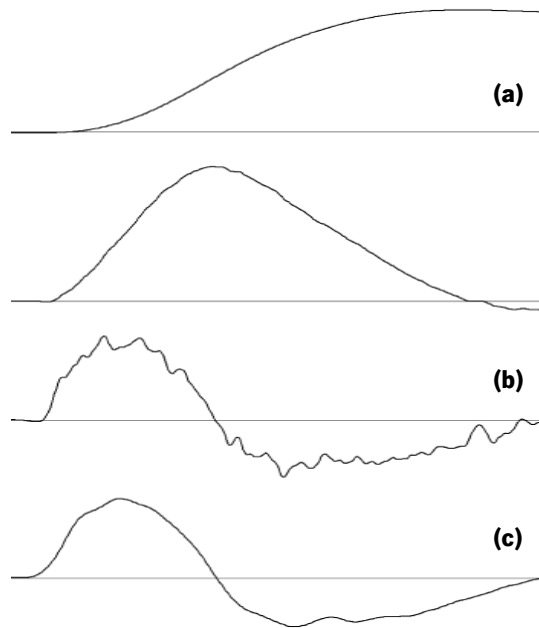


Figure 5.7 - Exemplificative data for acceleration acquisition: a) acquired data position; b) velocity and acceleration profiles derived from position; c) acceleration profile obtained directly from an accelerometer (adapted from (Khan *et al.*, 2006)).

CHAPTER 6 - RESULTS AND DISCUSSION

An analysis to the kinematic and kinetic results will be done for the representative test. In a second part, the results obtained for different test conditions and different anthropometric characteristics of the volunteers will be investigated.

In what refers to the experimental tests procedure, no subjects reported any discomfort, except subject 3 and 8. The complaints were rapidly overcome and did not affect the test results by any means. Interpretations related with sports activity were not possible since mostly the population tested did not practice any sport (see Table 4.1).

6.1 - Curve Analysis

In this subchapter, the analysis is done for the representative test and average cycle plots will be represented, if nothing in contrary is said.

6.1.1 - Linear Kinematics

Trajectory

Through the statistical treatment described in the subchapter 5.2, the average trajectory curve for a CaTraSys walking test was obtained. Figures 6.1 and 6.2 show the 3D average trajectory of the knee and ankle, respectively. For a better explanation, the arrows show the motion direction. The orange and pink arrows depict, respectively, the initial contact (the heel contact moment) and the preswing (the toe-off moment). Likewise, the gait phase between the orange and pink arrow correspond to the stance phase and the rest of the cycle to the swing

phase. The first correspond to the time the foot spends on the treadmill and the second to the moments when the foot is in the air.

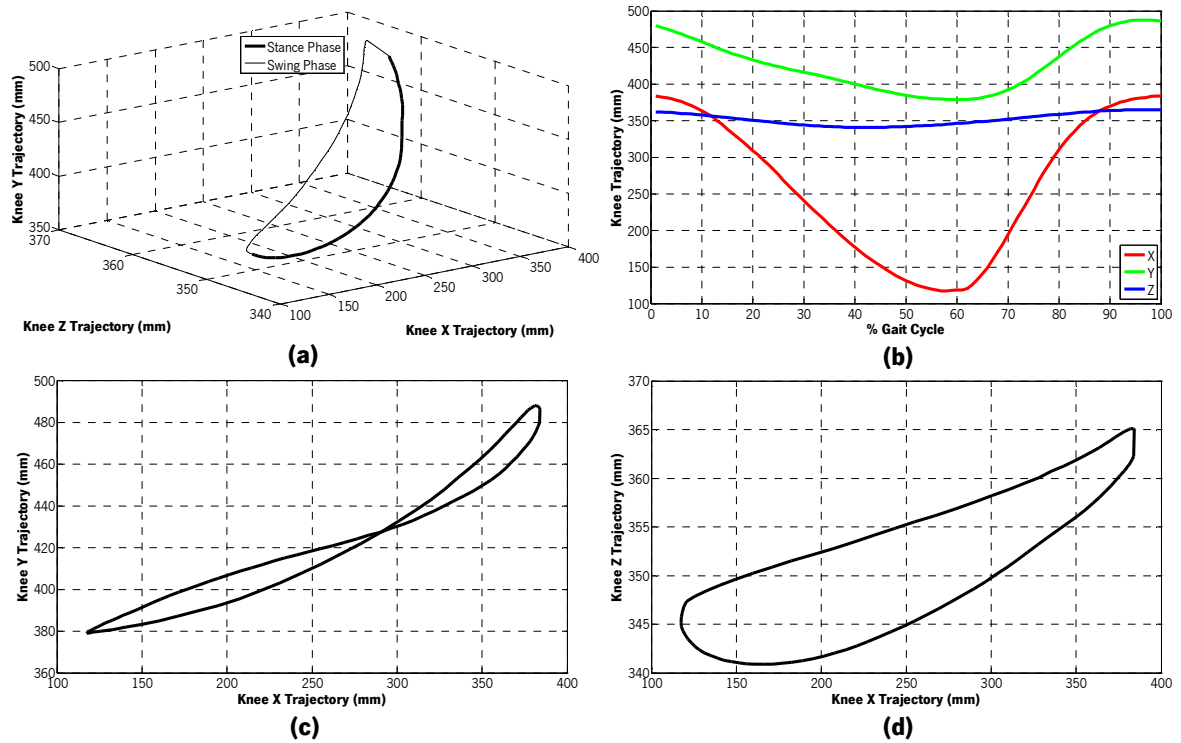


Figure 6.1 - Knee trajectory: (a) 3D; (b) X, Y and Z coordinates; (c) sagittal plane; (d) frontal plane. The arrows depict the movement direction.

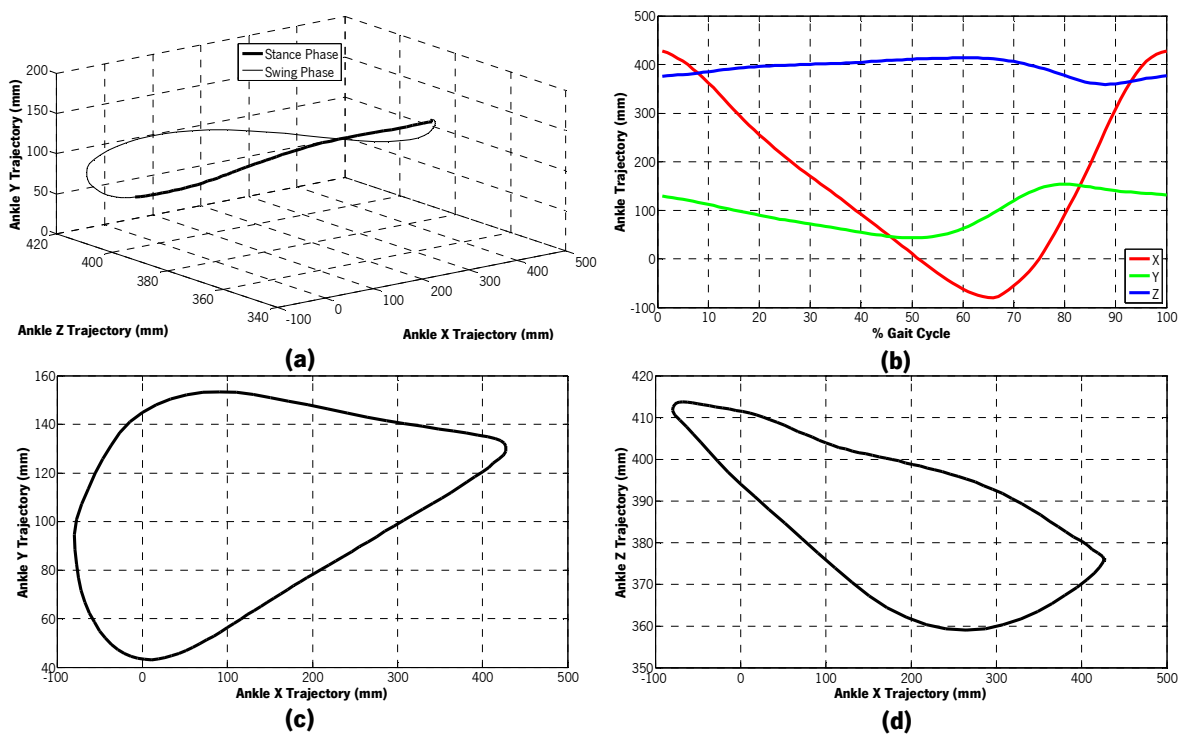


Figure 6.2 - Ankle trajectory: (a) 3D; (b) X, Y and Z coordinates; (c) sagittal plane; (d) frontal plane. The arrows depict the movement direction.

A detailed analysis will be done for the ankle trajectory in Fig. 6.2. The orange, pink and blue arrows show, respectively, the initial contact (the heel contact moment), the preswing (the toe off moment) and the initial swing (maximum knee flexion). Observing simultaneously Fig. 6.1b and 6.1c it can be pointed out that at the beginning of the gait cycle, the foot touches the ground (heel contact) and X and Y positions decrease till the end of stance phase. This corresponds to a back and down movement of the ankle. The slope in the sagittal plane is due to the 7.3° of inclination of the treadmill floor. Then, the heel lifts from the treadmill, the Y positions increase till the initial swing (ankle is being elevated), where maximum knee flexion occurs and so maximum ankle position is observed. At the same time, the X positions in the preswing moment continue to decrease till the ankle starts to move forward in the horizontal direction till the end of swing phase, maximum X position. Ankle Y positions decrease from the initial swing to the terminal swing, the knee is extending till the heel contact moment and X positions start to decrease again. Figure 6.1d represents the Z versus X trajectory. In the stance phase, Z positions increase which means the ankle performs lateral movement. During swing phase the ankle moves in the medial direction (Z positions decrease) and at the end start to increase again. Furthermore, during stance phase Z positions are more constant than in swing phase. This is because in the first the foot is in a more stable position, on the treadmill. The lateral movement is consistent with the optimization strategy of gait, where the individual adjust his centre of gravity (COG) in lateral direction in order to keep balance while walking (Li and Ceccarelli, 2011). Looking at Fig. 6.1, it can be confirmed that the lateral displacement is the minor one. The same type of analysis can be performed for Fig. 6.2.

In fact, observing together the 2D and 3D plots in Figs. 6.1 and 6.2, it can be concluded the specificity of the 3D motion may be overlooked when observing each plane of motion independently. This type of 3D plots can be named as trajectory *cyclogram* and they provide spatial but not temporal information (Tesio et al., 2010).

Figure 6.3a shows the knee and ankle 3D trajectory in the same plot. Observing the planar trajectory of Fig. 6.3b, it can be concluded that the amplitude of the horizontal movement in the ankle is much greater than the one of the knee and the amplitude of the vertical movement is also higher in the ankle, although not so different from the one of the knee. As for the lateral motion amplitude represented in Fig. 6.3c, it is much greater in the knee point than in the ankle. Logically, the minor displacement occurs for the lateral trajectory.

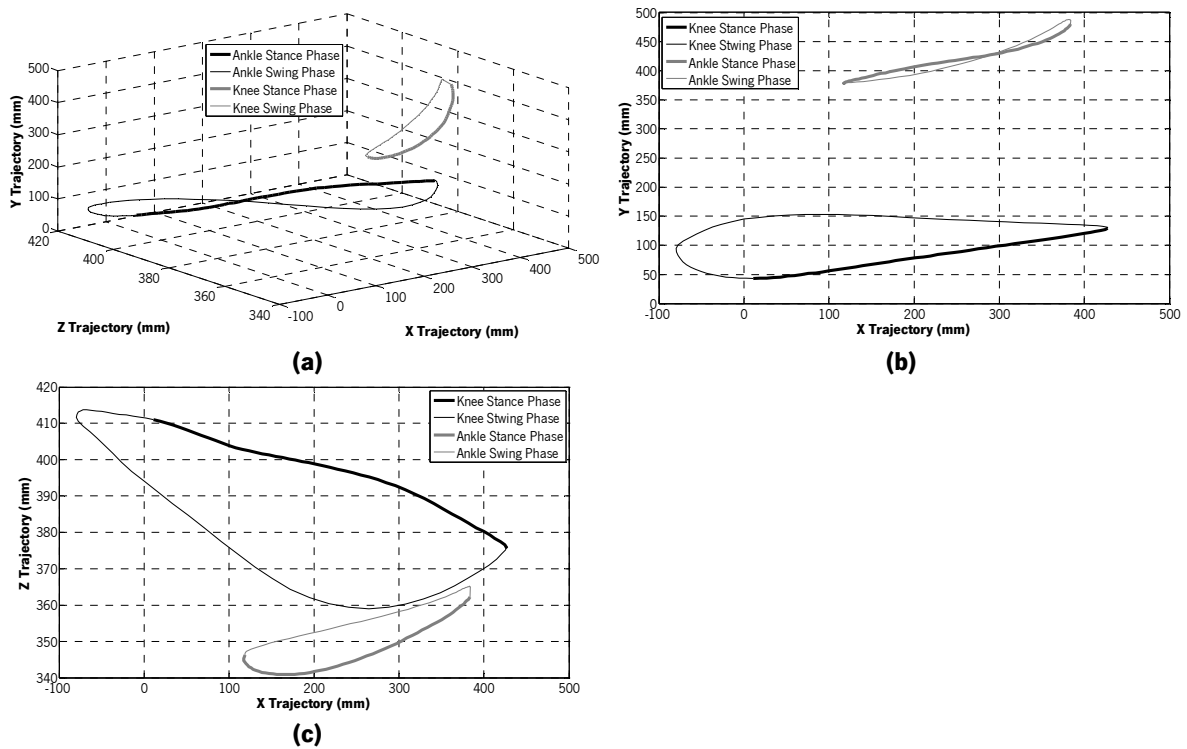


Figure 6.3 - Knee and ankle trajectories: (a) 3D; (b) sagittal plane; (c) frontal plane.

The vertical black lines in Fig. 6.4 pretend to represent the shank motion in the sagittal plane during the gait cycle. As the knee-ankle segment is considered a rigid body, its length should be a constant value, which is not verified in the study. A mean value of 329.95 mm and a SD value of 31.66 mm were calculated for the distance knee-ankle for the 654 tracked positions of the representative test. The errors associated with data acquisition and the changing in the end effector placement, i.e., the slippage of the strap around the evaluated point (in the study case, knee or ankle) can in fact give a rise to a change of the actual distance and therefore account for small estimation systematic errors. To overcome the error, an algorithm as an alignment procedure to eliminate the systematic error in the end-effector misalignment can be devised.

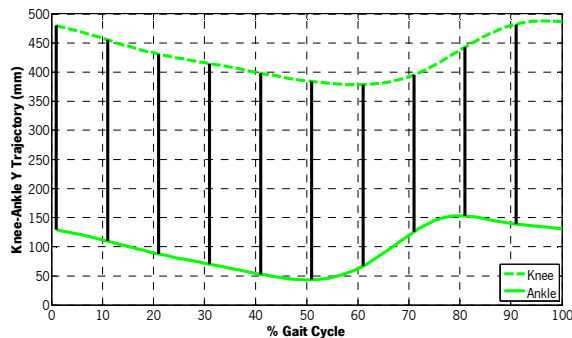


Figure 6.4 - Superior-inferior ankle trajectory.

Velocity and Acceleration

Figure 6.5 shows the velocity and acceleration experienced during a gait cycle by the knee and ankle point, respectively. Knee and ankle speed result from the vector module of the three respective directional components.

Average ankle speed (0.69 m/s) is higher than the knee one (0.38 m/s). The amplitude of the average velocity components decrease in the same way for both. Horizontal velocity amplitude is the highest, followed by the vertical and at last the lateral one. In fact, for the human walking motion is logical that the rate of the walking motion velocity components decrease in this way. In what refers to the acceleration, mean values of 1.7 m/s^2 and 2.8 m/s^2 were found for the knee and ankle point, respectively. The average acceleration amplitude is again superior in the ankle point, and the directional acceleration amplitude behaves in the same way as for the ankle. Periodic pattern was found in the velocity and acceleration results of the ankle and knee gait tests.

The correspondence of the physical events in the velocity and acceleration plot is not ideal due to the use of the differentiation and the filtering technique. Nevertheless, it is very clear in Fig. 6.5a a zero-crossing moment, in which velocity is 0 m/s , the heel contact moment. It is correspondent to a peak acceleration visible in Fig. 6.5c, corresponding to 4.7 m/s^2 . The same kind of event occurs in the ankle, but the values are not so high.

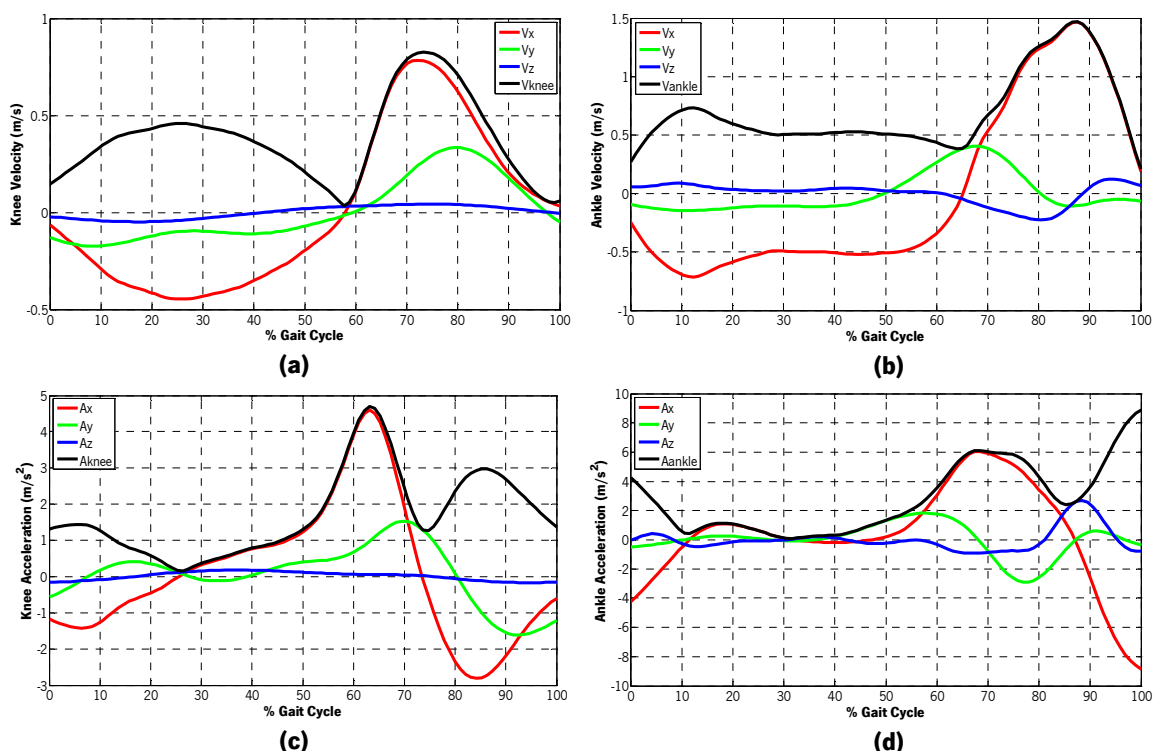


Figure 6.5 - Velocity and acceleration: (a) knee velocity; (b) ankle velocity; (c) knee acceleration; (d) ankle acceleration.

Angular Kinematics

In chapter 5.3, it was defined θ_s . The angles were defined as measured in a counterclockwise direction with the horizontal equal to 0° . Fig. 6.6 represent the θ_s in stance phase. It is clear that from the initial contact to the preswing the θ_s decrease, reaching 90° in maximum knee extension, i.e., midstance. Moreover:

- If the ankle point is anterior to the knee point, $\theta_s > 90^\circ$;
- If the ankle point is posterior to the knee point, $\theta_s < 90^\circ$.

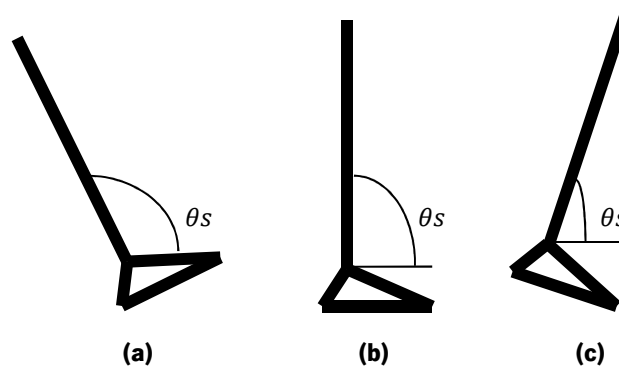


Figure 6.6 - Shank angle: (a) heel strike; (b) midstance ($\theta_s = 90^\circ$); (c) preswing.

A double pendulum model for swing and an inverse double pendulum model for stance was assumed (Salarian *et al.*, 2004).

The past values can be confirmed in Fig. 6.7a. After the data statistical treatment, it was possible to define the cycles to begin in the stance phase. In fact, if one cycle is observed, it is clear the heel contact is represented by a maximum angle value (average of 97°) and a minimum angle value for the toe-off moment (average of 48°) (Winter, 2005).

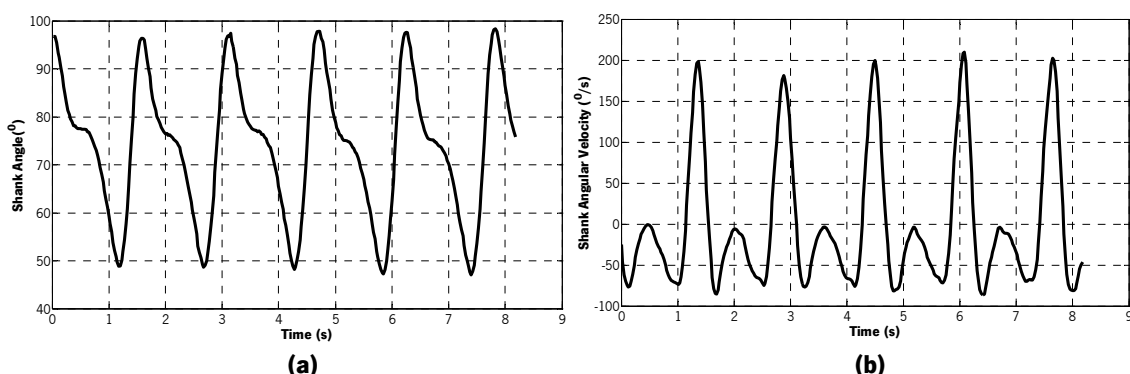


Figure 6.7 - Gait shank results: (a) shank angle; (b) shank angular velocity.

In what refers to the shank velocity presented in Fig. 6.7b, and beginning from the stance phase, some considerations will be done. Shank velocity begins with a negative peak value

related with heel strike, and during this phase only negative values are obtained. In the swing phase, a maximum angular velocity peak of shank velocity is obtained, corresponding to the midswing phase where maximum knee flexion occurs. Heel strike and heel off are represented by minimum negative peaks. Periodic feature was found for the both results.

6.1.2 - Kinetics

Some important considerations must be pointed out about the CaTraSys force results. In fact, they do not suitable represent the force behavior of the evaluated points (in the present case, knee and ankle). They are the result of the force exerted against the cable and their springs, which react pulling the leg toward the fixed platform, and also the force exerted to activate the treadmill conveyor belt. Other consequence of this force reaction is the possibility of obtaining a vibrated movement, especially in the arms (Ottaviano et al., 2001). Consequently, they are not representative of the force during the walking test.

However, they may indicate how the leg is exerting actions in the three components directions. Thus, the highest values may refer to the main direction of walking, just indicating the main actions of the ankle point in that direction.

Observing Fig. 6.8, it is clear the ankle force is higher than the force exerted by the knee. In fact, the ankle point needs to apply a higher force than the knee to perform the walking movement in the treadmill. The knee and ankle forces are vector modules. Periodic feature was also found for the forces results.

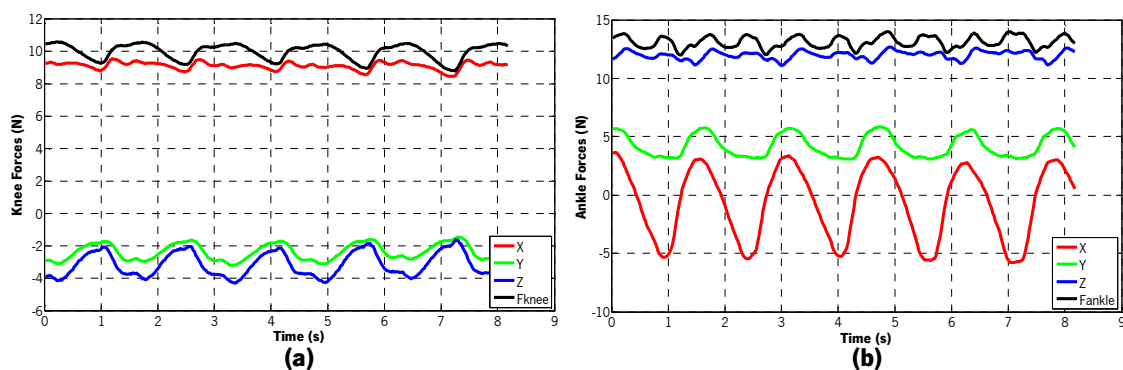


Figure 6.8- Forces results: (a) force exerted in the knee point; (b) force exerted in the ankle point.

6.2 - Comparative Gait Analysis

6.2.1 - Spatio-Temporal Parameters

For the 3D and two dimensional (2D) trajectory, a figure-of-eight shape for the knee and an approximately oval shape for the ankle are generally found across the diverse subjects and tested conditions, as previously highlighted in Figs. 6.1 and 6.2.

So that an objective analysis could be performed, each test result was quantified through numerical parameters. Using the complete/average signal from the ankle trajectory in the sagittal plane, spatio-temporal parameters were estimated for each test result (see Fig. 6.9):

- Walking Time (s) - defined as the time between the selected peaks of the horizontal trajectory (see Fig. 5.4c);
- Number of Cycles - determined as the number of selected peaks minus one (see Fig. 5.4c);
- Cycle Time (s) - obtained by dividing the walking time by the strides number;
- Cycle Cadence (cycles/s) - defined as the number of cycles per second, was calculated by dividing the total number of strides per the total walking time;
- Stance Phase (%) - to estimate the cycle percentage the foot spent on the treadmill, it was used the average vertical signal of the ankle. It was defined as the cycle percentage between the first position and the minimum position (see Fig. 6.9);
- Swing Phase (%) - corresponding to the time the foot spent in the air, it was defined as the cycle percentage between the minimum position and the last position of the average vertical signal of the ankle (see Fig. 6.9);
- Cycle Height (m) - indicates the amount by which the foot can be moved. It was defined by the difference between the minimum and maximum position of the average vertical trajectory (see Fig. 6.9);
- Cycle Length (m) - corresponds to the distance travelled by the foot in the forward direction, calculated as the difference between the minimum and maximum position of the average horizontal trajectory (see Fig. 6.9) (Whittle, 2007).
- Walking Distance (m) - estimated by multiplying the cycle length by the number of cycles;
- Cycle Medio-Lateral Movement (m) - indicating the amplitude of changes in the ankle lateral position, it was determined as the difference between the highest and the lowest lateral position of the average lateral trajectory (see Fig. 6.9).

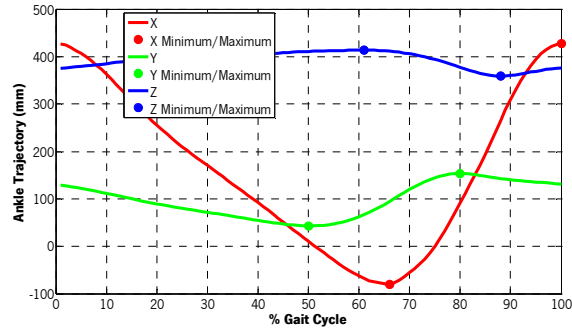


Figure 6.9 - Horizontal, vertical and lateral direction of the ankle trajectory.

Knee data was not considered in this analysis in a strategy to simplify the CaTraSys gait conclusions. Velocity, acceleration, shank parameters and forces were not part of the present evaluation since no added value was found in their analysis. The basic pattern was observed in the velocity and acceleration results for the different conditions, with some variation or addition of location peaks. In fact, at different walking speeds, the acceleration patterns, generally, have a moderate to low degree of variability (Zijlstra and Hof, 2003). CaTraSys forces output, as previously explained, do not completely represent the force during the walking motion.

Hereafter, examples of the parameters behavior (the ones visually detectable) are depicted. In Fig. 6.10, observing the trajectory of the largest stance phase curve, it is possible to detect in fact a high interval between the beginning of the stance phase and the minimum vertical position, corresponding to the end of the stance phase. This test has the highest stance phase of the experience, 50% of stance phase and 50% of swing phase. As for the curve with the highest swing phase, it is characterized by 63% of swing phase against 37% of stance phase. It can be seen that for the grey curve the vertical minimum position is reached very early.

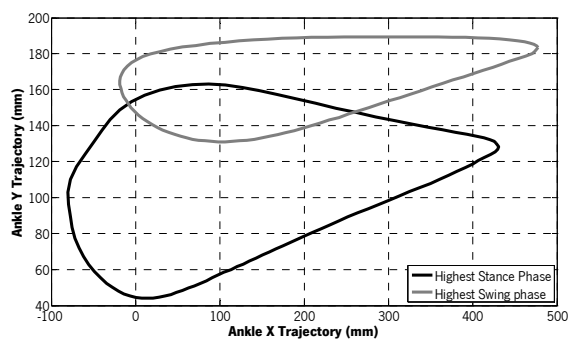


Figure 6.10 - Illustrative example of different stance and swing cycle periods (sagittal trajectories).

To demonstrate the range of the cycle length and height obtained with the CaTraSys experimental tests, it was ensembled in Fig. 6.11 the curves corresponding to the highest and lowest range of this feature. Observing the black curve, it is clear a high range of horizontal

position (cycle length) and vertical position (cycle height). The grey curve illustrates the minimum range of cycle length and height found in the tests results.

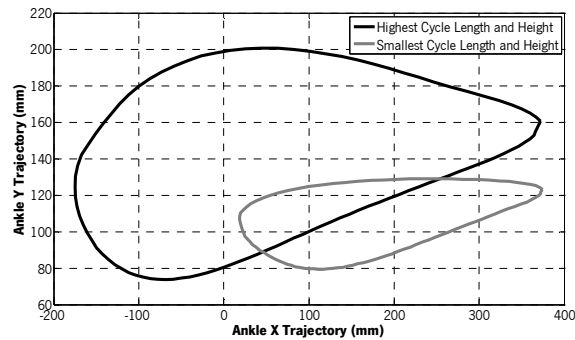


Figure 6.11 - Illustrative example of diverse cycle height and length (sagittal trajectories).

At last, Fig. 6.12 presents the tests results with the highest and lowest cycle lateral movement, which can be observed in the range of values of the ankle lateral trajectory.

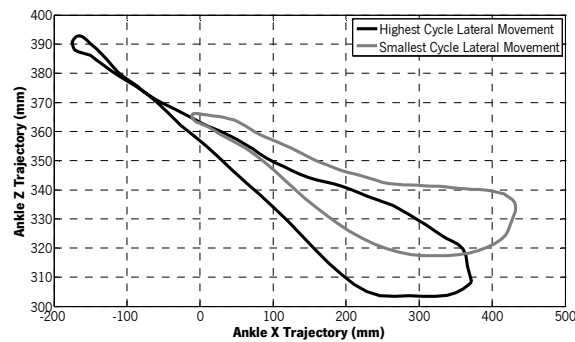


Figure 6.12 - Illustrative example of different cycle lateral displacements (transverse plane).

Table 6.1 presents the results of the parameters for the representative test. In fact, these parameters could be used to quantify the individual gait; for example to identify pathological matters, or also to reproduce it with specific software, which for example could be applied in biped robots (Ceccarelli *et al.*, 1999). In Appendix D (D.1 to D.8), tests information are provided for each individual who participated in the experimental tests.

Table 6.1 - Spatio-temporal parameters of the representative test.

Walking Distance (m)	4.0579
Walking Time (s)	12.5
Number of Cycles	8
Cycle Time (s)	1.5625
Cycle Cadence (cycles/s)	0.64
Stance Phase (%)	50
Swing Phase (%)	50
Cycle Height (m)	0.1102
Cycle Length (m)	0.5072
Cycle Lateral Movement (m)	0.0568

6.2.2 - Influence of the Test Conditions

Many investigations had concluded the human gait is highly adaptable to modifications in the mechanical demands of the task (e.g.: different speeds or types of surfaces) (Pepin *et al.*, 2003). One of the goals of the present work was to monitor the human gait taking into account different factors that could influence it. To accomplish the proposed objective four trial conditions were used: reference test, loaded test, footwear test and fast test. In order to run the comparative study the previous depicted parameters were used.

In order to compare the diverse test conditions, the three special test conditions, loaded test, footwear test and fast test, were studied against the corresponding reference test. Therefore, for each subject and parameter, the difference between its value for the reference test and for the other different test condition was calculated. With these values, it was determined the mean deviation (MD) and SD for each parameter and test condition (see Table 6.2).

Moreover, it was verified the behavior (increase/decrease) of those deviation values calculated firstly for each subject and parameter (see Table 6.3). Obviously, for each type of test, each table cell results from an inter calculation between subjects, and so it must be highlighted the behavior of all the parameters for that one test can possibly not be verified in a single test result (of the corresponding type).

The SD values in Table 6.2 are very high. In fact, this discrepancy of values between subjects can be the result of different individual selected velocities and anthropometric

parameters. The objective of Table 6.2 is indeed to give the possibility for an easy and general idea of the results, for each test condition and parameter.

Table 6.2 - Inter evaluation: MD and SD tests results.

	Loaded Test		Footwear Test				Fast Test	
	MD	SD	Men		Women		MD	SD
			MD	SD	MD	SD		
Cycle Cadence (cycles/s)	0.09	0.08	0.07	0.06	0.1	0.09	0.31	0.16
Stance Phase (%)	2.25	1.83	2.2	2.39	2	2.65	2.13	1.36
Swing Phase (%)	2.25	1.83	2.2	2.39	2	2.65	2.13	1.36
Cycle Height (mm)	10.24	7.14	11.28	7.72	6.77	7.35	15.41	12.35
Cycle Length (mm)	22.6	22.1	38.08	22.12	34.67	26.33	59.58	55.26
Cycle Lateral Movement (mm)	6.98	6.06	7.6	3.88	8.6	6.45	11.25	9.24

Table 6.3 - Inter evaluation: direction of the deviation values.

	Loaded Test		Footwear Test		Fast Test
			Men	Women	
Cycle Cadence	(62,5)↓	(80)↑	(100)↑	(100)↑	
Stance Phase	(87,5)↑	(40)	(66,7)↑	(62,5)↑	
Swing Phase	(87,5)↓	(40)	(66,7)↓	(62,5)↓	
Cycle Height	(87,5)↑	(60)↑	(100)↓	(100)↑	
Cycle Length	(62,5)↑	(60)↑	(66,7)↓	(100)↑	
Cycle Lateral Movement	(50)	(60)↑	(100)↑	(50)	

In Table 6.3, a positive deviation means an increase in the parameter value, a negative deviation means a decrease in the parameter value and a zero value means the parameter was equal for the both test conditions. The cases (50) constituted cases of 50/50 of growth and decrement. The cases (50)↑ and (50)↓ are the ones in which the deviation increment or reduction was predominantly positive or negative, respectively, since the rest of the percentage constituted cases of zero and negative deviation. As for the case (40), it illustrates a case in which occurs 40% of increment, 40% of decrement and 20% of non-alteration of values. Observing Table 6.3, important conclusions should be taken. In order to run an accurate analysis, it was only considered a pattern, i.e., it only constituted a conclusion to the present work if the parameter deviation direction was higher than 50%.

For the loading condition, it is concluded the cycle cadence is reduced in the majority of the cases, while stance phase, cycle height and length are increased. These values indicate so that for the subject carrying load on the shoulders while walking, a slower cycle frequency occurred,

the time the foot spent in the air was reduced and the amplitude of vertical and horizontal movement was also shorter. These conclusions can be observed in Table 6.3 and Fig. 6.13a.

In what refers to the footwear test, different conclusions were taken for men and women. From the present results, it can be concluded wearing sportive shoes increases cycle cadence, cycle height, length and lateral movement. These conclusions are not very accurate since the differences between the type of foot from the reference test (casual shoes) and the sportive shoes are probably not enough to allow its recognition from the CaTraSys results.

As for the heel-shoes tests results, it is adopted a quicker cadence and an increment in the stance phase. On the other hand, cycle height and length undergo a decrease and the lateral movement an increment. It can be thought that decreasing the cycle height and length is a defense strategy of the subject in order to maintain the stability. Wearing high heel shoes resulted in a 100% of increment in the lateral motion, which justifies the clear instability caused by this type of shoes and can lead to a modification of the body posture. Observing Table 6.3 and Fig. 6.13b, and comparing the curves from the reference and corresponding footwear test, it is evident an increment in all the vertical positions of the footwear curve. This modification is a consequence of being a heel shoes trial.

Relative to the fast test condition, it was observed a clear augmentation in the cycle cadence and stance phase as well as in the cycle height and length, as can be confirmed by Table 6.3 and Fig. 6.13c. The results are in accordance with literature. In fact, the adaptation to an increase of the walking speed is obtained with reduced cycles duration and higher cycles length, simultaneously (generally) or not (Pepin *et al.*, 2003). The medio-lateral amplitude of movement for the fast test was 50/50 of growth and decrement relative to the reference test. Despite the present results, it was expected a major percentage of decrement. Tesio *et al.* (2010) observed a decrease in the mediolateral movement of the body centre of mass with increasing speed, which is also coherent with Smeesters *et al.* (2001) that concluded sideway falls are more frequent at low speeds. Although the body centre of mass movement and lateral movement being distinct concepts, it would be consistent a higher percentage of decrement. As the results of the present work do not overcome the 50%, no conclusion should be inferred.

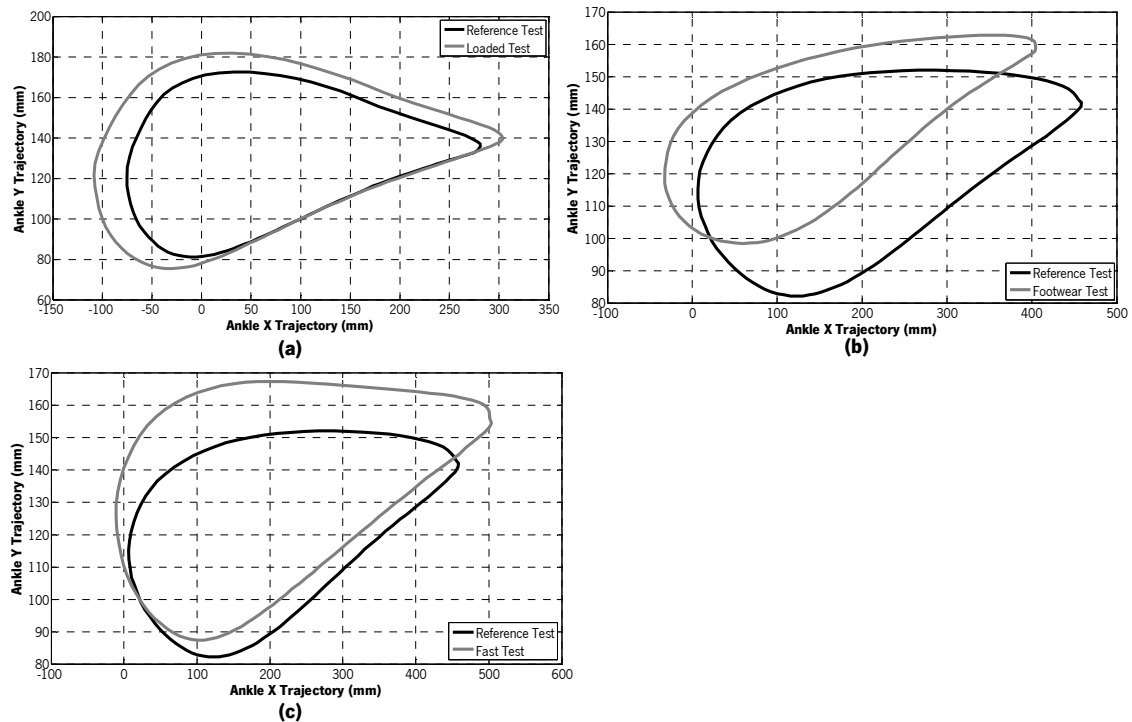


Figure 6.13 - Sagittal trajectories for the reference test and: (a) loaded test (subject 4); (b) footwear women test (subject 7); (c) fast test (subject 7).

6.2.3 - Influence of the Anthropometric Factors

The second type of comparison approach will be explained hereafter. Another aim of the present work was to monitor the human walking characteristics taking into account the anthropometric factors gender, age, height and weight.

For each type of test, it was verified the subjects parameters variation along with the anthropometric features. For the recognition, and as an example of the used method, having the parameters of the subjects for the reference test sorted in ascending order, it was verified if the behavior of any parameter coincided (approximately or totally) with the gender, age, height or weight sorting order. In fact, the CaTraSys results of the present work did not allow any accurate conclusion about behavior patterns of human gait according to anthropometric characteristics. This may obviously be caused by the low number of sampled individuals.

In order to give a general idea of the results for different anthropometric conditions, Figure 6.14 presents the sagittal trajectory of subjects with opposite values (maximum/minimum) of gender, age, height and weight, for the reference test condition.

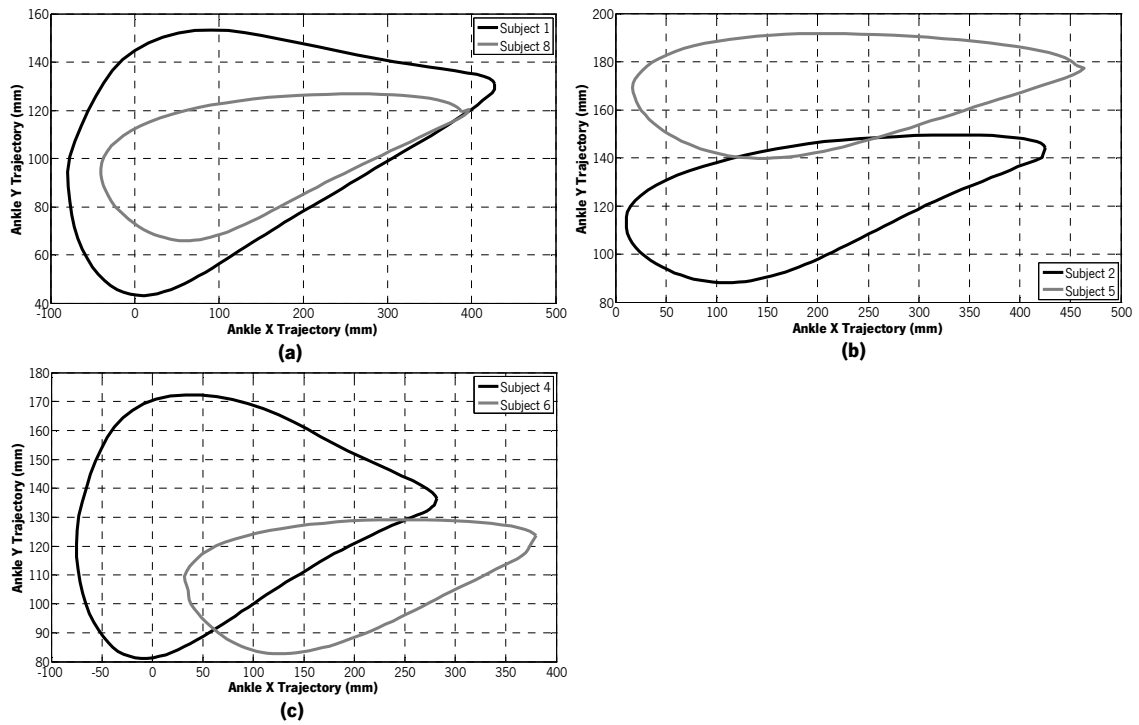


Figure 6.14 - Sagittal trajectories for different anthropometric characteristics, obtained in reference tests: (a) male and female subject (subject 1 and 8); (b) oldest and youngest subject of the test population (subject 2 and 5, 28 and 20 years old respectively); (c) subjects with the highest and lowest height and weight of the test population (subject 4 and 6).

CHAPTER 7 - CONCLUDING REMARKS

In the last chapter of the present thesis some concluding observations will be provided.

7.1 - Conclusions

In the present work, the use of CaTraSys for human walking characterization was proposed. The methodology of the experimental tests was reviewed. The data analysis techniques were discussed. A novel formulation was developed for determining kinematics and kinetics of a CaTraSys gait test.

Visual representation of CaTraSys results were provided and studied through the presented reference profiles. Although the deviations observed between tests, the basic patterns conclusions are fairly reproducible across all subjects and trial conditions. Estimation of spatio-temporal parameters for all the CaTraSys experimental results allowed running a comparative analysis and some findings about the behavior patterns for different walking conditions. The influence of the anthropometric characteristics on the population gait was also studied. In fact, the existence of standard values for these parameters could be a tool to distinct normal and pathological gait, or could be reproduced in software, which for example could be applied in biped robots. It was reported a limited number of results that can nevertheless be a basis for more sophisticated analyses with CaTraSys.

The presented methods and results prove the CaTraSys significance in the experimental characterization of the biomechanics of human walking, always respecting the principles of low-cost and easy operation of the proposed system.

The clinical application of CaTraSys was discussed and proved adequate for assessing purposes, for example in diagnosis or rehabilitation procedures of human limbs. The results of this work suggest hypotheses for further biomedical research.

7.2 - Future Work

For further developments of the present work the following items are suggested:

- Improve the study with a larger subject pool, which would allow generating reference spatio-temporal gait parameters for CaTraSys as well as more accurate conclusions;
- Use accelerometers to obtain accurate velocity and acceleration data;
- Include other end-effector schemes in the study, namely ones that include the hip and the left and right limb simultaneously;
- Improve the LabVIEW VI and the calibration procedure;
- Develop a formulation that considers the CaTraSys uncertainties, namely the end-effector misalignment;
- Devise a new end-effector, which would allow a more accurate data acquisition.

REFERENCES

- BARTLETT, R. (2007). *Introduction to Sports Biomechanics: Analysing Human Movement Patterns*. 2nd ed.: Taylor & Francis. 292 p.
- CECCARELLI, M., et al. (1999). CaTraSys (Cassino Tracking System): A New Measuring System for Workspace Evaluation of Robots. In Freyberger, F. & Schmidt, G. (eds) *Proceedings of 8th International Workshop on Robotics in Alpe-Adria-Danube Region (RAAD 1999)*, Munich, Germany, June 17-19, pp. 19-24.
- CECCARELLI, M., et al. (2000). Error Analysis and Experimental Tests of CaTraSys (Cassino Tracking System). In vol. 4 *Proceedings of 26th Annual Conference of the IEEE Industrial Electronics Society (IECON 2000)*, Nagoya, Japan, October 22-28, pp. 2371-2376: IEEE.
- CECCARELLI, M., et al. (2007, March 19-21). *Experimental Activity on Cable-Based Parallel Manipulators: Issues and Results at LARM in Cassino*. 2nd International Congress on Design and Modelling of Mechanical Systems (CMSM'2007), Monastir, Tunisia, p. 6.
- CECCARELLI, M. & ROMDHANE, L. (2009). Design Considerations for Human-Machine Interfaces in Cable-Based Parallel Manipulators for Physiotherapy Applications. In *Proceedings of 1st IFToMM International Symposium on Robotics and Mechatronics (ISRM 2009)*, Hanoi, Vietnam, September 21-23, pp. 1-8.
- CECCARELLI, M. (2010, September 14). *Problems and Experiences in Using Parallel Manipulators for Medical Applications*. International Workshop ROBOMED 2010: New Trends in the Development of Parallel Robots for Medical Applications, Cluj-Napoca, Romania, pp. 1-8.
- CECCARELLI, M. & ROMDHANE, L. (2010). Design Issues for Human-Machine Platform Interface in Cable-Based Parallel Manipulators for Physiotherapy Applications. *Journal of Zhejiang University - Science A (Applied Physics & Engineering)*, 11 (4): 231-239.
- CECCARELLI, M. (2011). Problems and Issues for Service Robots in New Applications. *International Journal of Social Robotics*, 3 (3): 299-312.
- CECCARELLI, M. (2012). The Historical Development of CaTraSys, a Cable System. In Koetsier, T. & Ceccarelli, M. (eds) vol. 15 *Proceedings of International Symposium on the History of Machines and Mechanisms (HMM2012), Explorations in the History of Machines and Mechanisms*, Amsterdam, Holland, April 05, pp. 365-379: Springer Netherland.
- CELESCO TRANSDUCER PRODUCTS INC. (2012). *PT101*. Available at: http://www.celesco.com/_datasheets/pt101.pdf (accessed: 2012.10.11).

- DEVITA, P. & BATES, B. T. (1988). Intraday Reliability of Ground Reaction Force Data. *Human Movement Science*, 7 (1): 73-85.
- DÍAZ, I., et al. (2011). Lower-Limb Robotic Rehabilitation: Literature Review and Challenges. *Journal of Robotics*, 2011 (2011): 11.
- GRANDÓN, C., et al. (2007). Certified Pose Determination under Uncertainties. In Merlet, J.-P. & Dahan, M. (eds) *Proceedings of 12th World Congress in Mechanism and Machine Science (12th IFToMM)*, Besançon, France, June 18-21, pp. 1-5.
- HAMILL, J. & KNUTZEN, K. M. (2009). *Biomechanical Basis of Human Movement*. 3rd ed.: Lippincott Williams & Wilkins.
- HOMMA, K., et al. (2002). Study of a Wire-Driven Leg Rehabilitation System. In vol. 2 *Proceedings of 2002 IEEE/RSJ International Conference on Intelligent Robots and Systems (IROS 2002)*, Lausanne, Switzerland, September 30-October 4, pp. 1451-1456: IEEE.
- IIDA, H. & YAMAMURO, T. (1987). Kinetic Analysis of the Center of Gravity of the Human Body in Normal and Pathological Gaits. *Journal of Biomechanics*, 20 (10): 987-995.
- KHAN, M. A., et al. (2006). Inferring Online and Offline Processing of Visual Feedback in Target-Directed Movements from Kinematic Data. *Neuroscience & Biobehavioral Reviews*, 30 (8): 1106-1121.
- KLIKA, V. (2009). *Biomechanics in Applications*. InTech.
- KUTZ, M. (2009). *Biomedical Engineering and Design Handbook, Volume 1: Fundamentals*. 2nd ed.: McGraw-Hill Companies, Inc.
- LAUMAS ELETTRONICA S.R.L. (2010). SA. Available at: http://www.laumas.com/files_pdf/sa.pdf (accessed: 2012.11.9).
- LAUMAS ELETTRONICA S.R.L. (2011). TPS. Available at: http://www.laumas.com/FILES_PDF/Tps.pdf (accessed: 2012.12.8).
- LI, T. & CECCARELLI, M. (2011). *An Experimental Analysis of Human Straight Walking*.
- MACELLARI, V. & GIACOMOZZI, C. (1996). Multistep Pressure Platform as a Stand-Alone System for Gait Assessment. *Medical and Biological Engineering and Computing*, 34 (4): 299-304.
- MOREIRA, P. (2009). *Development of a Three-Dimensional Contact Model for the Foot-Ground Interaction in Gait Simulations*. Msc Dissertation. Portugal: University of Minho. 119 p.
- Motion Capture Systems from Vicon*. Available at: <http://vicon.com/> (accessed: 2012.12.10).
- NATIONAL INSTRUMENTS CORPORATION. (2009). *NI USB-621x Specifications*. Available at: <http://www.ni.com/pdf/manuals/371932f.pdf> (accessed: 2012.10.7).

- NUNES, W. M., et al. (2011). Cable-Based Parallel Manipulator for Rehabilitation of Shoulder and Elbow Movements. In *Proceedings of 12th IEEE International Conference on Rehabilitation Robotics (ICORR 2011)*, Zurich, Switzerland, June 29-July 1, pp. 1-6: IEEE
- OTTAVIANO, E., et al. (2001). Experimental Determination of Workspace Characteristics of Human Arms. In *Proceedings of 9th Mediterranean Conference on Control and Automation (MED'01)*, Dubrovnik, Croatia, June 27–July 29, p. 6.
- OTTAVIANO, E., et al. (2002). CaTraSys (Cassino Tracking System): A Wire System for Experimental Evaluation of Robot Workspace. *Journal of Robotics and Mechatronics*, 14 (1): 78-87.
- OTTAVIANO, E. (2007). A System for Tension Monitoring in Cable-Based Parallel Architectures. In Merlet, J.-P. & Dahan, M. (eds) *Proceedings of 12th World Congress in Mechanism and Machine Science (12th IFToMM)*, Besançon, France, June 18-21, p. 6.
- OTTAVIANO, E., et al. (2009). An Experimental Evaluation of Human Walking. In *Proceedings of 3rd International Congress on Design and Modelling of Mechanical Systems (CMSM'2009)*, Hammamet, Tunisia, March 16-18, pp. 1-8.
- OTTAVIANO, E., et al. (2010). An application of CaTraSys, a Cable-Based Parallel Measuring System for an Experimental Characterization of Human Walking. *Robotica*, 28 (1): 119-133.
- OTTAVIANO, E. & GRANDE, S. (2012). A Monitoring System for the Gait Analysis of Lower Extremity. *Precision Instrument and Mechanology*, 1 (2): 48-56.
- PALMUCCI, F., et al. (2008). An Application of CaTraSys, a Cable-Based Parallel Measuring System for a Kinetostatic Analysis of Human Walking. In *Proceedings of 3rd IFToMM-FelbIM International Symposium on Multibody Systems and Mechatronics (MuSMe 2008)*, San Juan, Argentine, April 8-12, pp. 1-16.
- PAYTON, C., et al. (2008). *Biomechanical Evaluation of Movement in Sport And Exercise: The British Association Of Sport And Exercise Sciences Guidelines*. 1st ed.: Routledge.
- PEPIN, A., et al. (2003). Treadmill Walking in Incomplete Spinal-Cord-Injured Subjects: 1. Adaptation to Changes in Speed. *Spinal Cord*, 41 (5): 257-270.
- PERRY, J. (1992). *Gait Analysis: Normal and Pathological Function*. SLACK Incorporated.
- RACIC, V., et al. (2009). Experimental Identification and Analytical Modelling of Human Walking Forces: Literature Review. *Journal of Sound and Vibration*, 326 (1–2): 1-49.
- RILEY, P. O., et al. (2007). A Kinematic and Kinetic Comparison of Overground and Treadmill Walking in Healthy Subjects. *Gait & Posture*, 26 (1): 17-24.

- SALARIAN, A., et al. (2004). Gait Assessment in Parkinson's Disease: Toward an Ambulatory System for Long-Term Monitoring. *Biomedical Engineering, IEEE Transactions on*, 51 (8): 1434-1443.
- SMEESTERS, C., et al. (2001). Disturbance Type and Gait Speed Affect Fall Direction and Impact Location. *Journal of Biomechanics*, 34 (3): 309-317.
- TAVOLIERI, C., et al. (2006). Pose Determination for a Rigid Body by Means of CaTraSys II (Cassino Tracking System). In Husty, M. & Schröcker, H.-P. (eds) *Proceedings of 1st European Conference on Mechanism Science (EuCoMeS 2006)*, Obergurgl, Austria, February 21–26, pp. 21-26.
- TESIO, L., et al. (2010). The 3D Path of Body Centre of Mass During Adult Human Walking on Force Treadmill. *Journal of Biomechanics*, 43 (5): 938-944.
- WHITTLE, M. (2007). *Gait Analysis: an Introduction*. 4th ed.: Butterworth-Heinemann.
- WINTER, D. A. (1991). *The Biomechanics and Motor Control of Human Gait: Normal, Elderly and Pathological*. University of Waterloo Press.
- WINTER, D. A. (2005). *Biomechanics and Motor Control of Human Movement*. 3rd ed.: John Wiley & Sons, Inc.
- ZIJLSTRA, W. & HOF, A. L. (2003). Assessment of Spatio-Temporal Gait Parameters from Trunk Accelerations during Human Walking. *Gait & Posture*, 18 (2): 1-10.

LIST OF FIGURES

Figure 2.1 - Bones and joints of the lower limbs (Whittle, 2007).....	6
Figure 2.2 - Superficial muscles of the right leg (Whittle, 2007).....	8
Figure 2.3 - Standardized anatomical position with three reference planes and six fundamental directions (Racic <i>et al.</i> , 2009).	10
Figure 2.4 - The gait cycle (Racic <i>et al.</i> , 2009).....	10
Figure 2.5 - Gait phases and functional tasks: Initial Contact (IC); Loading Response (LR); Midstance (Mst); Terminal Stance (Tst); Preswing (Psw); Initial Swing (Isw), Mid-Swing (Msw); Terminal Swing (Tsw) (Racic <i>et al.</i> , 2009).	12
Figure 3.1 - CaTraSys: (a) prototype; (b) scheme (Li and Ceccarelli, 2011).	16
Figure 3.2 - Lay-out of PUMA robot applied to CaTraSys (Ceccarelli <i>et al.</i> , 2007).....	17
Figure 3.3 - VICON (black line) and CaTraSys (grey line) results for the ankle trajectory (Ottaviano and Grande, 2012).	18
Figure 3.4 - NI USB-6210 DAQ board used in CaTraSys (National Instruments Corporation, 2009).....	19
Figure 3.5 - Position transducer: (a) inside view of the plastic protective box; (b) spiral spring... 20	
Figure 3.6 - Set-up of the transducer, along with the two pulleys and the force sensor.....	20
Figure 3.7 - CaTraSys load cell (S.r.l., 2010).	21
Figure 3.8 - The 6 amplifiers together with the DAQ board.....	21
Figure 3.9 - CaTraSys end-effector: (a) attached to the knee and ankle in 3-3 configuration; (b) zoomed view.	22
Figure 3.10 - DAQ assistant configuration panel for transducer 1.	24
Figure 3.11 - NI MAX settings for position sensor 1.	25
Figure 3.12 - Tape measurement procedure for cable 1.	25
Figure 3.13 - Electronic scale device measuring the force exerted on the cable.	26
Figure 3.14 - CaTraSys 3-3 configuration: (a) treadmill walking test; (b) trilateration scheme (adapted from (Li and Ceccarelli, 2011)).....	27
Figure 3.15 - Scheme for the forces computation.	31
Figure 4.1 - Experimental tests conditions: (a) reference test; (b) loading test; (c) footwear test; (d) fast test.....	36
Figure 4.2 - Experimental footwear test for a male subject.	37

Figure 4.3- The different footwear types used in the experimental tests: (a) casual shoes; (b) sport shoes; (c) high heel shoes.	37
Figure 5.1 - Filtering: (a) raw signal; (b) final signal; (c) application of four cutoff frequencies; (d) zoomed view of (c).....	43
Figure 5.2 - Residual plot for the selection of an optimal cutoff frequency using residual analysis.	44
Figure 5.3 - Results of two different sessions (sagittal trajectories): (a) data with less dispersion; (b) rejected data.	46
Figure 5.4 - Detection of the heel strike moment in the horizontal trajectory: (a) local and global maximums; (b) zoomed view of (a); (c) global maximums uniquely; (d) original and medium curve.....	47
Figure 5.5 - Representation of the shank angle θ_s (adapted from (Winter, 2005))	48
Figure 5.6 - Finite-difference technique (adapted from (Winter, 2005)).	49
Figure 5.7 - Exemplificative data for acceleration acquisition: a) acquired data position; b) velocity and acceleration profiles derived from position; c) acceleration profile obtained directly from an accelerometer (adapted from (Khan <i>et al.</i> , 2006)).	50
Figure 6.1 - Knee trajectory: (a) 3D; (b) X , Y and Z coordinates; (c) sagittal plane; (d) frontal plane. The arrows depict the movement direction.....	52
Figure 6.2 - Ankle trajectory: (a) 3D; (b) X , Y and Z coordinates; (c) sagittal plane; (d) frontal plane. The arrows depict the movement direction.....	52
Figure 6.3 - Knee and ankle trajectories: (a) 3D; (b) sagittal plane; (c) frontal plane.....	54
Figure 6.4 - Superior-inferior ankle trajectory.	54
Figure 6.5 - Velocity and acceleration: (a) knee velocity; (b) ankle velocity; (c) knee acceleration; (d) ankle acceleration.	55
Figure 6.6 - Shank angle: (a) heel strike; (b) midstance ($\theta_s=90^\circ$); (c) preswing.	56
Figure 6.7 - Gait shank results: (a) shank angle; (b) shank angular velocity.	56
Figure 6.8- Forces results: (a) force exerted in the knee point; (b) force exerted in the ankle point.	57
Figure 6.9 - Horizontal, vertical and lateral direction of the ankle trajectory.....	59
Figure 6.10 - Illustrative example of different stance and swing cycle periods (sagittal trajectories).	59
Figure 6.11 - Illustrative example of diverse cycle height and length (sagittal trajectories).	60

Figure 6.12 - Illustrative example of different cycle lateral displacements (transverse plane). 60

Figure 6.13 - Sagittal trajectories for the reference test and: (a) loaded test (subject 4); (b) footwear women test (subject 7); (c) fast test (subject 7). 64

Figure 6.14 - Sagittal trajectories for different anthropometric characteristics, obtained in reference tests: (a) male and female subject (subject 1 and 8); (b) oldest and youngest subject of the test population (subject 2 and 5, 28 and 20 years old respectively); (c) subjects with the highest and lowest height and weight of the test population (subject 4 and 6). 65

LIST OF TABLES

Table 4.1 - Subjects anthropometric characteristics, sport activity frequencies and respective comments.....	39
Table 4.2 - Summary of the CaTraSys experimental protocol and estimative of the time spent with the respective task.....	40
Table 6.1 - Spatio-temporal parameters of the representative test.....	61
Table 6.2 - Inter evaluation: MD and SD tests results.....	62
Table 6.3 - Inter evaluation: direction of the deviation values.....	62

APPENDIX A – TECHNICAL SPECIFICATIONS OF CATRASYS COMPONENTS

A.1 - DAQ Board

NI USB-621x Specifications

Specifications listed below are typical at 25 °C unless otherwise noted. Refer to the *NI USB-621x User Manual* for more information about USB-621x devices.



Caution The input/output ports of this device are not protected for electromagnetic interference due to functional reasons. As a result, this device may experience reduced measurement accuracy or other temporary performance degradation when connected cables are routed in an environment with radiated or conducted radio frequency electromagnetic interference.

To ensure that this device functions within specifications in its operational electromagnetic environment and to limit radiated emissions, care should be taken in the selection, design, and installation of measurement probes and cables.

Français Deutsch 日本語 한국어 简体中文

ni.com/manuals

Analog Input

Number of channels	Input range.....	± 10 V, ± 5 V, ± 1 V, ± 0.2 V
USB-6210/6211/6212/ 6215/6216.....	8 differential or 16 single ended	
USB-6218.....	16 differential or 32 single ended	
ADC resolution.....	Maximum working voltage for analog inputs (signal + common mode).....	± 10.4 V of AI GND
16 bits	CMRR (DC to 60 Hz).....	100 dB
DNL.....	Input impedance	
No missing codes guaranteed	Device on	
INL.....	AI+ to AI GND.....	>10 G Ω in parallel with 100 pF
Refer to the <i>AI Absolute Accuracy Tables</i>	AI- to AI GND.....	>10 G Ω in parallel with 100 pF
Sampling rate	Device off	
Maximum	AI+ to AI GND.....	1200 Ω
USB-6210/6211/6215/6218... 250 kS/s single channel, 250 kS/s multichannel (aggregate)	AI- to AI GND.....	1200 Ω
USB-6212/6216.....	Input bias current.....	± 100 pA
400 kS/s single channel, 400 kS/s multichannel (aggregate)	Crosstalk (at 100 kHz)	
Minimum.....	Adjacent channels.....	-75 dB
0 S/s	Non-adjacent channels.....	-90 dB
Timing accuracy.....	Small signal bandwidth (-3 dB)	
50 ppm of sample rate	USB-6210/6211/6215/6218.....	450 kHz
Timing resolution.....	USB-6212/6216.....	1.5 MHz
50 ns		
Input coupling.....		
DC		



Input FIFO size.....	4,095 samples
Scan list memory.....	4,095 entries
Data transfers.....	USB Signal Stream, programmed I/O
Overvoltage protection (AI <0..31>, AI SENSE)	
Device on	±30 V for up to two AI pins
Device off	±20 V for up to two AI pins
Input current during overvoltage condition	±20 mA max/AI pin

Settling Time for Multichannel Measurements

Accuracy, full scale step, all ranges

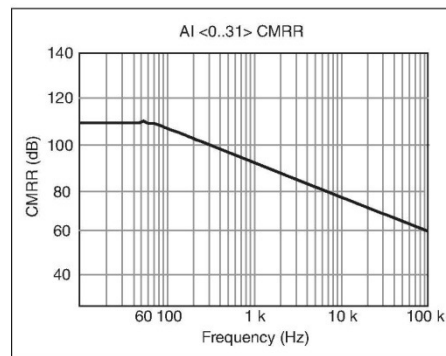
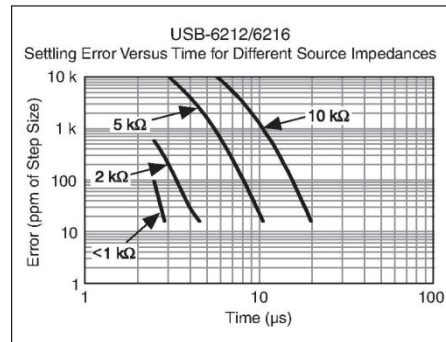
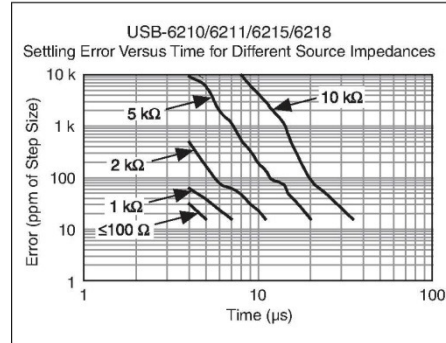
USB-6210/6211/6215/6218

- ±90 ppm of step (±6 LSB).....4 μs convert interval
- ±30 ppm of step (±2 LSB).....5 μs convert interval
- ±15 ppm of step (±1 LSB).....7 μs convert interval

USB-6212/6216

- ±90 ppm of step (±6 LSB).....2.5 μs convert interval
- ±30 ppm of step (±2 LSB).....3.5 μs convert interval
- ±15 ppm of step (±1 LSB).....5.5 μs convert interval

Typical Performance Graphs



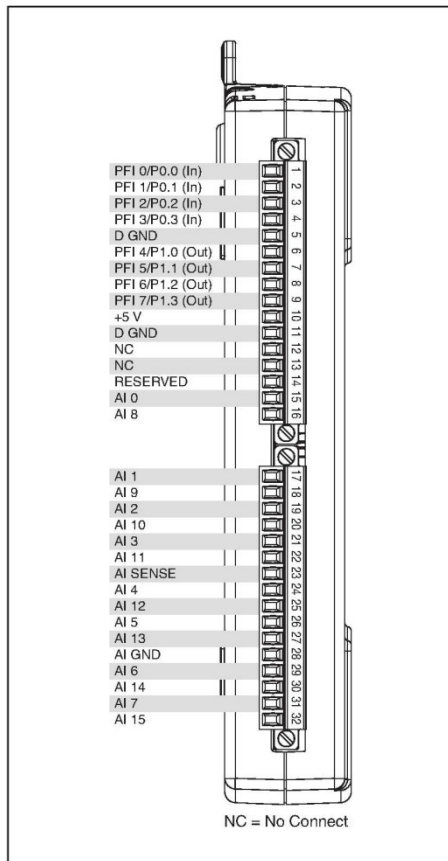


Figure 2. USB-6210 Pinout

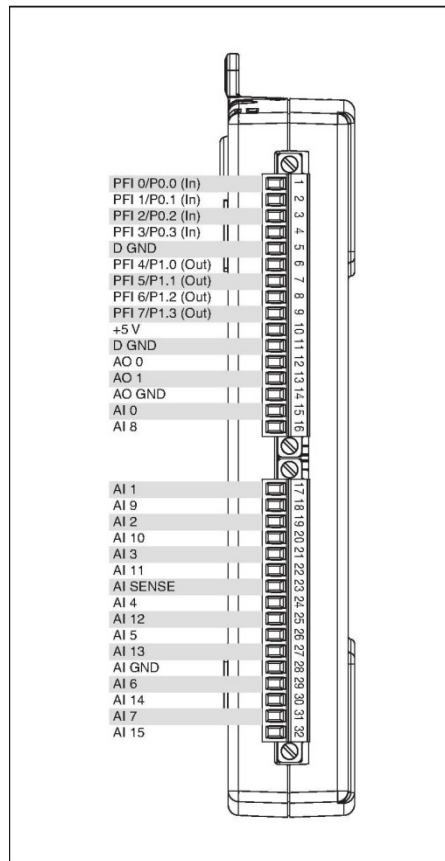


Figure 3. USB-6211/6215 Pinout

A.2 - Cable-Extension Position Transducer

Ordering Information:

Model Number:

PT101 - - 1 - 1 - 0

order code: A B C D E F G

Sample Model Number:

PT101 - 0025 - 111 - 1110

- A** range: 25 inches
- B** measuring cable tension: standard - 5 oz.
- C** cable exit: top
- D** sensing circuit: 500 ohms
- E** electrical connection: 6-pin plastic connector

Full Stroke Range:

order code:	0002	0005	0010	0015	0020	0025	0030	0040	0050	0060	0075	0080	0100
full stroke range, min:	2 in.	5 in.	10 in.	15 in.	20 in.	25 in.	30 in.	40 in.	50 in.	60 in.	75 in.	80 in.	100 in.
accuracy (% of f.s.):	0.25%		0.15%		0.10%		0.15%		0.10%				
potentiometer cycle life*:	2.5 x 10 ⁶		5 x 10 ⁵		2.5 x 10 ⁵		5 x 10 ⁵		2.5 x 10 ⁵				

*-1 cycle is defined as the travel of the measuring cable from full retraction to full extension and back to full retraction

celesco
celesco.com • info@celesco.com

tel: 800.423.5483 • +1.818.701.2750 • fax: +1.818.701.2799

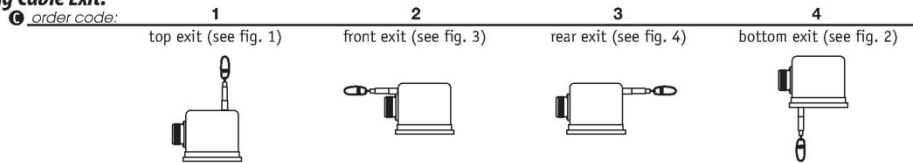
Ordering Information (cont.):

Measuring Cable Tension:

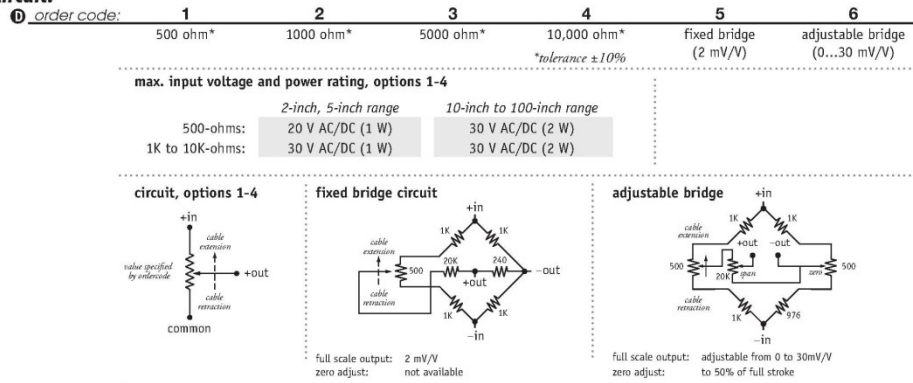
	1		H		2*	3*
	standard tension	high tension	tension, ±20%	max acceleration		
2, 10, 20 inch range:	12 oz.	• 11 g	65 oz.	• 53 g	72 oz.	144 oz.
5, 25, 50 inch range:	5 oz.	• 2 g	26 oz.	• 11 g	30 oz.	60 oz.
15, 30 inch range:	8 oz.	• 3 g	43 oz.	• 23 g	48 oz.	96 oz.
40 inch range:	6 oz.	• 4 g	33 oz.	• 16 g	48 oz.	96 oz.
60 inch range:	13 oz.	• 4 g	22 oz.	• 8 g	26 oz.	52 oz.
75, 80 inch range:	10 oz.	• 3 g	40 oz.	• 12 g	20 oz.	40 oz.
100 inch range:	13 oz.	• 5 g	52 oz.	• 20 g	26 oz.	52 oz.
measuring cable:	.019-in. dia. nylon-coated stainless steel				.024-in. dia. stainless steel	

**note – outline dimensions for these options are not controlled on this datasheet!*

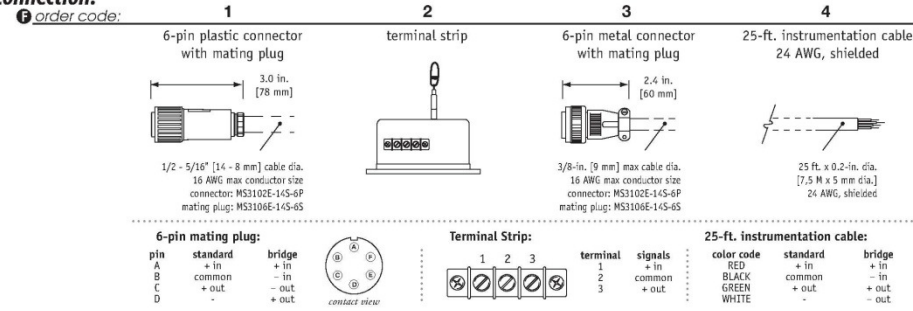
Measuring Cable Exit:



Sensing Circuit:



Electrical Connection:



tel: 800.423.5483 • +1.818.701.2750 • fax: +1.818.701.2799



celesco
celesco.com • info@celesco.com

PT101 | 3

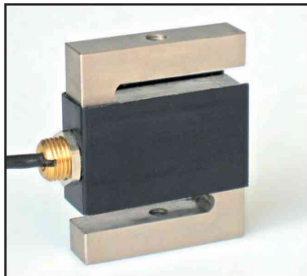
A.3 - Tension (Compression) Load Cell

SA

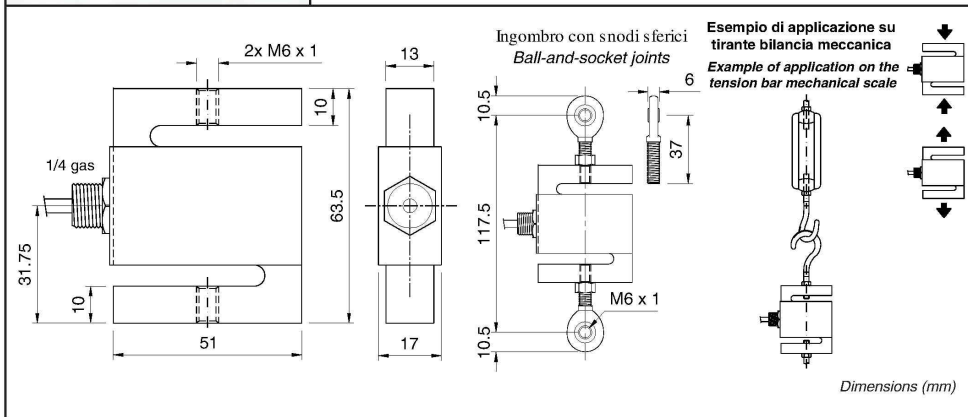
CELLE DI CARICO A TRAZIONE (COMPRESSIONE) TENSION (COMPRESSION) LOAD CELLS

SA kg 15, 30, 60.....
Snodo EM6 M6x1 con dado / Joint EM6 M6x1 with nut..... cad./each
Approvazione ATEX  II 1 G  II 2 D (zone 0-1-2-21-22) / ATEX approved (zone 0-1-2-21-22).....

 APPROVAZIONE OIML R60 C3
C3 OIML R60 C3 APPROVED



- ESECUZIONE IN ACCIAIO SPECIALE
- ERRORE COMBINATO $\leq \pm 0,02\%$
- GRADO DI PROTEZIONE IP 65
- SPECIAL STEEL CONSTRUCTION
- COMBINED ERROR $\leq \pm 0,02\%$
- PROTECTION RATING IP 65



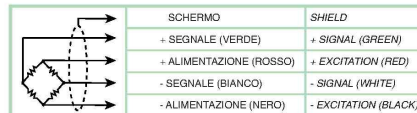
CARATTERISTICHE TECNICHE

SENSIBILITA'	2 mV/V $\pm 10\%$
EFFETTO DELLA TEMPERATURA SULLO ZERO	0.0017 % / °C
EFFETTO DELLA TEMPERATURA SUL FONDO SCALA	0.0013 % / °C
COMPENSAZIONE TERMICA	- 10°C / + 40°C
CAMPO DI TEMPERATURA DI LAVORO	- 20°C / + 60°C
CREEP A CARICO NOMINALE DOPO 4 ORE	0.03 %
TENSIONE DI ALIMENTAZIONE MAX TOLLERATA	15 Volt
RESISTENZA D'INGRESSO	381 ohm ± 20
RESISTENZA DI USCITA	350 ohm ± 4
BILANCIAMENTO DI ZERO	± 1 %
RESISTENZA D'ISOLAMENTO	> 5000 Mohm
CARICO STATICO MASSIMO (% sul Fondo Scala)	120 %
CARICO DI ROTTURA (% sul Fondo Scala)	> 300 %
DEFLESSIONE A CARICO NOMINALE	0.2 mm

TECHNICAL FEATURES

RATED OUTPUT
TEMPERATURE EFFECT ON ZERO
TEMPERATURE EFFECT ON SPAN
COMPENSATED TEMPERATURE RANGE
OPERATING TEMPERATURE RANGE
CREEP AT NOMINAL LOAD IN 4 HOURS
MAX SUPPLY VOLTAGE WITHOUT DAMAGE
INPUT RESISTANCE
OUTPUT RESISTANCE
ZERO BALANCE
INSULATION RESISTANCE
SAFE OVERLOAD (% of Full Scale)
ULTIMATE OVERLOAD (% of Full Scale)
DEFLECTION AT NOMINAL LOAD

CAVO	CABLE
LUNGHEZZA	3 m
DIAMETRO	4 mm
FILI CONDUTTORI	4 x 0.24 mm ²
LENGTH	DIAMETER
	CORES



A.4 - Analog Weight Transmitter

TRASMETTITORE ANALOGICO DI PESO 0-20mA; 4-20mA; 0-10VDC +/-5VDC ANALOG WEIGHT TRANSMITTER 0-20mA; 4-20mA; 0-10VDC +/-5VDC

TPS

JOLLYTPS calibrazione e selezione uscita analogica (0-20mA/4-20mA/0-10VDC) a cura del cliente / calibration and analog output (0-20mA/4-20mA/0-10VDC) selectable by the customer.....

TPS 0-20mA / 4-20mA / 0-10VDC

TPS +/- 5VDC (= +/-20mV).....

OPZIONI A RICHIESTA :

- Maggiorazione per celle di carico 3mV/V (escluso +/-5VDC).....

OPTIONS ON REQUEST :

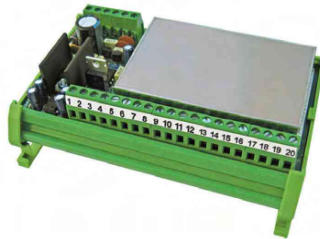
- Additional for 3mV/V cells (except ± 5VDC).....

GOST R
Russian
Standards



A richiesta
on request

**POSSIBILITA' DI SOPPRIMERE
LA TARA ED OTTENERE IL VALORE
MASSIMO DI USCITA
SINO AD 1/6 DEL F.S CELLE**
**ABILITY TO RESET THE TARE
AND GET THE
MAXIMUM OUTPUT VALUE
UP TO 1/6 OF FULL SCALE**



**USCITA ANALOGICA
RESISTENZA DI CARICO**
Loading resistance
Analog output

0-20 mA DC	max.	400 ohm
4-20 mA DC	max.	400 ohm
0-10 VDC	min.	2000 ohm
+/-5 VDC	min.	2000 ohm

Trasmettitore adatto per montaggio su barra Omega/DIN a retro quadro oppure in cassetta stagna.

Dimensioni: 123 mm x 90 mm x h 65 mm.

Provisto di filtro analogico per smorzare le oscillazioni di peso mediante vite di regolazione a un giro. Utilizzabile con schede analogico/digitali installate normalmente su PLC.

Weight transmitter for Omega/DIN rail mounting suitable for back panel or junction box.

Dimensions: 123 mm x 90 mm x height 65 mm.

Includes analogue filter to decrease the weight oscillations. Ideal for use with analog/digital boards normally installed on PLC.

CARATTERISTICHE TECNICHE

ALIMENTAZIONE	24 VDC +/-15%
LINEARITA'	0.01 % Full Scale
DERIVA TERMICA	0.005 % F.S./°C
POTENZA ASSORBITA	6 W
CAMPO DI MISURA	3 - 24 mV (*TPS +/-5VDC: +/-8 to +/-20mV)
FILTRO ANALOGICO (10-90%)	100 - 1000 msec
N° CELLE DI CARICO IN PARALLELO	max 6 (350 ohm)
ALIMENTAZIONE CELLE DI CARICO	10 VDC / 180 mA
UMIDITA' (non condensante)	85 %
TEMPERATURA DI STOCCAGGIO	-20°C + 70°C
TEMPERATURA DI ESERCIZIO	-10°C + 50°C

TECHNICAL FEATURES

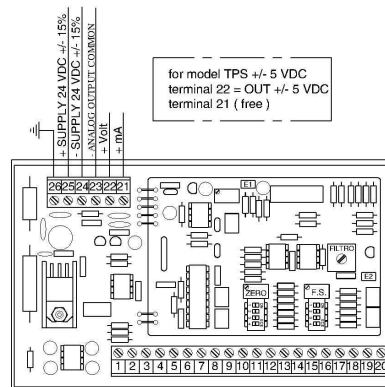
POWER SUPPLY
LINEARITY
THERMAL DRIFT
POWER CONSUMPTION
MEASURING RANGE
ANALOG FILTER (10-90%)
NUMBER OF LOAD CELLS IN PARALLEL
LOAD CELL SUPPLY
HUMIDITY (condensate free)
STORAGE TEMPERATURE
WORKING TEMPERATURE

CALIBRAZIONE

ZERO GROSS: 4 mini-interruttori da 0 a 17 mV (TPS +/-5VDC: +/-17mV)
ZERO FINE tramite potenziometro a 10 giri, 10% del campo
FONDO SCALA GROSS: 4 mini-interruttori da 3 a 24 mV (1/6 F.S.)*
FONDO SCALA FINE tramite potenziometro a 10 giri, 10% del campo

CALIBRATION

COARSE ZERO by 4 dip-switches from 0 to 17mV (TPS +/-5VDC: +/-17)
FINE ZERO by trimmer 10% range
COARSE FULL SCALE by 4 dip-switches from 3 to 24mV (1/6 F.S.)*
FINE FULL SCALE by trimmer 10% range



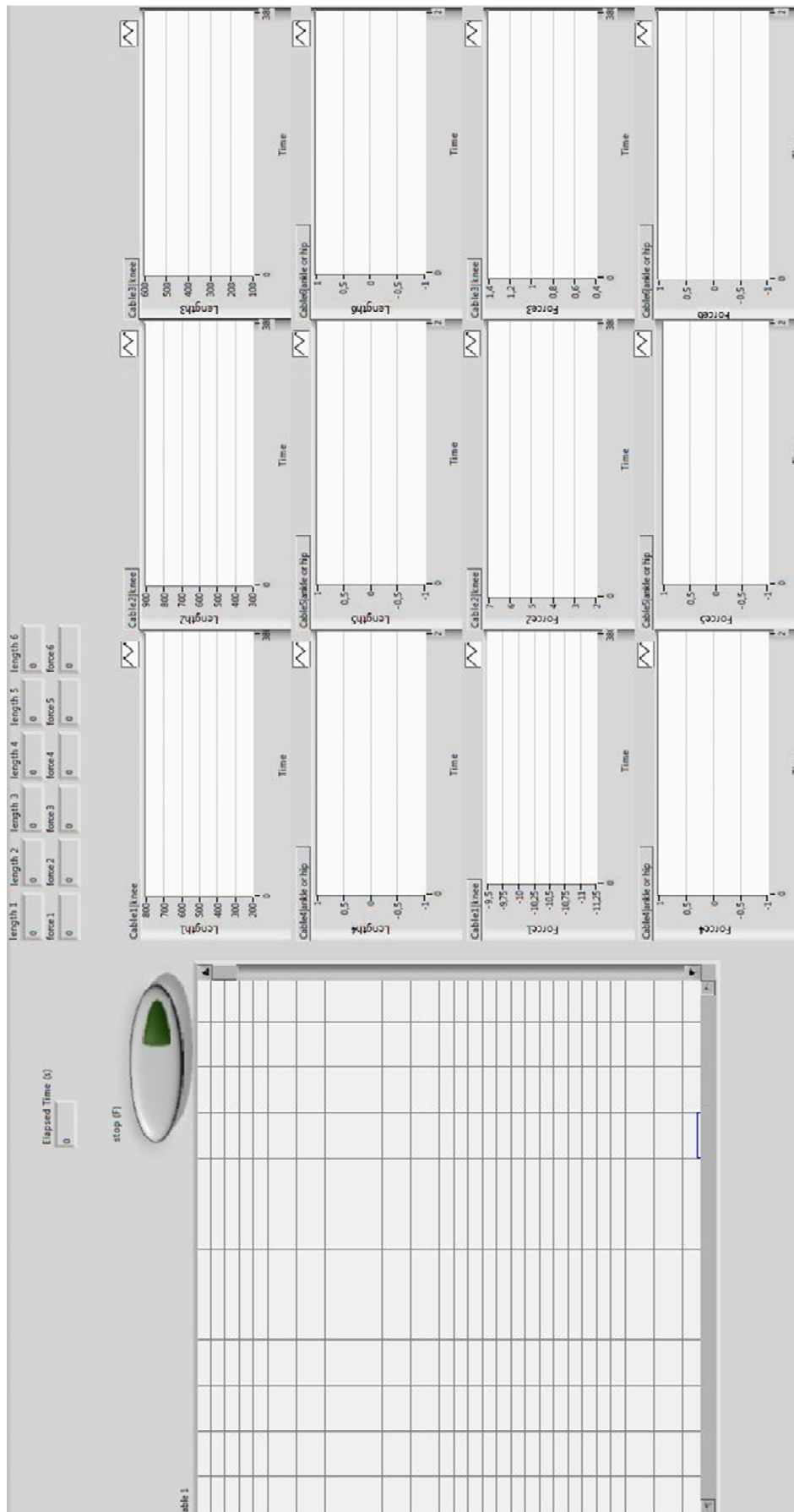
for model TPS +/- 5 VDC
terminal 22 = OUT +/- 5 VDC
terminal 21 (free)

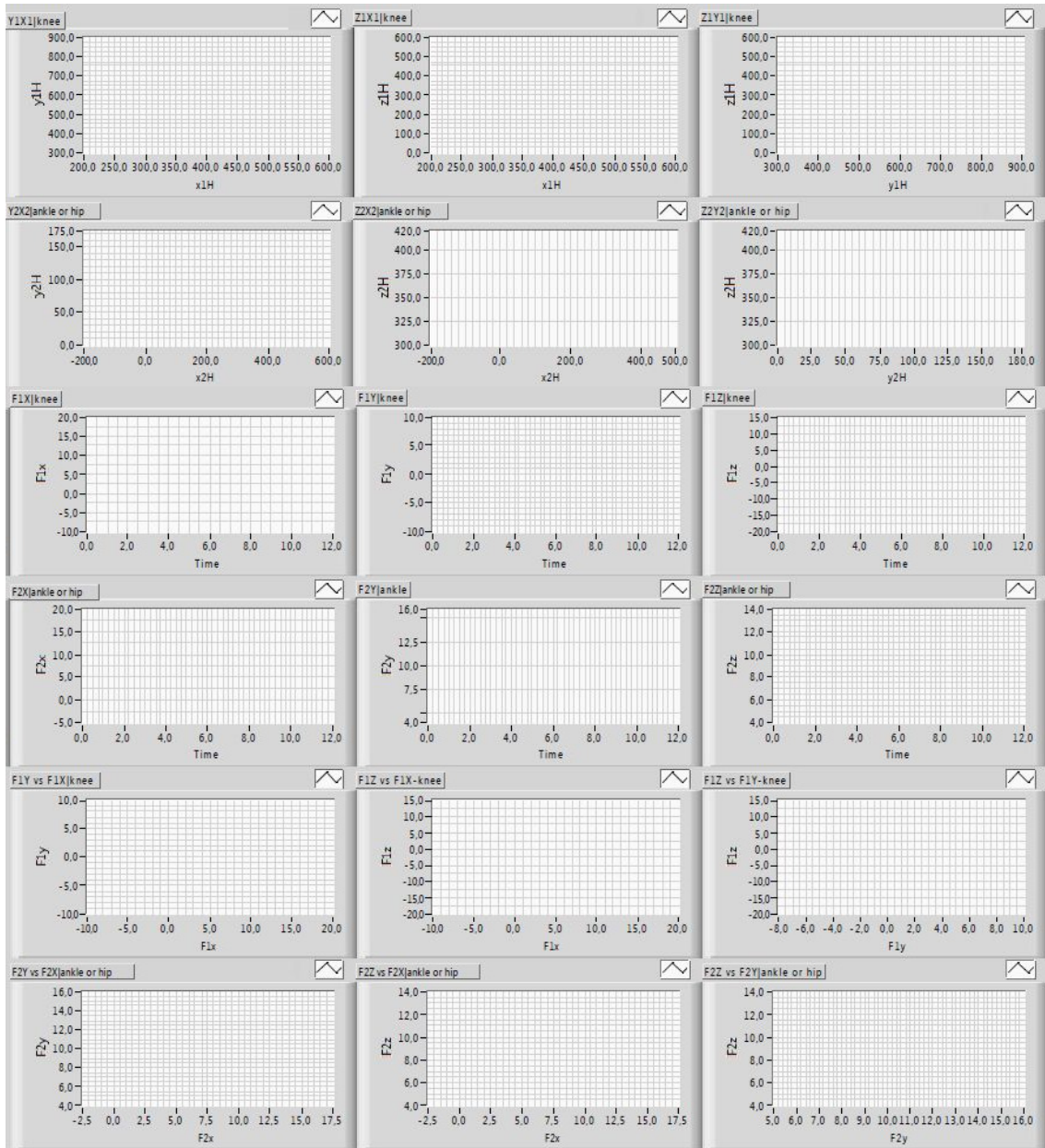
- 1 = - LOAD CELL EXCITATION 10 VDC
- 2 = + LOAD CELL EXCITATION 10 VDC
- 3 = - SIGNAL CELL
- 4 = + SIGNAL CELL
- 5 = SHIELD
- 6 = - LOAD CELL EXCITATION 10 VDC
- 7 = + LOAD CELL EXCITATION 10 VDC
- 8 = - SIGNAL CELL
- 9 = + SIGNAL CELL
- 10 = SHIELD
- 11 = - LOAD CELL EXCITATION 10 VDC
- 12 = + LOAD CELL EXCITATION 10 VDC
- 13 = - SIGNAL CELL
- 14 = + SIGNAL CELL
- 15 = SHIELD
- 16 = - LOAD CELL EXCITATION 10 VDC
- 17 = + LOAD CELL EXCITATION 10 VDC
- 18 = - SIGNAL CELL
- 19 = + SIGNAL CELL
- 20 = SHIELD

125

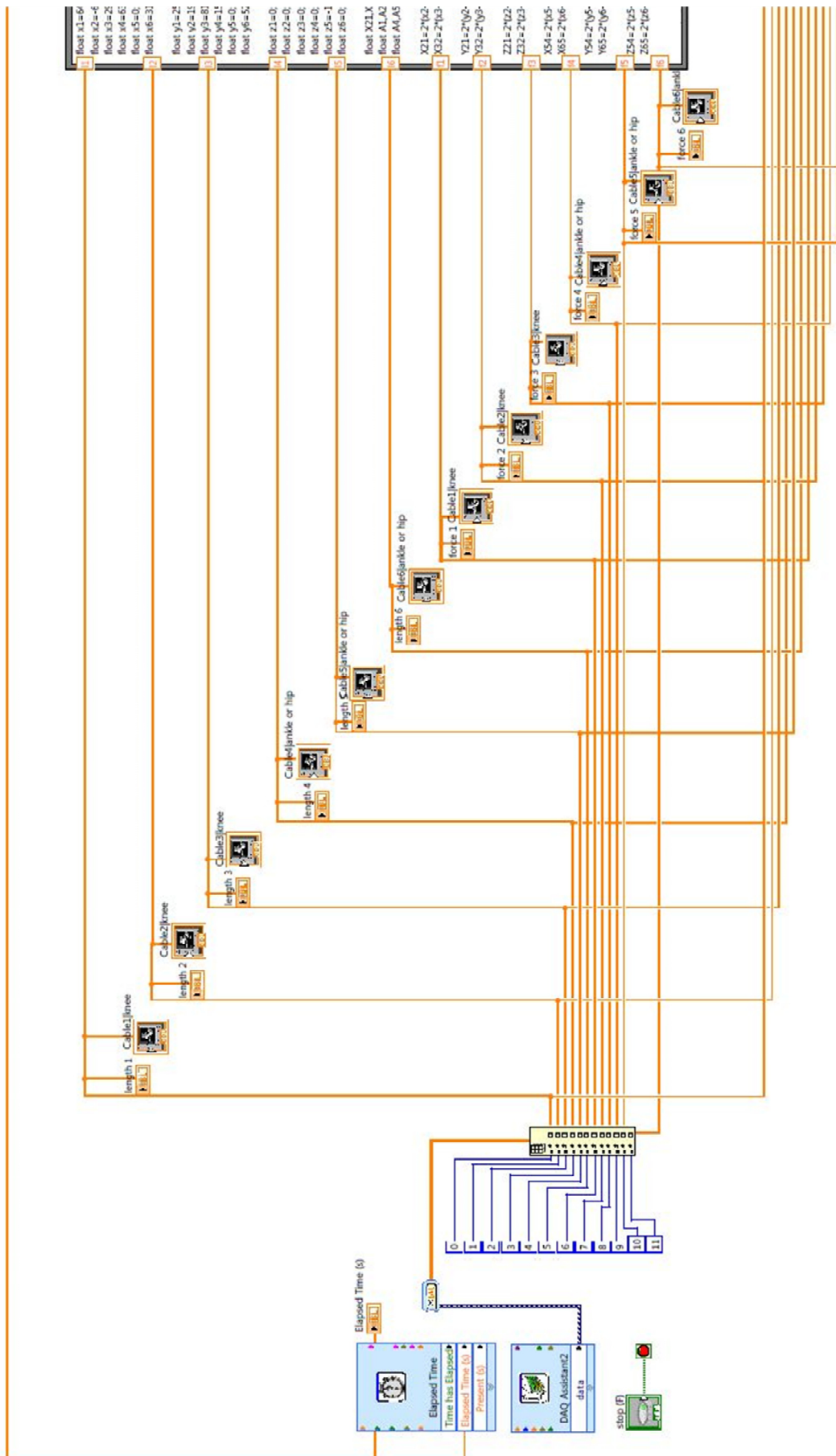
APPENDIX B – LABVIEW VI

B.1 - Front Panel





B.2 - Block Diagram



**APPENDIX C – FORM FOR CATRASYS EXPERIMENTAL TEST ON HUMAN
WALKING CHARACTERIZATION**



Thesis Title: Biomechanical Analysis of the Human Gait Cycle for Different Scenarios
Scientific Domain: Biomedical Engineering – Biomechanics
Operator: Maria João Varela
Institutions: LARM of UCassino (Italy) and CT2M of UMinho (Portugal)

University of Cassino and South Latium
Civil and Mechanical Engineering Department
LARM, Laboratory of Robotics and Mechatronics
Via G. Di Biasio 43, 03043 Cassino - Fr (Italy)
<http://webuser.unicas.it/weblarm/larmindex.htm>

FORM FOR CATRASYS EXPERIMENTAL TEST ON HUMAN WALKING CHARACTERIZATION

Operator Section		
Test Identification	Tests Validated (___ of ___)	Duration (s)
Pre-Comment		
After-Comment		

Subject Section			All information must be provided (capital letters)
Nationality	Gender (M/F)	Birth Date (dd/mm/yyyy)	
Height (m)		Weight (kg)	
Health Disorders (Past/Present)	Date (yyyy)	Description	
	Date (yyyy)	Description	
Sport Activity	Identification	Frequency (Times per Week)	
After-Comment (e.g.: Difficulties/Suggestions)			

Terms and Conditions: This personal information is being collected under the authority of a LARM project on human walking characterization. Its disclosure is governed by the privacy provisions of the privacy Italian law number 196 of 30 June, 2003. If you have any questions about the collection of this information, please contact Professor Marco Ceccarelli at the address listed above.

Legal Name	Surname	First Name
Contact Information	Mailing Address	Phone Number
Signature		Date(dd/mm/yyyy)

APPENDIX D – INDIVIDUAL TESTS INFORMATION

D.1 - Subject 1

Subject	Nationality	Gender (M/F)	Age (Years)	Weight (kg)	Height (m)	Shoes Size	Sport Activity (Times/Week)	Comments
1	Chinese	M	28	61	1.68	41	No	No
Parameter								
Parameter		Reference Walking	Loaded Walking	Footwear Walking	Fast Walking			
Walking Distance (m)		4.0579	3.5776	3.7306	3.7744			
Walking Time (s)		12.5	11.275	11.9	9.1			
Number of Cycles		8	7	8	8			
Cycle Time (s)		1.5625	1.6107	1.4875	1.1375			
Cycle Cadence (cycles/s)		0.64	0.6208	0.6723	0.8791			
Stance Phase (%)		50	50	47	46			
Swing Phase (%)		50	50	53	54			
Cycle Height (m)		0.1102	0.1191	0.0955	0.1093			
Cycle Length (m)		0.5072	0.5111	0.4663	0.4718			
Cycle Lateral Movement (m)		0.0568	0.068	0.0662	0.0569			
Supervisor Comment		One swing phase very different from the others.	No	Cycles not very uniform.	No			

D.2 - Subject 2

Subject	Nationality	Gender (M/F)	Age (Years)	Weight (kg)	Height (m)	Shoes Size	Sport Activity (Times/Week)	Comments
2	Chinese	M	28	65	1.68	39	No	No
Parameter								
	Reference Walking	Loaded Walking	Footwear Walking	Fast Walking				
Walking Distance (m)	3.7304	3.2457	4.0006	4.0898				
Walking Time (s)	12.8	11.55	13.3	9.15				
Number of Cycles	9	8	9	9				
Cycle Time (s)	1.4222	1.4438	1.4778	1.0167				
Cycle Cadence (cycles/s)	0.7031	0.6926	0.6767	0.9836				
Stance Phase (%)	43	49	43	42				
Swing Phase (%)	57	51	57	58				
Cycle Height (m)	0.0614	0.0775	0.0658	0.0872				
Cycle Length (m)	0.4145	0.4057	0.4445	0.4544				
Cycle Lateral Movement (m)	0.0765	0.0736	0.0699	0.0616				
Supervisor Comment	No	No	No	No				

D.3 - Subject 3

Subject	Nationality	Gender (M/F)	Age (Years)	Weight (kg)	Height (m)	Shoes Size	Sport Activity (Times/Week)	Comments
3	Romanian	M	28	58	1.75	41	No	Discomfort caused by the ankle ee
Parameter								
Parameter	Reference Walking	Loaded Walking	Footwear Walking	Fast Walking				
Walking Distance (m)	2.8088	3.0902	3.3293	3.1687				
Walking Time (s)	8.7	10.3	9.075	6.375				
Number of Cycles	7	8	8	7				
Cycle Time (s)	1.2429	1.2875	1.1344	0.9107				
Cycle Cadence (cycles/s)	0.8046	0.7767	0.8815	1.098				
Stance Phase (%)	42	44	41	41				
Swing Phase (%)	58	56	59	59				
Cycle Height (m)	0.0774	0.085	0.074	0.0865				
Cycle Length (m)	0.4013	0.3863	0.4162	0.4527				
Cycle Lateral Movement (m)	0.0487	0.0530	0.0578	0.0594				
Supervisor Comment	Very circular curvature of the cycles.	No	No	Very circular curvature of the cycles.				

D.4 - Subject 4

Subject	Nationality	Gender (M/F)	Age (Years)	Weight (kg)	Height (m)	Shoes Size	Sport Activity (Times/Week)	Comments
4	Greek	M	21	82	1.80	43	No	No
Parameter								
Parameter	Reference Walking	Loaded Walking	Footwear Walking	Fast Walking				
Walking Distance (m)	2.8544	3.7109	3.0153	3.8278				
Walking Time (s)	10.925	13.425	8.825	7.725				
Number of Cycles	8	9	7	7				
Cycle Time (s)	1.3656	1.4917	1.2607	1.1036				
Cycle Cadence (cycles/s)	0.7323	0.6704	0.7932	0.9061				
Stance Phase (%)	48	49	49	44				
Swing Phase (%)	52	51	51	56				
Cycle Height (m)	0.0913	0.1064	0.1031	0.1269				
Cycle Length (m)	0.3568	0.4123	0.4308	0.5468				
Cycle Lateral Movement (m)	0.0601	0.0802	0.0615	0.0895				
Supervisor Comment	Cycles not very uniform.	No	No	One swing phase very different from the others.				

D.5 - Subject 5

Subject	Nationality	Gender (M/F)	Age (Years)	Weight (kg)	Height (m)	Shoes Size	Sport Activity (Times/Week)	Comments
5	Italian	M	20	65	1.72	42	Basketball (3)	No
Parameter		Reference Walking		Loaded Walking		Footwear Walking		Fast Walking
Walking Distance (m)		3.5747		4.4678		3.0233		4.4058
Walking Time (s)		11.2		14.675		7.877		9.3
Number of Cycles		8		9		7		9
Cycle Time (s)		1.4		1.6306		1.2237		1.0333
Cycle Cadence (cycles/s)		0.7143		0.6133		0.7872		0.9677
Stance Phase (%)		35		37		49		38
Swing Phase (%)		65		63		51		62
Cycle Height (m)		0.0519		0.0584		0.1451		0.074
Cycle Length (m)		0.4468		0.4964		0.4898		0.4895
Cycle Lateral Movement (m)		0.0693		0.0657		0.0675		0.0666
Supervisor Comment		No		No		No		No

D.6 - Subject 6

Subject	Nationality	Gender (M/F)	Age (Years)	Weight (kg)	Height (m)	Shoes Size	Sport Activity (Times/Week)	Comments
6	Chinese	F	28	49	1.55	36	No	No
Parameter								
		Reference Walking		Loaded Walking		Footwear Walking		Fast Walking
Walking Distance (m)		2.4388		2.8458		2.8794		3.1808
Walking Time (s)		9.25		11.55		11.875		7.825
Number of Cycles		7		8		8		8
Cycle Time (s)		1.3214		1.44375		1.4844		0.9781
Cycle Cadence (cycles/s)		0.7568		0.6926		0.6737		1.0224
Stance Phase (%)		40		41		43		41
Swing Phase (%)		60		59		57		59
Cycle Height (m)		0.0465		0.0496		0.049		0.0655
Cycle Length (m)		0.3484		0.3557		0.351		0.3976
Cycle Lateral Movement (m)		0.0667		0.065		0.0578		0.0565
Supervisor Comment		Cycles not very uniform.		Knee: Stance phase with zz positions very stable.		Ankle: Very sharp curve.		One swing phase very different from the others.

D.7 - Subject 7

Subject	Nationality	Gender (M/F)	Age (Years)	Weight (kg)	Height (m)	Shoes Size	Sport Activity (Times/Week)	Comments
7	Portuguese	F	23	56	1.63	37	Swimming (2)	No
Parameter								
Parameter	Reference Walking		Loaded Walking		Footwear Walking		Fast Walking	
Walking Distance (m)	3.1659		4.5309		3.5007		5.1475	
Walking Time (s)	11.95		15.05		13.25		11.325	
Number of Cycles	7		10		8		10	
Cycle Time (s)	1.7071		1.505		1.6563		1.1325	
Cycle Cadence (cycles/s)	0.5858		0.6645		0.6038		0.883	
Stance Phase (%)	43		46		48		45	
Swing Phase (%)	57		54		52		55	
Cycle Height (m)	0.0698		0.0679		0.0644		0.0799	
Cycle Length (m)	0.4523		0.4531		0.4376		0.5148	
Cycle Lateral Movement (m)	0.0627		0.0677		0.0787		0.0684	
Supervisor Comment	No		No		No		No	

D.8 - Subject 8

Subject	Nationality	Gender (M/F)	Age (Years)	Weight (kg)	Height (m)	Shoes Size	Sport Activity (Times/Week)	Comments
8	Spanish	F	22	62	1.65	38	No	Difficult on treadmill walking
Parameter		Reference Walking	Loaded Walking	Footwear Walking	Fast Walking			
Walking Distance (m)		3.9397	3.9781	4.1292	3.9885			
Walking Time (s)		13.975	11.2	11.875	6.65			
Number of Cycles		9	10	10	9			
Cycle Time (s)		1.5528	1.12	1.1875	0.7389			
Cycle Cadence (cycles/s)		0.644	0.8928	0.8421	1.3534			
Stance Phase (%)		41	44	41	42			
Swing Phase (%)		59	56	59	58			
Cycle Height (m)		0.061	0.0837	0.0463	0.0617			
Cycle Length (m)		0.4377	0.3978	0.4129	0.4432			
Cycle Lateral Movement (m)		0.0653	0.0583	0.0709	0.049			
Supervisor Comment		Cycles not very uniform.	Knee: Stance phase with zz positions very stable.	Ankle: Very sharp curve.	One swing phase very different from the others.			